



UNIVERSIDAD DE GUANAJUATO
CAMPUS IRAPUATO-SALAMANCA
DIVISIÓN DE INGENIERÍAS

“ANALYTICAL AND NUMERICAL STUDY OF THE
PLATE TWIST TEST IN COMPOSITE LAMINATES AND
SANDWICH PANELS”

TESIS

QUE PARA OBTENER EL GRADO DE:
DOCTOR EN INGENIERÍA MECÁNICA

PRESENTA

M. EN I. RENNY JESÚS GUILLÉN RUJANO

DIRECTORES:

DR. ADRIÁN HERNÁNDEZ PÉREZ

DR. AGUSTÍN VIDAL LESSO

SALAMANCA GTO.

MAYO 2020

Salamanca, Gto., a 20 de Abril del 2020.

M. en I. HERIBERTO GUTIÉRREZ MARTÍN
JEFE DE LA UNIDAD DE ADMINISTRACIÓN ESCOLAR
PRESENTE.-

Por medio de la presente, se otorga autorización para proceder a los trámites de impresión, empastado de tesis y titulación al alumno(a) Renny Jesús Guillén Rujano del Programa de Doctorado en Ingeniería Mecánica y cuyo número de NIA es: 145804 del cual soy director. El título de la tesis es: Analytical and numerical study of the plate twist test in composite laminates and sandwich panels.

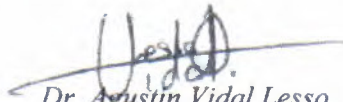
Hago constar que he revisado dicho trabajo y he tenido comunicación con los sinodales asignados para la revisión de la tesis, por lo que no hay impedimento alguno para fijar la fecha de examen de titulación.

ATENTAMENTE



Dr. Adrián Hernández Pérez

NOMBRE Y FIRMA
DIRECTOR DE TESIS
SECRETARIO



Dr. Agustín Vidal Lesso

NOMBRE Y FIRMA
DIRECTOR DE TESIS



Dr. Ledania Orozco, Elías Rigoberto

NOMBRE Y FIRMA
PRESIDENTE



Dr. Balvanthin García Antonio de Jesús

NOMBRE Y FIRMA
VOCAL



Dr. Avilés Cetina Francis

NOMBRE Y FIRMA
VOCAL



Dr. José de Jesús Kú Herrera

NOMBRE Y FIRMA
VOCAL



Universidad
Guanajuato



To my Lord
To my family
To Venezuela



Universidad
Guanajuato



Acknowledgements

To: Conacyt-Mexico, Universidad de Guanajuato, Universidad Nacional Experimental del Táchira, Advisor Dr. Adrián Hernández Pérez, Dr. José de Jesús Kú Herrera, Dr. Francis Avilés, Dr. Agustín Vidal Lesso, Dr. Kristofer Gamstedt, Lic. Sayuri Mendieta Grimaldo, Alexa Morones Mendieta, Grimaldo's family, Cobarrubias' family, to my family and to all those who contributed in over way to achieve this goal. Thank you, a lot. God bless them.



Universidad
Guanajuato

Abstract

An analytical and numerical research work related to the plate twist test of specially orthotropic plates is developed in this thesis. Two finite element models and two analytical closed-form solutions are developed for deflections and rotations of thick specially orthotropic materials under twisting loads by using the first-order shear deformation theory. These solutions show good agreement in the compliance predictions with respect to previously reported measurements and finite element estimations. The first solution considers the effect solely of the stiffness D_{66} and A_{44}, A_{55} in the compliance, assuming shear correction factors of $2/3$ and a twisting moment $M_{xy} = P/4$. The second solution not only considers the influence of D_{66} and A_{44}, A_{55} on the compliance but also that by D_{11}, D_{12}, D_{22} stiffnesses, varying the shear correction factors and M_{xy} according to the material system and geometry. The results of the parametrical analysis show that both solutions are able to adequately predict the deflections of specially orthotropic plates from low to moderately high side-length to thickness ratios ($1 \leq \text{side-lengths/thickness} \leq 20$ and $(1 \leq \text{side-lengths/thickness} \leq 61)$, respectively; also both solutions can be used for rectangular plates with ratios between sides-length ($1 \leq \text{side-length in } x \text{ axis/side-length in } y \text{ axis} \leq 10$). Examination of the in-plane shear modulus ratio between face sheets and core (G_{12f}/G_{12c}) points out that the first solution slightly underpredicts the compliance with respect to finite element method (FEM), specially for G_{12f}/G_{12c} ratios larger than 100, whilst the second solution match very well for those ratios. Examination of the M_{xy} by finite element method showed that M_{xy} has a parabolic behavior for sandwich panels with compliant cores, reaching a maximum value at the center of the plate different to $P/4$ and being dependent of the material properties.



Universidad
Guanajuato

List of symbols

Nomenclature

Latin Letters

A_{ij}	Components of the extensional stiffness matrix
A_i	Constants of the proposed polynomial to be determined
B_{ij}	Bending-extensional coupling stiffness
B_i	Constants of the proposed polynomial to be determined
c_1	Calibration factor in the Avilés' semi-empirical solution
C	Compliance
C_i	Constants of the proposed polynomial to be determined
C_o	Displacement of the center of the plate in z direction
D_{ij}	Bending stiffness ($i, j = 1, \dots, 6$)
E	Young's modulus of isotropic materials
E_1, E_2, E_3	Young's modulus of one lamina at the material coordinate 1 (0°), 2 (90°) and 3, respectively
E_c, E_f	Young's modulus of the core and face for sandwich materials
G	Shear modulus of isotropic materials
G_{12}, G_{13}, G_{23}	In-plane shear modulus at the material plane 1 – 2, 1 – 3, 2 – 3, respectively
G_c, G_f	Shear modulus of the isotropic core and isotropic face in sandwich materials, respectively
G_{12c}, G_{12f}	Shear modulus of the core and face sheet in sandwich materials at material plane 1 – 2, respectively
$g_x(z), g_y(z)$	Continuum functions used to define the shear stresses $\tau_{xz}(z), \tau_{yz}(z)$ in order to define the shear correction factors K_{11} and K_{22} , respectively
h	Total plate thickness
h_c, h_f	Core and face sheet thickness of the sandwich panel
h_i	Thickness of the i -th ply in a composite laminate
$H_{11}(z), H_{22}(z)$	Functions obtained from integration of $g_x(z)$ and $g_y(z)$ required to define K_{11} and K_{22} , respectively
k	Dummy index that refers to the ply number in a laminated material
K_{ij}	Shear correction factor for FSDT
K_{11}, K_{22}	Shear correction factor for the FSDT in yz and xz plane
L_x, L_y	Span-length along x and y -axes
L'_x, L'_y	Side-length of the plate with overhang along x and y axes
m	Number of nodes in the plane xy at z location
m_o	Current number of the terms in the double Fourier series
M_o	Maximum number of terms in the double Fourier series

M_x, M_y	Bending moment resultant per unit of length along x and y direction, respectively
M_{xy}	Twisting moment resultant per unit of length relative at xy plane
$(M_{xy})_{ave}$	Average twisting moment at mid-plane
$(M_{xy})_{max}$	Maximum twisting moment per unit of length at mid-plane
n	Number of nodes along the thickness of the model at (x, y) position
n_o	Current number of the terms in the double Fourier series
N_o	Maximum number of terms in the double Fourier series
N	Total amount of plies
N_x, N_y	Normal in-plane force resultant per unit of length in x and y direction, respectively
N_{xy}	In-plane shear force resultant per unit of length relative to xy plane
P	Total applied load over the plate
q	Load per unit of area acting along z direction over the plate
Q_{ij}	Plane stress-reduced stiffness
$(\bar{Q}_{ij})_k$	Transformed plane stress-reduced stiffness
$\bar{Q}_{11}^{(k)}, \bar{Q}_{22}^{(k)}$	Transformed reduced stiffnesses of the k -th ply along the material axis 1 (longitudinal) and 2 (transverse), respectively
Q_x, Q_y	Transverse shear load resultant per unit of length tangential to the yz and xz planes, respectively
R_i	Variable to be minimized by using the theorem of minimum potential
\bar{S}_{ij}	Material compliance coefficients
$[T]$	Transformation matrix
u_o, v_o	Displacement of a point in x and y direction of the middle plane on $z = 0$, respectively
$u(x, y)$	General displacement in x direction
V	Strain energy
$v(x, y)$	General displacement in y direction
$w(x, y), w$	Deflection along the z direction
w_o	Deflection along the z direction at mid-plane on $z = 0$
z_i, z_{i-1}	i -th and $(i - 1)$ -th nodal coordinates in z direction

Greek letters

$\gamma_{xy}, \gamma_{xz}, \gamma_{yz}$	In-plane and transverse shear strain shear at xy , xz , and yz planes, respectively
$\gamma_{12}, \gamma_{13}, \gamma_{23}$	In-plane and transverse shear strain shear at 1 – 2, 1 – 3, and 2 – 3 planes, respectively
δ	Maximum deflection of the plate
$\epsilon_x, \epsilon_y, \epsilon_z$	Longitudinal strains relatives to x -, y - and z -axis, respectively
$\epsilon_1, \epsilon_2, \epsilon_3$	Longitudinal strains relatives to 1-, 2- and 3-axis, respectively
θ	Orientation angle for the fibers in the k -th layer

$\kappa_x, \kappa_y, \kappa_{xy}$	Bending and twisting curvatures of the middle surface along to x -, y -axes and xy plane, respectively
λ_x, λ_y	Functions that define the parabolic behaviour of the shear strain and shear stresses in TSDT
ν	Poisson's ratio of isotropic materials
$\nu_{12}, \nu_{13}, \nu_{23}$	Poisson's ratio at the 1 – 2 , 1 – 3 and 2 – 3 planes, respectively
$\sigma_x, \sigma_y, \sigma_z$	Normal stresses along x, y and z -axis
$\sigma_1, \sigma_2, \sigma_3$	Normal stresses along 1,2 and 3-axis
$\tau_{xy}, \tau_{xz}, \tau_{yz}$	Shear stress in the xy, xz and yz planes, respectively
$\tau_{12}, \tau_{13}, \tau_{23}$	Shear stress in the 1 – 2, 1 – 3 and 2 – 3 planes, respectively
$\tau_{xy}^i, \tau_{xy}^{i-1}$	In-plane shear stresses at the i -th and $(i - 1)$ -th nodal coordinate in z direction, respectively
$\tau_{xz}(z), \tau_{yz}(z)$	Shear stress distribution along the thickness in xz and yz planes, respectively
Φ_x, Φ_y	Rotation of a transverse normal about the x and y -axes, associated at u and v displacement fields, respectively
φ_x, φ_y	Functions without physical interpretation in SSDT associated at u and v displacement fields
Ω	Planform area of the plate
$\Omega^{FEM}, \Omega^{FSDT}$	Areas enclosed by the γ_{xy} curve along center-line $y = L_y/2$ for FEM and FSDT

List of acronyms

ASTM	American Society for Testing and Materials
CLPT	Classical laminated plate theory
ECT	Edge crack torsion
ESL	Equivalent single layer
EXP	Reported experiments
FEM	Finite element method
FSDT	First-order shear deformation theory
LM	Laminate composite
PT	Plate twist
PTS	Plate twist specimen
PVC	Polyvinyl chloride
SSDT	Second-order shear deformation theory
SW	Sandwich panel
TSDT	Third-order shear deformation theory



Universidad
Guanajuato

Index

Acknowledgements	v
Abstract	vii
List of symbols	ix
Index	xiii
List of Tables	xvii
List of Figures	xix
Introduction	xxiii
Hypothesis	xxiv
Objectives	xxiv
Justification	xxiv
Scope	xxv
Chapter I. The Plate Twist Specimen	1
1 Background	2
1.1 Composite material	2
1.2 Composite laminates	2
1.3 Sandwich panels	3
1.4 The stress and strain relationship	4
1.5 Laminated plate theories	7
1.5.1 Classical laminate plate theory	7
1.5.2 First-order shear deformation laminated plate theory	8
1.5.3 Second-order laminated plate theory	9
1.5.4 Third-order shear deformation laminated plate theory	9
1.6 First-order shear deformation laminated plate theory	11
1.6.1 Displacement field	11
1.6.2 Strain field	12
1.6.3 Stress field	13
1.6.4 Laminate constitutive equations	13
1.6.5 Equilibrium equations	15
1.6.6 Governing equations	16
1.6.7 Theorem of minimum potential energy	18

1.7	The plate twist specimen	18
1.7.1	Some analytical solutions previously reported for thin plates	19
1.8	Finite element method	21
1.8.1	Description of the SOLID185 element	22
Chapter II. Examination of the plate twist specimen for thick specially orthotropic laminated composites and sandwich plates by using first-order shear deformation theory		27
2.1	Introduction	28
2.2	Analytical solution using first-order shear deformation theory	29
2.2.1	The plate twist specimen	29
2.2.2	First-order shear deformation solution	32
2.3	Finite element analysis	37
2.4	Results and discussion	38
2.4.1	Displacement, rotations, and strain fields	38
2.4.2	Parametric investigation	46
2.4.3	Comparison with experiments	50
2.5	Conclusions	52
Chapter III. A closed-form solution for anticlastic bending of laminated composite plates		53
3.1	Introduction	54
3.2	First-order shear deformation theory	55
3.2.1	Kinematics	55
3.2.2	Governing differential equations	57
3.3	Plate twist solution	58
3.3.1	Boundary conditions	58
3.3.2	Closed-form polynomial solution	59
3.4	Finite element analysis	64
3.5	Results and discussion	66
3.5.1	Examination of the twisting moment	67
3.5.2	Prediction of displacements and transverse shear strains	73
3.5.3	Parametric analysis	77
3.6	Conclusions	80
Conclusions		83
Appendix A: Effect of the shear correction factor		85



Appendix B: Calculation of the shear correction factors	86
References	89



Universidad
Guanajuato

List of Tables

Table 2.1. Elastic properties of baseline panels.	32
Table 2.2. Compliance, measured and predicted by other authors and by the current FSDT solution [16, 17, 42] in ($\mu\text{m}/\text{N}$) and [11] in (10^{-4} in/Lb).	51
Table 3.1. Dimensions and properties of the baseline orthotropic panels.	65
Table 3.2. Comparison between previously reported compliance measurements and predictions by FEM and FSDT of this work.	66



Universidad
Guanajuato

List of Figures

Figure 1. 1. Schematic of a composite laminate and laminated construction.	3
Figure 1. 2. Schematic of typical sandwich cores. (a) Solid core. (b) Web core. (c) Corrugated core.	4
Figure 1. 3. Generalized stress components in a solid body.	5
Figure 1. 4. Undeformed and deformed geometries of an edge of a plate under the assumptions of the CLPT [3].....	8
Figure 1. 5. Undeformed and deformed geometries of an edge of a plate under the assumptions of the TSDT [3].	11
Figure 1. 6. Undeformed and deformed geometries of an edge of a plate under the assumptions of FSDT [3].....	11
Figure 1. 7. Schematic general representation in a composite laminate of longitudinal strain ε_x , transversal shear strain γ_{xz} and shear stress τ_{xz} in FSDT and real shear stress τ_{xz}	12
Figure 1. 8. Force and moment resultants on a rectangular plate.....	14
Figure 1. 9. Representation of the mid-plane area and global coordinate system.....	18
Figure 1. 10. Loading configurations of the plate twist specimen. (a) First. (b) Second..	19
Figure 1. 11. SOLID185 element. (a) Homogeneous structural solid. (b) Layered structural solid [31].....	22
Figure 1. 12. Coordinate systems of the SOLID185 element. (a) Global. (b) Natural or intrinsic coordinates s,t and g [30].....	23
Figure 2. 1. The PTS. (a) Composite laminate. (b) Sandwich panel.	30
Figure 2. 2. Equivalent force and moment diagrams for the PTS. (a) Original free body diagram. (b) Equivalent free body diagram with force and moment resultants. (c) Resultant transverse shear loads and twist moments in one quarter plate.	31
Figure 2. 3. Finite element models of the baseline materials. (a) Laminated composite. (b) Sandwich panel.....	38
Figure 2. 4. Normalized mid-plane deflection (w/P) for the square $[(0/90)_6]_s$ composite laminate. (a) FSDT. (b) FEM. (c) Along $y = L_y/2$	40
Figure 2. 5. Normalized mid-plane deflection (w/P) of the square AL/H45 sandwich panel. (a) FSDT. (b) FEM. (c) Along $y = L_y/2$	42

Figure 2. 6. Mid-plane transverse shear strain γ_{xz} distribution along the AL/H45 sandwich panel. (a) $y = L_y/2$. (b) $x = 0$ centerline.	44
Figure 2. 7. Rotation function ϕ_x , slope $\partial w/\partial x_{FSDT}$, slope $\partial w/\partial x_{CLPT}$ and transverse shear strain γ_{xz} at the xz plane for the (a) $[(0/90)_6]_s$ laminate. (b) AL/H45 sandwich panel.	45
Figure 2. 8. Effect of normalized side-length L_x/h on the compliance of square composites. (a) Cross-ply $[(0/90)_n]_s$ laminate. (b) AL/H45 sandwich panel.	47
Figure 2. 9. Effect of the ratio between in-plane shear stiffness of the face sheet and core (G_{12f}/G_{12c}) on the compliance of square sandwich twist panels.	48
Figure 2. 10. Effect of G_{23}/G_{12} shear stiffness ratio on the compliance of cross-ply laminates.	49
Figure 2. 11. Effect of in-plane aspect ratio L_x/L_y in the compliance of $[(0/90)_{12}]_s$ laminates.	50
Figure 3. 1. Schematic of the PTS. (a) Representation of rotations ϕ_x , slopes $\partial w/\partial x$ and transverse shear strains γ_{xz} . (b) Isometric view.	56
Figure 3. 2. Schematic of the FEM of the PTS.	65
Figure 3. 3. Distribution of normalized twisting moment M_{xy}/P calculated by FSDT and FEM at the mid-plane ($z = 0$) of the LM baseline panel. (a) FEM. (b) FSDT. (c) along the center line $y = 0$	69
Figure 3. 4. Distribution of normalized twisting moment M_{xy}/P calculated by FSDT and FEM at the mid-plane ($z = 0$) of the SW baseline panel. (a) FEM. (b) FSDT. (c) along the center line $y = 0$	71
Figure 3. 5. Maximum and average M_{xy}/P (Eq. (3.29)) versus E_f/E_c ratios for different sandwich panels using the panel SW as baseline. (a) $1 \leq E_f/E_c \leq 200$. (b) $200 \leq E_f/E_c \leq 1768$	73
Figure 3. 6. Normalized displacement fields $w(x, y)/P$ for the baseline SW at mid-plane ($z = 0$). (a) FEM. (b) FSDT. (c) along center line $y = 0$	75
Figure 3. 7. Comparison of normalized mid-plane transverse shear strain (γ_{xz}/P) for the baseline panels listed in Table 3.1 at the edge $y = L_y/2$. (a) LM. (b) SW.	77
Figure 3. 8. Effect of normalized length L_x/h on the compliance of square panels based on baselines plates. (a) LM. (b) SW with $h_f = 2\text{mm}$	78
Figure 3. 9. Effect of the in-plane shear modulus ratio on the compliance of the square sandwich panels.	79



Figure A – 1. Normalized mid-plane deflection (w/P) predicted by FEM, CLPT and FSDT (employing four values of K_{ij}) for the square AL/H45 sandwich panel at the edge $y = L_y/2$ 85



Universidad
Guanajuato

Introduction

Composite materials represent a big part of the available materials to use in engineering process and design. They are the result of combining on macroscopic scale two or more materials with different properties to form a useful third material [1, 2]. The study of these materials is conducted by experimental testing, numerical methods or theoretical analysis. The last one is performed using theory of elasticity or simplifications from this one, such as the classical laminate plate theory (CLPT) or the first-, second- or third-order shear deformation theories [3, 4] among others. Many problems like bending, vibration, buckling, torsion, fatigue in beams, columns, bars, plates, shells, etc., have been solved for composite materials by using these approaches [2-8].

The plate twist (PT) is an interesting torsion problem to be studied for composite materials since many engineering components are subjected to torsion. Its study is important and may help to prevent failure in machinery components as turbine blades, helicopter propellers, transmission shafts among others throughout the determination of the shear modulus and prediction of the elastic behavior of the materials [9, 10]. The PT may be employed to determine the elastic behavior of moderate thick and thin plates before the action of torsional loads if the material properties are known, i.e., prediction of the deflections, rotations, stress and strain field over the material under the action of twisting loads [6, 11, 12]. The PT has been used to study the anticlastic bending of rectangular laminate composite plates [12] which is generated by the action of twisting couples along the edge of the plate which may lead to a failure known as delamination in composite materials (plies separation). The PT consists in a thin or moderate thick plate supported in two diagonal corners and subjected to two-point loads in the opposite other two corners [9]. This problem has been addressed by several researchers using CLPT and First-Order Shear Deformation Theory (FSDT), but until now there is not an accurate solution to predict the compliance of rigid and compliant composite plates. Therefore, this doctoral thesis devotes to analytical and numerically study the PT test in composite laminates and sandwich panels.

The analysis of the PT specimen is addressed herein by using the FSDT. The study is divided in three chapters. In Chapter I some theoretical background needed to understand the border conditions, constitutive equations, equilibrium equations, governing equations and develop analytical and numerical solutions for the PT problem, is shown. In Chapter II is developed an analytical polynomial solution which considers the action of twisting moment (M_{xy}), assuming that M_{xy} has a constant value of $P/4$ in the whole plate; the bending moments (M_x, M_y) are vanished; and the shear forces (Q_x, Q_y) are considered as constants. In Chapter III another polynomial solution is developed considering a variable M_{xy} ($M_{xy} \neq P/4$), keeping M_x, M_y not negligible, and considering Q_x, Q_y as variables along the entire plate, and the general conclusions of this thesis work are presented at the end of this manuscript.

Hypothesis

It is possible to deduce a mathematical expression that accurately predicts the compliance of thick laminated composite plates loaded in torsion considering the effects of transversal shear loads, bending and twisting moments by using FSDT.

Objectives

General

To analyze theoretically and numerically the elastic response of laminated composite plates and sandwich panels under twisting loads using the PT configuration, considering the effects due to transverse shear forces, bending and twisting moments on the plate deflection.

Specifics

- a. To develop compliance equations using polynomials for thick and thin specially orthotropic plates subjected to torsion under the PT configuration by using the FSDT.
- b. To determine the compliance, modeling composite laminates and sandwich panels subjected to torsion by using the finite element method.
- c. To determine and examine the transversal shear strain field of the plates predicted by FEM and the models developed.
- d. To determine and examine the influence of twisting moment on the plates by using FEM and the models developed.
- e. To establish the validation of the developed models using the previously reported results.
- f. To define the range of application of the developed models conducting a parametric analysis.

Justification

Twisting behavior of laminated composite materials is important because structures and devices made with these materials may undergo torsion during their working life, inducing mechanical damage such as creep, degradation of elastic properties, fatigue, fracture of the constituents and delamination (separation of the layers that form the composite material). Common examples of composite structures under twisting loads includes rotatory blades of helicopters, wind turbines, rotating machinery, airplane wings and transmission shafts [13]. Some test methods as the torsion pendulum and the PT are standardized methods to study the

torsional behavior of isotropic materials [14], wood-based structural panels [9] and fiber-reinforced unidirectional plastic composites [10, 15]. The PT test is a recognized international test method to determine the torsional stiffness of plywood [9] and metal panels [11, 15], also it has been employed to determine the in-plane shear modulus of the face sheets, transverse shear modulus of the soft core and twist stiffness in sandwich panels [16].

Despite the PT has been extensively studied [6, 17, 18], to date there is not an accurate closed-form mathematical expression for the compliance of laminated composite and sandwich structures materials which includes the influence of shear forces (Q_x, Q_y), bending moments (M_x, M_y) and twisting moment (M_{xy}). In fact, it is important to study the behavior and influence of the M_{xy} in the problem of plate torsion, due to this resultant load seems to be the most important according to Avilés et al. [17], Timoshenko and Woinowsky-Krieger [12] and Nadaí [19] solutions among others. Until now every reported research has considered M_{xy} as a constant value of $P/4$ and have not considered its dependence to the material system, additionally, they have not analytically considered the influence of the transversal shear forces. On the other hand, FSDT employs a shear correction factor K_{ij} which depends of the materials system [3] and becomes important to accurately predict the behavior of the PT specimen. Given this background, this research aims to develop closed-form expressions for the compliance of specially orthotropic laminates and sandwich panels considering all these parameters.

Scope

The scope of this research is to obtain, validate and establish the range of application of at least an analytical expression to analyze the torsional behavior of specially orthotropic composite laminate plates and sandwich panels with isotropic core and faces under PT configuration using FSDT.



Universidad
Guanajuato



Chapter I. The Plate Twist Specimen

1 Background

1.1 Composite material

A composite material is the combination of two or more materials on the macroscopic scale [2], where each part may have different mechanical and chemical properties [20] to form a useful third material with desirable properties that cannot be achieved with any of the constituents alone [3]. Composite materials are normally made of one or more discontinuous phases distributed in one continuous phase. The continuous phase is called the matrix and the discontinuous phase is called the reinforcement. The properties of a composite material depend on the properties of the constituents, their geometrical distribution, their interactions, among others [21]. Composite materials can be classified by the form of the reinforcement [2, 20] as fiber composites, particle composites, laminated composites and combinations of some or all of the three types mentioned.

1.2 Composite laminates

A composite is called a laminated when it consists of layers (at least two) or when two or more different materials are bonded together (see, Figure 1.1). Lamination combines the best aspects of the constituent layers to achieve a more useful material. The ability to structure and orient material layers (Figure 1.1) in a prescribed sequence leads to several significant advantages of composite materials compared with conventional monolithic materials. The most important ability is to tailor or align the lamina properties and orientations to the prescribed structural loads. Some properties that can be emphasized by lamination are strength, stiffness, corrosion resistance, low weight, etc. [20]. An international code to represent the stacking sequence of a composite laminate was presented in the 1973 edition of the “Advanced Composites Design Guide” and is explained widely by Adams et al.[1]. An example of this code is: $[(0/90)_2]_s$, where the square brackets “[]” indicates the beginning and end of the code. The subscript s indicates that there is a symmetric laminate. The parenthesis “()” contain in this case only the plies on the one side of the mid-plane due the laminates is a symmetric material. The numbers 0 and 90 represent the θ orientation of each ply with respect to one reference system, where 0 normally is parallel to x -axis. The number 2 in this case is indicating that the stacking sequence is repeat twice. In this example, there are 8 plies and could be expressed in an extended form as follow: $[0/90/0/90]_s$ or $[0/90/0/90/90/0/90/0]$. The numbers 1,2,3 in Figure 1.1, represent the material coordinate system, where 1 identifies the orientation of the fiber, 2 is normal to the fiber, 3 is considered normal to the plane where the fibers are contained (1 – 2). The composite material employed in this thesis work is a cross ply laminate $[(0/90)_n]_s$ which are typically employed in the automotive, sport and naval industries [2].

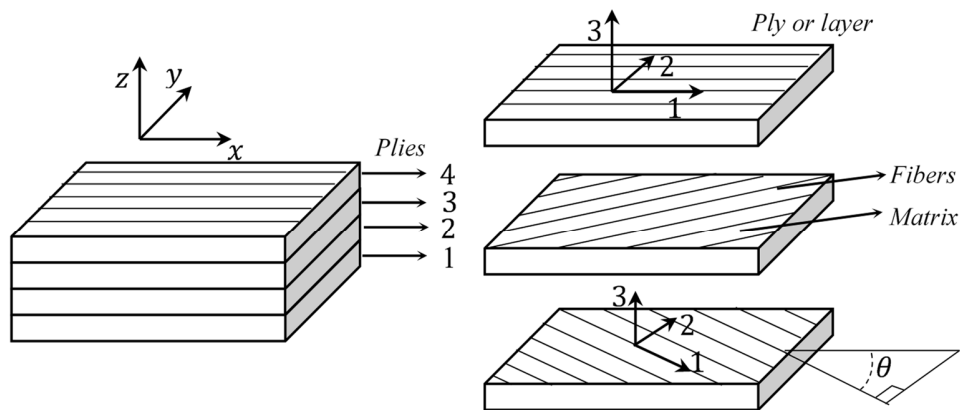


Figure 1. 1. Schematic of a composite laminate and laminated construction.

1.3 Sandwich panels

Sandwich structures are a composite material that can be defined as a subset of multilayered composite structures, optimized for the anticipated lifetime loading conditions [22]. They are formed by two face sheets, which are relatively thin and stiff, enclosed by a core which is relatively thick and light, and which has adequate stiffness in a direction normal to the face sheets of the panel [21, 23-25]. Great alternative forms of sandwich structures may be obtained by combining different face sheets and core materials. Such face sheets may be steel, aluminum, wood, fiber-reinforced plastic or even concrete. The core may be made of cork, balsa wood, rubber, solid plastic material (polyethylene), rigid foam material (polyurethane, polystyrene, phenolic foam), mineral wool slabs or from honeycombs of metal or even paper, corrugated in single or double wall, etc. [25, 26]. The function of the core in a sandwich panel is to resist the shear effects, increase the strength/weight ratio, and avoid the buckling [7, 23, 25]; and the function of the face sheets in the sandwich panels is to resist the normal stress produced by bending loads [7, 24]. The objective of a sandwich construction is to make a structure combining lightness and flexural stiffness to allow optimization of structures that are weight-critical such as parts of airplanes, space structures, sporting goods, naval structures, and blades for wind-power generation [24]. Figure 1.2 shows three sandwich structures with different core configurations. Some characteristics of sandwich structures that makes them frequently used are: Mass savings with respect to conventional structures, high specific stiffness (bending stiffness with respect to the mass), good fatigue properties, sound-damping properties, good thermal and acoustical insulation properties, excellent airtightness, economical mass production to pre-cut lengths of components of uniform high quality between others [25, 27]. This work employs typical sandwich structures made of polyurethane of high density with metal face sheets (Rigid sandwich), normally used in the airports, buildings, laboratories, electrical central, among

others, and sandwich structures with a core made of polyurethane of low density (compliant sandwich), frequently found in many industrial sectors, specially in the food industry to build frigorific chambers, also in the civil industry used to build administrative offices and furniture too fast, etc [23, 24].

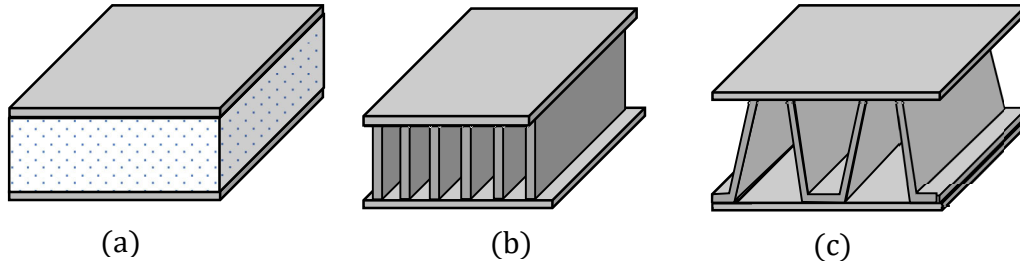


Figure 1.2. Schematic of typical sandwich cores. (a) Solid core. (b) Web core. (c) Corrugated core.

1.4 The stress and strain relationship

According to classical theory of elasticity, the generalized linear strain field for small displacements is given by [3, 28, 29],

$$\{\varepsilon\} = \begin{Bmatrix} \varepsilon_x \\ \varepsilon_y \\ \varepsilon_z \\ \gamma_{xy} \\ \gamma_{yz} \\ \gamma_{xz} \end{Bmatrix} = \begin{Bmatrix} \partial u / \partial x \\ \partial v / \partial y \\ \partial w / \partial z \\ \frac{\partial u}{\partial y} + \frac{\partial v}{\partial x} \\ \frac{\partial v}{\partial z} + \frac{\partial w}{\partial y} \\ \frac{\partial w}{\partial x} + \frac{\partial u}{\partial z} \end{Bmatrix} \quad (1.1)$$

where $\varepsilon_x, \varepsilon_y, \varepsilon_z$ are the generalized normal strain respect to the x -axis, y -axis, z -axis whereas $\gamma_{xy}, \gamma_{xz}, \gamma_{yz}$ are the generalized engineering shear strains at the planes xy, xz, yz , respectively.

The stress field in the solid body is represented in Figure 1.3 by six components. Where $\sigma_x, \sigma_y, \sigma_z$ are the normal stress in x -, y -, z -axis and $\tau_{xy}, \tau_{xz}, \tau_{yz}$ are the shear stress at the planes xy, yz and xz , respectively.

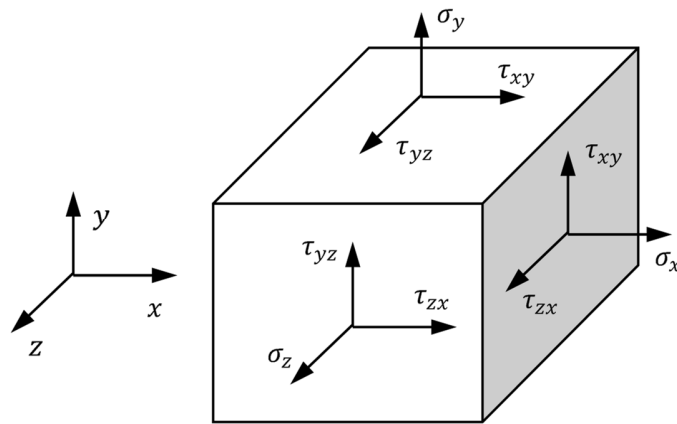


Figure 1.3. Generalized stress components in a solid body.

The Eq. (1.1) has a directly relationship with the stresses present in the body caused by the action of the external loads. The equations that establish the relations between stresses and strains are known as constitutive equations or Generalized Hooke's Law equation for small deformations [3, 30].

For homogeneous elastic body having anisotropy of a general type, i.e., without elastic symmetry, the relationship between stress and strains is established by 21 independent material constants [28]. The elastic symmetry depends on the internal structures of the body and some properties may be identical in some directions as is the case of natural wood, delta wood, plywood, composite laminates, etc [28]. When there is elastic symmetry in a body, the constants that establish the relationship between stress and strains is reduced [28]. The most important cases of elastic symmetry are: a) One plane of elastic symmetry: in this case the number of independent constants are reduced to 13; b) three planes of the elastic symmetry or also called orthogonal-anisotropic or simply orthotropic: the number of independent constants are reduced to 9; c) a plane of isotropy or commonly known as transversely isotropic: the number of independent constants are reduced to 5, and finally, d) complete symmetry or isotropic body: this is the simplest material and only have 2 independent constants. For a further explanation of this kind of elastic symmetric the reader is referred to reference [28].

The Hooke's Law can be written in compact form as

$$\{\sigma\} = [D]\{\varepsilon\} \quad (1.2a)$$

Also, this law is written as

$$\begin{Bmatrix} \varepsilon_1 \\ \varepsilon_2 \\ \varepsilon_3 \\ \gamma_{12} \\ \gamma_{23} \\ \gamma_{13} \end{Bmatrix} = [D]^{-1} \begin{Bmatrix} \sigma_1 \\ \sigma_2 \\ \sigma_3 \\ \tau_{12} \\ \tau_{23} \\ \tau_{13} \end{Bmatrix} \quad (1.2b)$$

where $[D]$ and $[D]^{-1}$ are the stiffness and compliance matrices, respectively. $[D]^{-1}$ arranges the elastic properties of the elastic body according to Eq. (1.2c) in function of the 9 engineering constants for an orthotropic body [3, 28, 29, 31].

$$[D]^{-1} = \begin{bmatrix} 1/E_1 & -\nu_{12}/E_1 & -\nu_{13}/E_1 & 0 & 0 & 0 \\ -\nu_{21}/E_2 & 1/E_2 & -\nu_{23}/E_2 & 0 & 0 & 0 \\ -\nu_{31}/E_3 & -\nu_{32}/E_3 & 1/E_3 & 0 & 0 & 0 \\ 0 & 0 & 0 & 1/G_{12} & 0 & 0 \\ 0 & 0 & 0 & 0 & 1/G_{23} & 0 \\ 0 & 0 & 0 & 0 & 0 & 1/G_{13} \end{bmatrix} \quad (1.2c)$$

$$\frac{\nu_{21}}{E_2} = \frac{\nu_{12}}{E_1}; \quad \frac{\nu_{31}}{E_3} = \frac{\nu_{13}}{E_1}; \quad \frac{\nu_{32}}{E_3} = \frac{\nu_{23}}{E_2} \quad (1.2d)$$

where E_1, E_2, E_3 are the modulus of elasticity or Young's modulus in 1, 2, and 3 directions, respectively; $\nu_{12}, \nu_{23}, \nu_{13}$ are the Poisson's ratios at the planes 1 – 2, 2 – 3, and 1 – 3, respectively; and G_{12}, G_{23}, G_{13} are the shear modulus at the planes 1 – 2, 2 – 3, and 1 – 3, respectively. The subscripts 1,2,3 correspond to the directions of the material coordinate system (see, Figure 1.1). Eq. (1.2b) may be written in a most general form referred to a global coordinate system using the transformation matrix $[T]$ given by [2, 3, 32],

$$[T] = \begin{bmatrix} \cos^2 \theta & \sin^2 \theta & 0 & 0 & 0 & \sin(2\theta) \\ \sin^2 \theta & \cos^2 \theta & 0 & 0 & 0 & -\sin(2\theta) \\ 0 & 0 & 1 & 0 & 0 & 0 \\ 0 & 0 & 0 & \cos(\theta) & -\sin(\theta) & 0 \\ 0 & 0 & 0 & \sin(\theta) & \cos(\theta) & 0 \\ -\sin(\theta)\cos(\theta) & \sin(\theta)\cos(\theta) & 0 & 0 & 0 & \cos^2 \theta - \sin^2 \theta \end{bmatrix} \quad (1.2e)$$

$$\begin{Bmatrix} \varepsilon_x \\ \varepsilon_y \\ \varepsilon_z \\ \gamma_{xy} \\ \gamma_{yz} \\ \gamma_{xz} \end{Bmatrix} = [T]^{-1}[D]^{-1}[T] \begin{Bmatrix} \sigma_x \\ \sigma_y \\ \sigma_z \\ \tau_{xy} \\ \tau_{yz} \\ \tau_{xz} \end{Bmatrix} \quad (1.2f)$$

1.5 Laminated plate theories

A plate is defined as a solid material bounded by two parallel planes whose transverse dimension (thickness) is small compared to the other two dimensions [21]. The plate analysis is a simplification of the 3-D continuum problem to a 2-D problem, in which a heterogeneous laminated plate is treated as statically equivalent single layer having a complex constitutive behavior [3]. The equivalent single layer (ESL) theories are developed by assuming the form of the displacement field or stress field as a linear combination of unknown functions and the coordinate along the thickness [3]. The most relevant ESL laminated plate theories are the CLPT, the FSDT, the second-order shear deformation theory (SSDT) and the third-order laminated plate theory (TSDT) [3, 4], all these consider that the plate is under a state of plane stress because the thickness is small compared to the in-plane dimensions [3]. As the order of the theory increases, so does the difficulty of the analysis and its computational effort, increasing the accuracy of the calculations due to the reduction of the assumptions, approaching to the theory of elasticity. In the section 1.6.6, the FSDT is widely explained since this theory is employed to develop two closed-form solutions for the PT specimen.

1.5.1 Classical laminate plate theory

The CLPT is the simplest laminated plate theory and it is based on the Kirchhoff's hypothesis. This hypothesis establishes that lines normal to the mid-plane remains perpendicular to such a plane without any change in length after deformation; i.e., a normal line to the mid-plane does not stretch after deformation; it simply translates and rotates as a consequence of the deformation [32]. As consequence of this, the transverse shear and transverse normal effects are neglected; i.e., deformation is due entirely to bending and in-plane stretching [3]. The interpretation of this assumptions leads to the conclusion that the transverse displacement is independent of the coordinate along the thickness, and the transverse normal and shear strains are zero.

In addition to the Kirchhoff's hypothesis, CLPT requires one additional assumption and some restrictions to develop its kinematic framework. The assumption required is that the layers are perfectly bonded together, i.e., there are not relative sliding between layers. The restrictions required are: the material of each layer is linearly elastic and has three planes of material symmetry (Orthotropic material); each layer has a constant thickness; the strain and displacements are small and finally the transverse shear stresses on the top and the bottom

surface of the laminate are zero [3, 32]. Therefore, CLPT is based on the following displacement field

$$u(x, y) = u_o(x, y) - z(\partial w/\partial x) \quad (1.3a)$$

$$v(x, y) = v_o(x, y) - z(\partial w/\partial y) \quad (1.3b)$$

$$w(x, y) = w_o(x, y) \quad (1.3c)$$

where $u(x, y), v(x, y), w(x, y)$ are called the generalized displacement functions. u_o, v_o, w_o denote the displacement of a point at mid-plane $z = 0$. The displacement field given by Eqs. (1.3a – c) implies that straight lines normal to the xy -plane before deformation remain straight and normal to the mid-surface after deformation [3] (Figure 1.4), thus, the Kirchhoff's hypothesis is satisfied.

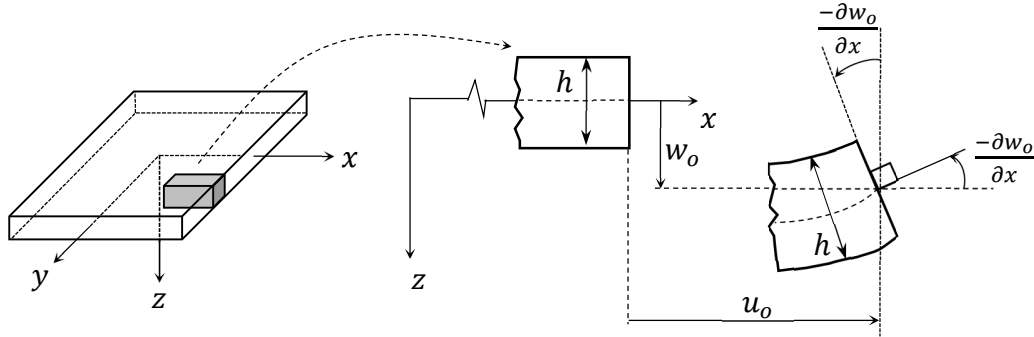


Figure 1.4. Undeformed and deformed geometries of an edge of a plate under the assumptions of the CLPT [3].

1.5.2 First-order shear deformation laminated plate theory

The next theory in the hierarchy of ESL plate theories is the FSDT, which is based on the following displacement field [3],

$$u(x, y) = u_o(x, y) + z\phi_x(x, y) \quad (1.4a)$$

$$v(x, y) = v_o(x, y) + z\phi_y(x, y) \quad (1.4b)$$

$$w(x, y) = w_o(x, y) \quad (1.4c)$$

where ϕ_x and ϕ_y denote the rotations about the y -axis and x -axis, respectively. The FSDT extends the kinematic of the CLPT by including a gross transverse shear deformation in its kinematic assumptions; i.e., the transverse shear strains are assumed to be constant along the plate thickness. Inclusion of this rudimentary form of shear deformation allows to determine the transverse shear stresses, representing an advantage with respect to CLPT, however the

FSDT requires shear correction factors, which are difficult to determine for arbitrarily laminated composite plates [3, 33, 34].

If the inextensibility and/or straightness of transverse normal are removed, i.e., if the deformation and the warping along the thickness are considered, the second and higher-order ESL laminated plate theories can be formulated (The terms “inextensibility” makes reference to the Kirchhoff’s hypothesis, which assumes that the transversal lines does not change length; i.e., the thickness remains constant [32]).

In theories of lamination, the FSDT seems to provide the best compromise of solution, accuracy and simplicity [3] for thin and moderately thick laminate plates to determine the stress and displacement fields in composite plates. The only difference between FSDT and CLPT is the fact that FSDT assumes that transverse shear strains are constant along the transversal normal (i.e., along the thickness) [3] and CLPT does not consider it. In this thesis work, only the FSDT will be explained in detail and used to develop the analytical models.

1.5.3 Second-order laminated plate theory

Second and higher-order ESL laminated plate theories use higher-order polynomials in the expansion of the displacement component through the thickness of the laminate [3]. The second-order theory with transverse inextensibility (deformation along the thickness is neglected) is based on the displacement field [3],

$$u(x, y) = u_o(x, y) + z\phi_x(x, y) + z^2\varphi_x(x, y) \quad (1.5a)$$

$$v(x, y) = v_o(x, y) + z\phi_y(x, y) + z^2\varphi_y(x, y) \quad (1.5b)$$

$$w(x, y) = w_o(x, y) \quad (1.5c)$$

where φ_x and φ_y are functions that are often difficult to interpret in physical terms; they give rise to the higher-order stress and increase the accuracy of calculations. This theory considers a quadratic variation of the transverse shear strain and does not require the shear correction factor employed in FSDT.

1.5.4 Third-order shear deformation laminated plate theory

The TSDT formulated by Reddy [3, 4] with transverse inextensibility is based on the displacement field

$$u(x, y) = u_o(x, y) + z\phi_x(x, y) + z^2\varphi_x(x, y) + z^3\lambda_x(x, y) \quad (1.6a)$$

$$v(x, y) = v_o(x, y) + z\phi_y(x, y) + z^2\varphi_y(x, y) + z^3\lambda_y(x, y) \quad (1.6b)$$

$$w(x, y) = w_o(x, y) \quad (1.6c)$$

where $\Phi_x, \Phi_y, \varphi_x, \varphi_y, \lambda_x, \lambda_y$ are functions to be determined. λ_x, λ_y are functions introduced to represent the parabolic behavior of the shear stresses and strains along the thickness of the plate.

By imposing traction-free boundary conditions on the top and bottom faces of the laminate, i.e., $\tau_{xz}(x, y, \pm h/2) = 0$ and $\tau_{yz}(x, y, \pm h/2) = 0$, Reddy [3, 4] found that φ_x and φ_y are zero and λ_x, λ_y are defined as follow

$$\lambda_x = -\frac{4}{3h^2} \left(\phi_x + \frac{\partial w_o}{\partial x} \right); \quad \lambda_y = -\frac{4}{3h^2} \left(\phi_y + \frac{\partial w_o}{\partial y} \right) \quad (1.6d-e)$$

Substituting Eqs. (1.6d – e) into (1.6a – c) the displacement field of the Reddy's theory is finally rewritten as,

$$u(x, y) = u_o(x, y) - z\phi_x(x, y) + z^3(-4/(3h^2))(\phi_x + \partial w_o/\partial x) \quad (1.6f)$$

$$v(x, y) = v_o(x, y) - z\phi_y(x, y) + z^3(-4/(3h^2))(\phi_y + \partial w_o/\partial y) \quad (1.6g)$$

$$w(x, y) = w_o(x, y) \quad (1.6h)$$

where h is the plate thickness. In Eqs. (1.6f – g) is observed that the displacement field accommodates quadratic variation of transverse shear strains (and hence stresses) and vanishing of transverse shear stresses on the top and bottom of a general laminate composed of monoclinic layers (imposed condition). Thus, there is no need to use shear correction factors in the TSDT. The assumptions of the Kirchhoff's hypothesis are applied in TSDT with the particularity that the transversal line is not normal to the mid-plane; i.e., this line is not straight and has an additional rotation occasioned by the transversal shear forces [3] (see, Figure 1.5). The TSDT provides an increase in accuracy relative to the FSDT, at expense of an increase in computational effort [3]. The accuracy of this theory, and the other ESL theories are affected when the laminate becomes thicker, and have the inconvenient that are often incapable of accurately describing the state of stress and strain at the ply level near geometric and material discontinuities or near regions of intense loading [3]. The CLPT and FSDT could be obtained from TSDT with the difference that to obtain the FSDT from TSDT, the shear correction factor must be introduced after the simplification of the TSDT.

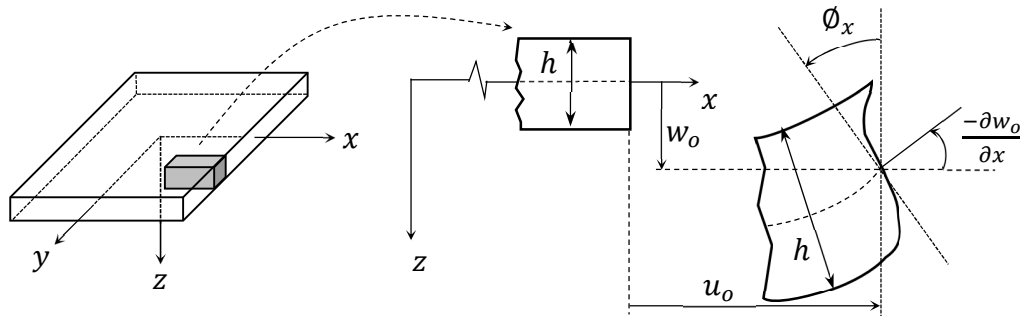


Figure 1.5. Undeformed and deformed geometries of an edge of a plate under the assumptions of the TSDT [3].

1.6 First-order shear deformation laminated plate theory

1.6.1 Displacement field

To describe the strains and displacement fields in FSDT (Eq. (1.4)), the assumptions of the Kirchhoff's hypothesis are employed with the particularity that the transversal line normal to the mid-plane in CLPT is not normal to the mid-plane in FSDT; i.e., this line has an additional rotation occasioned by the transversal shear forces [3] (see, Figure 1.6). Since the FSDT assumes that transverse shear strains are constants along the plate thickness (Figure 1.6) a shear correction factor K_{ij} is introduced in the constitutive equations [3] (Eq. (1.11c)). This factor depends not only on the geometric parameter, but also on the loading and boundary conditions of the plate [4]. More information about this factor have been annexed in appendices A and B.

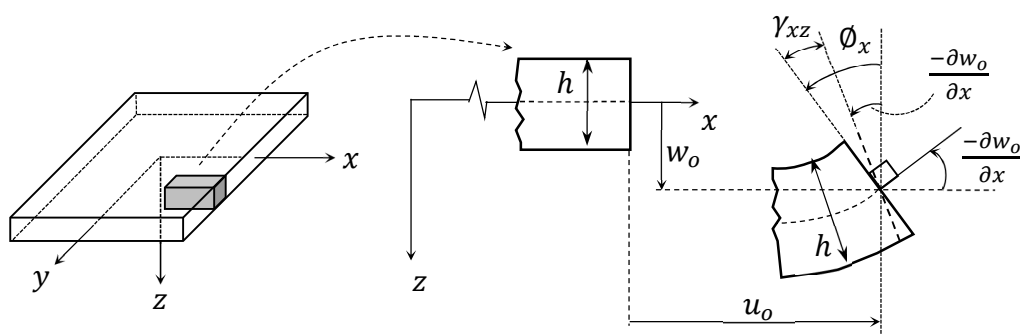


Figure 1.6. Undeformed and deformed geometries of an edge of a plate under the assumptions of FSDT [3].

1.6.2 Strain field

Considering the strain field given by Eq. (1.1); the strains associated with the displacement field (Eqs. (1.4)) are given by,

$$\varepsilon_x = \frac{\partial u_o}{\partial x} + z \frac{\partial \phi_x}{\partial x} = \varepsilon_x^o + z\kappa_x \quad (1.7a)$$

$$\varepsilon_y = \frac{\partial v_o}{\partial y} + z \frac{\partial \phi_y}{\partial y} = \varepsilon_y^o + z\kappa_y \quad (1.7b)$$

$$\varepsilon_z = 0 \quad (1.7c)$$

$$\gamma_{xy} = \left(\frac{\partial u_o}{\partial y} + \frac{\partial v_o}{\partial x} \right) + z \left(\frac{\partial \phi_x}{\partial y} + \frac{\partial \phi_y}{\partial x} \right) = \gamma_{xy}^o + z\kappa_{xy} \quad (1.7d)$$

$$\gamma_{xz} = \frac{\partial w_o}{\partial x} + \phi_x \quad (1.7e)$$

$$\gamma_{yz} = \frac{\partial w_o}{\partial y} + \phi_y \quad (1.7f)$$

where, ε_x , ε_y , ε_z are the longitudinal strains relative to the x -, y - and z -axes; γ_{xy} is the in-plane shear strain whereas γ_{xz} , γ_{yz} are the transverse shear strains associated with the xy , xz , and yz planes, respectively. The superscript "o" is used to designate mid-plane values. κ_x and κ_y are known as curvatures around x -axis and y -axis, respectively, and κ_{xy} is known as twist curvature of the middle surface, respectively.

Note that the longitudinal strains ε_x , ε_y and the in-plane shear strain γ_{xy} are linear through the laminate thickness, while the transverse shear strains are constant through the thickness of the laminates in the FSDT (see, Figure 1.7).

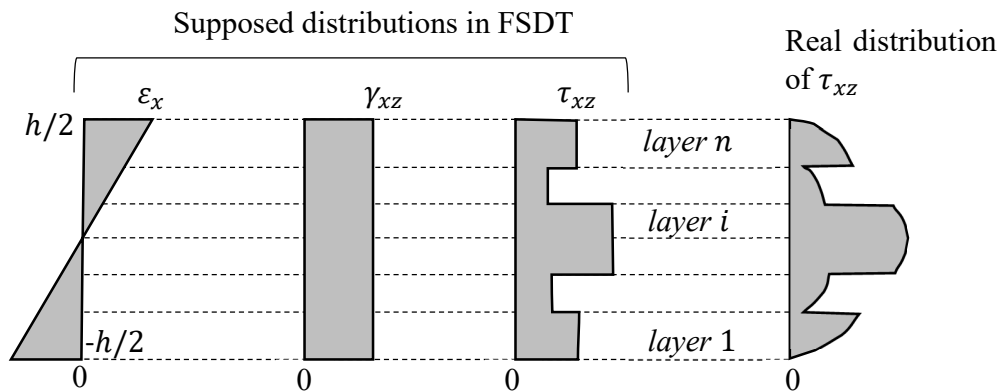


Figure 1. 7. Schematic general representation in a composite laminate of longitudinal strain ε_x , transversal shear strain γ_{xz} and shear stress τ_{xz} in FSDT and real shear stress τ_{xz} .

1.6.3 Stress field

The stresses in the k -th layer of a laminated composite can be expressed in terms of the mid-surface strains and curvatures as [2, 3, 21], i.e.,

$$\begin{Bmatrix} \sigma_x \\ \sigma_y \\ \tau_{xy} \end{Bmatrix}_k = \begin{bmatrix} \bar{Q}_{11} & \bar{Q}_{12} & \bar{Q}_{16} \\ \bar{Q}_{12} & \bar{Q}_{22} & \bar{Q}_{26} \\ \bar{Q}_{16} & \bar{Q}_{26} & \bar{Q}_{66} \end{bmatrix}_k \begin{Bmatrix} \varepsilon_{xx} \\ \varepsilon_{yy} \\ \gamma_{xy} \end{Bmatrix} = \begin{bmatrix} \bar{Q}_{11} & \bar{Q}_{12} & \bar{Q}_{16} \\ \bar{Q}_{12} & \bar{Q}_{22} & \bar{Q}_{26} \\ \bar{Q}_{16} & \bar{Q}_{26} & \bar{Q}_{66} \end{bmatrix}_k \begin{Bmatrix} \varepsilon_{xx}^o \\ \varepsilon_{yy}^o \\ \gamma_{xy}^o \end{Bmatrix} + z \begin{Bmatrix} \kappa_x \\ \kappa_y \\ \kappa_{xy} \end{Bmatrix} \quad (1.8a)$$

$$\begin{Bmatrix} \tau_{yz} \\ \tau_{xz} \end{Bmatrix}_k = \begin{bmatrix} \bar{Q}_{44} & \bar{Q}_{45} \\ \bar{Q}_{45} & \bar{Q}_{55} \end{bmatrix}_k \begin{Bmatrix} \gamma_{yz} \\ \gamma_{xz} \end{Bmatrix} \quad (1.8b)$$

here $(\bar{Q}_{ij})_k$ are the transformed plane stress-reduced stiffness ($i, j = 1, 2, 6$ to Eq. (1.8a) and $i, j = 4, 5$ to Eq. (1.8b)) which are given by

$$\begin{aligned} \bar{Q}_{11} &= Q_{11} \cos^4 \theta + 2(Q_{12} + 2Q_{66}) \sin^2 \theta \cos^2 \theta + Q_{22} \sin^4 \theta \\ \bar{Q}_{12} &= (Q_{11} + Q_{22} - 4Q_{66}) \sin^2 \theta \cos^2 \theta + Q_{12} (\sin^4 \theta + \cos^4 \theta) \\ \bar{Q}_{22} &= Q_{11} \sin^4 \theta + 2(Q_{12} + 2Q_{66}) \sin^2 \theta \cos^2 \theta + Q_{22} \cos^4 \theta \\ \bar{Q}_{16} &= (Q_{11} - Q_{12} - 2Q_{66}) \sin \theta \cos^3 \theta + (Q_{12} - Q_{22} + 2Q_{66}) (\sin^3 \theta + \cos \theta) \\ \bar{Q}_{26} &= (Q_{11} - Q_{12} - 2Q_{66}) \sin^3 \theta \cos \theta + (Q_{12} - Q_{22} + 2Q_{66}) (\sin \theta + \cos^3 \theta) \\ \bar{Q}_{66} &= (Q_{11} + Q_{22} - 2Q_{12} - 2Q_{66}) \sin^2 \theta \cos^2 \theta + Q_{66} (\sin^4 \theta + \cos^4 \theta) \\ \bar{Q}_{44} &= Q_{44} \cos^2 \theta + Q_{55} \sin^2 \theta \\ \bar{Q}_{45} &= (Q_{55} - Q_{44}) \cos \theta \sin \theta \\ \bar{Q}_{55} &= Q_{55} \cos^2 \theta + Q_{44} \sin^2 \theta \end{aligned} \quad (1.9)$$

where θ is the orientation angle of the fibers for the k -th layer (Figure 1.1). And Q_{ij} are the reduced stiffnesses ($i, j = 1, 2, 4, 5, 6$) which are related to the engineering constants as follows

$$\begin{aligned} Q_{11}^{(k)} &= \frac{E_1^{(k)}}{1 - \nu_{12}^{(k)} \nu_{21}^{(k)}}; & Q_{12}^{(k)} &= \frac{\nu_{12}^{(k)} E_2^{(k)}}{1 - \nu_{12}^{(k)} \nu_{21}^{(k)}}; & Q_{22}^{(k)} &= \frac{E_2^{(k)}}{1 - \nu_{12}^{(k)} \nu_{21}^{(k)}} \\ Q_{66}^{(k)} &= G_{12}^{(k)}; & Q_{44}^{(k)} &= G_{23}^{(k)}; & Q_{55}^{(k)} &= G_{13}^{(k)} \\ \frac{\nu_{12}^{(k)}}{E_1^{(k)}} &= \frac{\nu_{21}^{(k)}}{E_2^{(k)}} \end{aligned} \quad (1.10)$$

1.6.4 Laminate constitutive equations

The resultant laminate forces and moments acting on a laminate (Figure 1.8) are obtained by integration of the stresses through each ply thickness as is indicated as [2, 3, 21, 28],

$$\begin{bmatrix} N_x \\ N_y \\ N_{xy} \end{bmatrix} = \int_{-h/2}^{h/2} \begin{bmatrix} \sigma_x \\ \sigma_y \\ \tau_{xy} \end{bmatrix} dz = \sum_{k=1}^N \int_{z_k}^{z_{k+1}} \begin{bmatrix} \sigma_x \\ \sigma_y \\ \tau_{xy} \end{bmatrix}_k dz \quad (1.11a)$$

$$\begin{bmatrix} M_x \\ M_y \\ M_{xy} \end{bmatrix} = \int_{-h/2}^{h/2} \begin{bmatrix} \sigma_x \\ \sigma_y \\ \tau_{xy} \end{bmatrix} z dz = \sum_{k=1}^N \int_{z_k}^{z_{k+1}} \begin{bmatrix} \sigma_x \\ \sigma_y \\ \tau_{xy} \end{bmatrix}_k z dz \quad (1.11b)$$

$$\begin{bmatrix} Q_y \\ Q_x \end{bmatrix} = K_{ij} \int_{-h/2}^{h/2} \begin{bmatrix} \tau_{yz} \\ \tau_{xz} \end{bmatrix} dz = K_{ij} \sum_{k=1}^N \int_{z_k}^{z_{k+1}} \begin{bmatrix} \tau_{yz} \\ \tau_{xz} \end{bmatrix}_k dz \quad (1.11c)$$

where N_x and N_y are normal forces along x and y -axes, N_{xy} is an in-plane shear force relative to xy plane, M_x and M_y are bending moments relative to x - and y -axis, M_{xy} is the twisting moment relative at the xy plane, and Q_x and Q_y are the transverse shear forces tangential to the yz and xz planes, respectively. All these loads are oriented as shown in Figure 1.8 and are measured per unit length of the corresponding plate side-length.

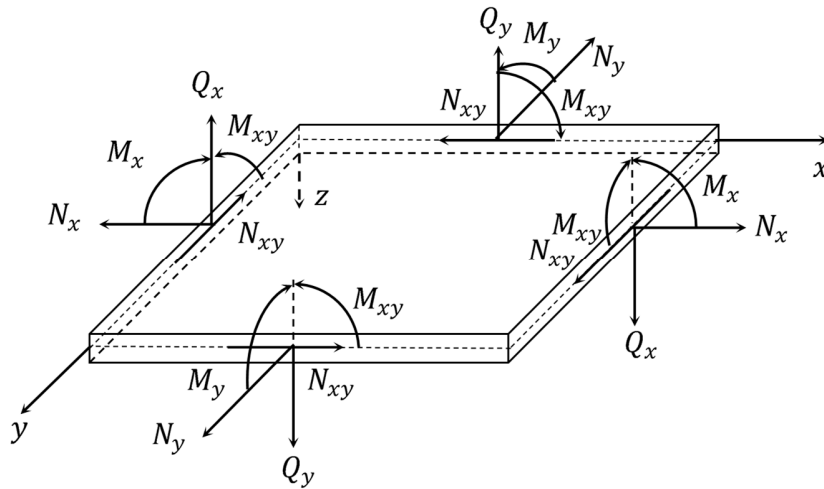


Figure 1.8. Force and moment resultants on a rectangular plate.

Replacing Eqs. (1.7a – f) into (1.8a – b) and these last ones into (1.11a – c), the constitutive equations become,

$$\begin{Bmatrix} N_x \\ N_y \\ N_{xy} \end{Bmatrix} = \begin{bmatrix} A_{11} & A_{12} & A_{16} \\ A_{12} & A_{22} & A_{26} \\ A_{16} & A_{26} & A_{66} \end{bmatrix} \begin{Bmatrix} \frac{\partial u_o}{\partial x} + \frac{1}{2} \left(\frac{\partial w_o}{\partial x} \right)^2 \\ \frac{\partial v_o}{\partial y} + \frac{1}{2} \left(\frac{\partial w_o}{\partial y} \right)^2 \\ \frac{\partial u_o}{\partial y} + \frac{\partial v_o}{\partial x} + \frac{\partial w_o}{\partial x} \frac{\partial w_o}{\partial y} \end{Bmatrix} + \begin{bmatrix} B_{11} & B_{12} & B_{16} \\ B_{12} & B_{22} & B_{26} \\ B_{16} & B_{26} & B_{66} \end{bmatrix} \begin{Bmatrix} \frac{\partial \phi_x}{\partial x} \\ \frac{\partial \phi_y}{\partial y} \\ \frac{\partial \phi_x}{\partial y} + \frac{\partial \phi_y}{\partial x} \end{Bmatrix} \quad (1.12a)$$

$$\begin{Bmatrix} M_x \\ M_y \\ M_{xy} \end{Bmatrix} = \begin{bmatrix} B_{11} & B_{12} & B_{16} \\ B_{12} & B_{22} & B_{26} \\ B_{16} & B_{26} & B_{66} \end{bmatrix} \begin{Bmatrix} \frac{\partial u_o}{\partial x} + \frac{1}{2} \left(\frac{\partial w_o}{\partial x} \right)^2 \\ \frac{\partial v_o}{\partial y} + \frac{1}{2} \left(\frac{\partial w_o}{\partial y} \right)^2 \\ \frac{\partial u_o}{\partial y} + \frac{\partial v_o}{\partial x} + \frac{\partial w_o}{\partial x} \frac{\partial w_o}{\partial y} \end{Bmatrix} + \begin{bmatrix} D_{11} & D_{12} & D_{16} \\ D_{12} & D_{22} & D_{26} \\ D_{16} & D_{26} & D_{66} \end{bmatrix} \begin{Bmatrix} \frac{\partial \phi_x}{\partial x} \\ \frac{\partial \phi_y}{\partial y} \\ \frac{\partial \phi_x}{\partial y} + \frac{\partial \phi_y}{\partial x} \end{Bmatrix} \quad (1.12b)$$

$$\begin{Bmatrix} Q_y \\ Q_x \end{Bmatrix} = \begin{bmatrix} K_{44}A_{44} & K_{45}A_{45} \\ K_{45}A_{45} & K_{55}A_{55} \end{bmatrix} \begin{Bmatrix} \phi_y + \frac{\partial w_o}{\partial y} \\ \phi_x + \frac{\partial w_o}{\partial x} \end{Bmatrix} \quad (1.12c)$$

where A_{ij} , B_{ij} and D_{ij} are called the extensional stiffnesses, the bending-extensional coupling stiffnesses and the bending stiffnesses, respectively. The subscripts i, j take the values 1, 2 and 6 in Eqs. (1.12a – b), and 4 and 5 in Eq. (1.12c). A_{ij} , B_{ij} and D_{ij} are defined in terms of \bar{Q}_{ij}^k as

$$A_{ij} = \sum_{k=1}^N \bar{Q}_{ij}^k (z_{k+1} - z_k) \quad (1.13a)$$

$$B_{ij} = \frac{1}{2} \sum_{k=1}^N \bar{Q}_{ij}^k (z_{k+1}^2 - z_k^2) \quad (1.13b)$$

$$D_{ij} = \frac{1}{3} \sum_{k=1}^N \bar{Q}_{ij}^k (z_{k+1}^3 - z_k^3) \quad (1.13c)$$

In Eq. (1.13c), K_{ij} are the shear correction factors, which should be selected according to the material system and boundary conditions of the problem as is shown in the Appendix A, or accord to the selection explained by Whitney and Pagano [35], Kaneko [36] and others; or could be determined as indicated in the Appendix B, by using a specific procedure, e.g., Chow [34], Whitney [37, 38], Bert [39] or Birman [33].

1.6.5 Equilibrium equations

The equilibrium equations by FSDT are obtained by making a balance of force and moment resultants [3], which results,

$$\frac{\partial N_x}{\partial x} + \frac{\partial N_{xy}}{\partial y} = 0 \quad (1.14a)$$

$$\frac{\partial N_{xy}}{\partial x} + \frac{\partial N_y}{\partial y} = 0 \quad (1.14b)$$

$$\frac{\partial Q_x}{\partial x} + \frac{\partial Q_y}{\partial y} + q = 0 \quad (1.14c)$$

$$\frac{\partial M_x}{\partial x} + \frac{\partial M_{xy}}{\partial y} - Q_x = 0 \quad (1.14d)$$

$$\frac{\partial M_{xy}}{\partial x} + \frac{\partial M_{yy}}{\partial y} - Q_y = 0 \quad (1.14e)$$

where q is the total distributed transverse load over the plate.

1.6.6 Governing equations

The governing equations by FSDT result from the combination of equilibrium and constitutive equations (they are also called equation of motion in terms of displacements [3]), which are given by,

$$\begin{aligned} & A_{11} \left(\frac{\partial^2 u_o}{\partial x^2} + \frac{\partial w_o}{\partial x} \frac{\partial^2 w_o}{\partial x^2} \right) + A_{12} \left(\frac{\partial^2 v_o}{\partial y \partial x} + \frac{\partial w_o}{\partial y} \frac{\partial^2 w_o}{\partial y \partial x} \right) \\ & + A_{16} \left(\frac{\partial^2 u_o}{\partial y \partial x} + \frac{\partial^2 v_o}{\partial x^2} + \frac{\partial^2 w_o}{\partial x^2} \frac{\partial w_o}{\partial y} + \frac{\partial w_o}{\partial x} \frac{\partial^2 w_o}{\partial y \partial x} \right) + B_{11} \frac{\partial^2 \phi_x}{\partial x^2} + B_{12} \frac{\partial^2 \phi_y}{\partial y \partial x} \\ & + B_{16} \left(\frac{\partial^2 \phi_x}{\partial x \partial y} + \frac{\partial^2 \phi_y}{\partial x^2} \right) + A_{16} \left(\frac{\partial^2 u_o}{\partial x \partial y} + \frac{\partial w_o}{\partial x} \frac{\partial^2 w_o}{\partial x \partial y} \right) \\ & + A_{26} \left(\frac{\partial^2 v_o}{\partial y^2} + \frac{\partial w_o}{\partial y} \frac{\partial^2 w_o}{\partial y^2} \right) + A_{66} \left(\frac{\partial^2 u_o}{\partial y^2} + \frac{\partial^2 v_o}{\partial x \partial y} + \frac{\partial^2 w_o}{\partial x \partial y} \frac{\partial w_o}{\partial y} + \frac{\partial w_o}{\partial x} \frac{\partial^2 w_o}{\partial y^2} \right) \\ & + B_{16} \frac{\partial^2 \phi_x}{\partial x \partial y} + B_{26} \frac{\partial^2 \phi_y}{\partial y^2} + B_{66} \left(\frac{\partial^2 \phi_x}{\partial y^2} + \frac{\partial^2 \phi_y}{\partial y \partial x} \right) = 0 \end{aligned} \quad (1.15a)$$

1.6.7 Theorem of minimum potential energy

The strain energy V in composite laminated plates is obtained from the integration of the strain energy density function around the elastic body volume, plus the work of external forces [40, 41]. The strain energy in terms of displacement is given by,

$$\begin{aligned}
 V = \iint_{\Omega} \left\{ \frac{A_{11}}{2} \left(\frac{\partial u_0}{\partial x} \right)^2 + \frac{B_{11}}{2} \frac{\partial u_0}{\partial x} \frac{\partial \phi_x}{\partial x} + \frac{D_{11}}{2} \left(\frac{\partial \phi_x}{\partial x} \right)^2 + A_{12} \frac{\partial u_0}{\partial x} \frac{\partial v_0}{\partial y} + B_{12} \left[\frac{\partial u_0}{\partial x} \frac{\partial \phi_y}{\partial y} + \frac{\partial v_0}{\partial y} \frac{\partial \phi_x}{\partial x} \right] + \right. \\
 D_{12} \frac{\partial \phi_y}{\partial y} \frac{\partial \phi_x}{\partial x} + A_{16} \left[\frac{\partial u_0}{\partial x} \frac{\partial v_0}{\partial y} + \frac{\partial u_0}{\partial x} \frac{\partial v_0}{\partial x} \right] + D_{16} \left[\frac{\partial \phi_x}{\partial x} \frac{\partial \phi_y}{\partial y} + \frac{\partial \phi_x}{\partial x} \frac{\partial \phi_y}{\partial x} \right] + B_{16} \left[\frac{\partial u_0}{\partial x} \frac{\partial \phi_x}{\partial y} + \frac{\partial u_0}{\partial x} \frac{\partial \phi_y}{\partial x} \right] + \\
 \frac{\partial u_0}{\partial y} \frac{\partial \phi_x}{\partial x} + \frac{\partial v_0}{\partial y} \frac{\partial \phi_x}{\partial x} \left. \right\} + \frac{A_{22}}{2} \left(\frac{\partial v_0}{\partial y} \right)^2 + B_{22} \frac{\partial v_0}{\partial y} \frac{\partial \phi_y}{\partial y} + \frac{D_{22}}{2} \left(\frac{\partial \phi_y}{\partial y} \right)^2 + A_{26} \left[\frac{\partial v_0}{\partial y} \frac{\partial u_0}{\partial y} + \frac{\partial v_0}{\partial y} \frac{\partial v_0}{\partial x} \right] + \\
 B_{26} \left[\frac{\partial v_0}{\partial x} \frac{\partial \phi_x}{\partial y} + \frac{\partial v_0}{\partial y} \frac{\partial \phi_0}{\partial x} + \frac{\partial u_0}{\partial y} \frac{\partial \phi_y}{\partial y} + \frac{\partial v_0}{\partial x} \frac{\partial \phi_y}{\partial y} \right] + D_{26} \left[\frac{\partial \phi_x}{\partial y} \frac{\partial \phi_y}{\partial y} + \frac{\partial \phi_y}{\partial x} \frac{\partial \phi_y}{\partial y} \right] + K_{12} A_{45} \left(\phi_x \phi_y + \phi_x \frac{\partial w}{\partial y} + \right. \\
 \left. \phi_y \frac{\partial w}{\partial x} + \frac{\partial w}{\partial x} \frac{\partial w}{\partial y} \right) + K_{22} A_{55} \left[\frac{\phi_x^2}{2} + \phi_x \frac{\partial w}{\partial x} + \frac{1}{2} \left(\frac{\partial w}{\partial x} \right)^2 \right] + K_{11} A_{44} \left[\frac{\phi_y^2}{2} + \phi_y \frac{\partial w}{\partial y} + \frac{1}{2} \left(\frac{\partial w}{\partial y} \right)^2 \right] + \\
 A_{66} \left[\frac{1}{2} \left(\frac{\partial u_0}{\partial y} \right)^2 + \frac{\partial u_0}{\partial y} \frac{\partial v_0}{\partial x} + \frac{1}{2} \left(\frac{\partial v_0}{\partial x} \right)^2 \right] + B_{66} \left[\frac{\partial u_0}{\partial y} \frac{\partial \phi_x}{\partial y} + \frac{\partial u_0}{\partial y} \frac{\partial \phi_y}{\partial x} + \frac{\partial v_0}{\partial x} \frac{\partial \phi_x}{\partial y} + \frac{\partial v_0}{\partial x} \frac{\partial \phi_y}{\partial x} \right] + \\
 D_{66} \left[\frac{1}{2} \left(\frac{\partial \phi_x}{\partial y} \right)^2 + \frac{\partial \phi_x}{\partial y} \frac{\partial \phi_y}{\partial x} + \frac{1}{2} \left(\frac{\partial \phi_y}{\partial x} \right)^2 \right] - q(x, y) w(x, y) \} dy dx
 \end{aligned} \tag{1.16}$$

Ω refers to the $x - y$ mid-plane area of the plate whose dimensions are $-L_x/2 \leq x \leq L_x/2$ and $-L_y/2 \leq y \leq L_y/2$ (see, Figure 1.9). The Theorem of Minimum Potential Energy can be stated as: “of all of the displacements satisfying compatibility and the prescribed boundary conditions, those which satisfy the equilibrium equations make the potential energy minimum” [40]. This is mathematically represented as,

$$\frac{\partial V}{\partial R_i} = 0 \tag{1.17}$$

where R_i is the variable which the potential energy is minimized.

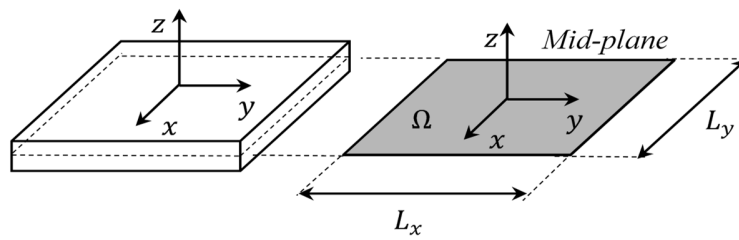


Figure 1. 9. Representation of the mid-plane area and global coordinate system.

1.7 The plate twist specimen

There are two loading configurations for the PT: the first one consists in a thin or moderate thick plate supported in three corners with a point-load P applied in one corner (Figure

1.10a) while the second configuration consists on a thin or moderate thick plate supported in two diagonal corners and subjected to two loads each one of magnitude $P/2$ in the opposite other two corners [9, 24] (Figure 1.10b). Both specimens have been employed to analyze isotropic materials [11, 15], composite materials [6, 9, 10, 15] and sandwich panels [6, 17, 42] in order to determine not only the shear properties but also those of their constituents.

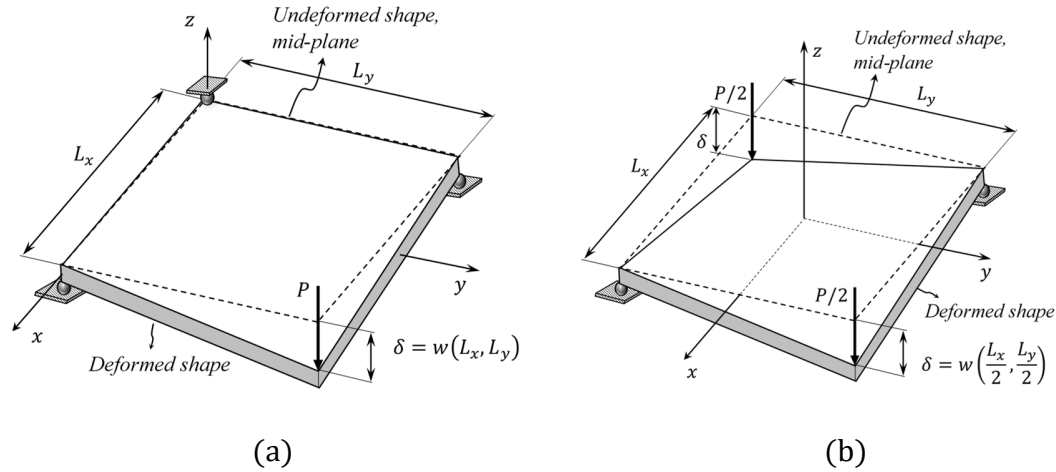


Figure 1. 10. Loading configurations of the plate twist specimen. (a) First. (b) Second.

1.7.1 Some analytical solutions previously reported for thin plates

Many authors have reported the same polynomial expression as solution for the PTs employing the theory of elasticity [11, 19, 28, 43, 44], CLPT [17] and the theorem of minimum potential energy [6]; other two expressions were reported using a semi-empirical method [42] and a double Fourier series with FSDT [45], and a geometrically nonlinear extended high-order sandwich plate theory was developed to be implemented using FEM [46].

Hearmon and Adams [11] carried out an extensive study about the bending and twisting behavior of anisotropic plates based on the previous study reported by Thielemann [43]. According to Hearmon and Adams, the deflection of w_o of an isotropic thin plate is given by,

$$\begin{aligned}
 h^3 w_o = & 6M_x(\bar{S}_{11}x^2 + \bar{S}_{12}y^2 + \bar{S}_{16}xy) \\
 & + 6M_y(\bar{S}_{12}x^2 + \bar{S}_{22}y^2 + \bar{S}_{26}xy) \\
 & + 6M_{xy}(\bar{S}_{16}x^2 + \bar{S}_{26}y^2 + \bar{S}_{66}xy)
 \end{aligned} \tag{1.18}$$

where \bar{S}_{ij} represents the compliance coefficients, and x and y are aligned with the diagonals of the plate. By neglecting bending effects ($M_x, M_y = 0$ [11, 12]) and considering a constant twisting moment $M_{xy} = P/4$ [12, 44], Eq. (1.18) becomes

$$w_o = \frac{3P}{2h^3} (\bar{S}_{16}x^2 + \bar{S}_{26}y^2 + \bar{S}_{66}xy) \quad (1.19a)$$

by considering an isotropic material ($S_{16} = S_{26} = 0$ and $S_{66} = 1/G$), Eq. (1.19a) becomes

$$w_o = \frac{3P}{2h^3G} xy \quad (1.19b)$$

Eq. (1.19b) coincides with equation employed by the international standard ASTM D3044-95 [9] to determine the shear modulus of wood-based structural panels.

Vinson [6] developed polynomial expressions for a specially orthotropic PTs using the theorem of minimum potential energy (Eq. (1.17))

$$w_o = C_1 + C_2x + C_3y + \dots + C_{12}x^3y + C_{13}x^2y^2 + C_{14}xy^3 + C_{15}y^4 \quad (1.20a)$$

$$u_o = A_1 + A_2x + A_3y + A_4x^2 + A_5xy + A_6y^2 \quad (1.20b)$$

$$v_o = B_1 + B_2x + B_3y + B_4x^2 + B_5xy + B_6y^2 \quad (1.20c)$$

Vinson [6] also considered the following conditions to address the problem; i.e., he considered null displacements and null slopes at the center of the plate, maximum and equal displacements at the corners, and a free-edge border condition [4, 40, 47].

$$w_o(0,0) = u_o(0,0) = v(0,0) = \frac{\partial w}{\partial x} = \frac{\partial w}{\partial y} = 0 \quad (1.21a-e)$$

$$w_o\left(\frac{L_x}{2}, \frac{L_y}{2}\right) = w_o\left(-\frac{L_x}{2}, -\frac{L_y}{2}\right) = w_o\left(\frac{L_x}{2}, -\frac{L_y}{2}\right) = w_o\left(-\frac{L_x}{2}, \frac{L_y}{2}\right) \quad (1.21f-i)$$

$$N_x, N_{xy}, M_x, M_{xy} = 0 \quad \text{at } x = \pm \frac{L_x}{2} \quad (1.21j-m)$$

$$N_y, N_{xy}, M_y, M_{xy} = 0 \quad \text{at } y = \pm \frac{L_y}{2} \quad (1.21n-q)$$

By substituting Eqs. (1.21) into the proposed polynomials, the deflection w_o becomes,

$$w_o = \frac{P}{4D_{66}} xy \quad (1.22)$$

If an isotropic materials is analyzed ($D_{66} = Gh^3/12$) the deflection given by Eq. (1.22) results in, $w_o = 3Pxy/(Gh^3)$ which coincides with Nadai's solution [19]. An identical solution to Eq. (1.22) was obtained by Avilés et al. [17] with the exception that they employed a 45° rotated coordinate system and CLPT. In a subsequent paper, Avilés et al. [42] developed a semi-empirical equation for the deflection of sandwich structures. Such equation employed a calibration factor c_1 to account the deflection due to transverse shear deformation in compliant cores. In such a model, the maximum deflection attains the following form,

$$\delta = w_o \left(\frac{L_x}{2}, \frac{L_y}{2} \right) = \frac{PL_x L_y}{16D_{66}} \left(1 + \frac{16c_1 D_{66}}{L_x L_y h_c \sqrt{(G_{13})_c (G_{23})_c}} \right) \quad (1.23)$$

where C_1 is calculated from a parametric analysis of the panel dimensions and thicknesses by FEM, and the subscript c corresponds to the sandwich core.

Hernández et al. [45] developed a solution for the PT by using Fourier series; representing the antisymmetric point load per unit area as,

$$q(x, y) = \sum_{m_o=1}^{M_o} \sum_{n_o=1}^{N_o} q_{m_o n_o} \sin \left(\frac{m_o \pi x}{L_x} \right) \sin \left(\frac{n_o \pi y}{L_y} \right) \quad (1.24)$$

where m_o and n_o are positive integers and the term $q_{m_o n_o}$ are determined using the classical Fourier theory [48]. Applying the constitutive (Eq. (1.12)), equilibrium (Eq. (1.14)) and governing equations (Eq. (1.15)), Hernández-Pérez et al. [45] found that the deflection of the plate can be predicted by using the Eq. (1.25) with $N_o = M_o = 40$, i.e.,

$$w(x, y) = \sum_{m_o=1}^{40} \sum_{n_o=1}^{40} \frac{q_{m_o n_o}}{D_{11} \left(\frac{m_o \pi}{L_x} \right)^4 + 2(D_{12} + 2D_{66}) \left(\frac{m_o \pi}{L_x} \right)^2 \left(\frac{n_o \pi}{L_y} \right)^2 + D_{22} \left(\frac{n_o \pi}{L_y} \right)^4} \quad (1.25)$$

Equation (1.25) was found suitable to predict deflections of compliant sandwich structures but inadequate for stiff composite laminates. From this section is concluded that the solutions previously developed do not consider the transverse shear strains which are important for sandwich structures as is mentioned in [17].

1.8 Finite element method

The FEM is a numerical method that approximate the differential equations that describe a physical phenomenon as an algebraic system using matrix algebra [49, 50]. FEM can be used to obtain an approximate solution of complex problems in areas of engineering such as

structural analysis, heat transfer, fluid flow, mass transport, and electromagnetic potential [30, 49, 50]. FEM consists in modeling a body by dividing it into an equivalent of smaller bodies or units (finite elements) interconnected at points common to two or more elements (nodal points or nodes) and/or boundary lines or/and surfaces; this process of dividing is called discretization [30, 50]. This method lets to solve complex problems formulating the equations for each finite element that conform the body and combining them to obtain the solution of the whole body. In this thesis the commercial software (ANSYS11.0) is employed to develop the numerical models.

1.8.1 Description of the SOLID185 element

FEM was employed to compare predictions with the FSDT solutions developed herein. The SOLID185 element is suitable for modeling general 3-D solid structures [31]. This is a solid tetrahedral element defined by eight nodes (one node in each corner: 1,2,3,4,5,6,7,8, Figure 1.11a) with three free degrees of freedom at each node (translation in the nodal x, y , and z directions) and the orthotropic material properties. This element may be employed as Homogeneous structural solid for Sandwich panels (Figure 1.11a) or as Layered structural solid for composite laminates (Figure 1.11b) [31]. The unknown displacements in each node i of the element is given by,

$$\{d\} = \begin{Bmatrix} u_1 \\ v_1 \\ w_1 \\ \vdots \\ u_i \\ v_i \\ w_i \end{Bmatrix} ; \quad i = 1, \dots, 8 \quad (1.26)$$

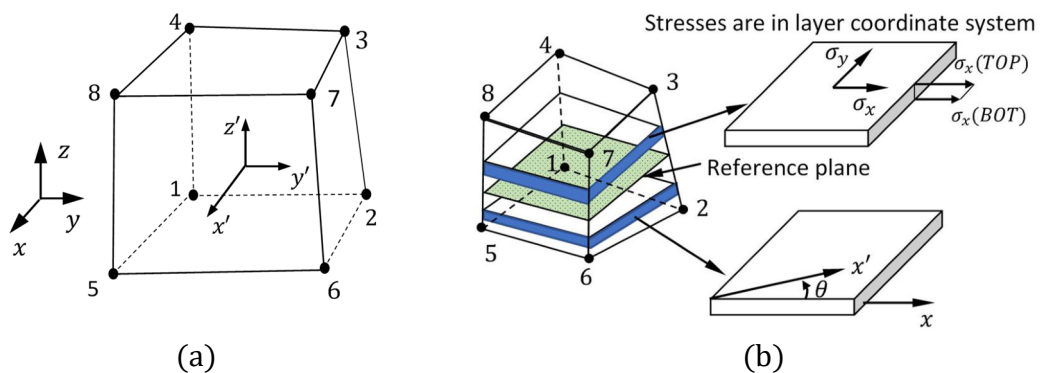


Figure 1. 11. SOLID185 element. (a) Homogeneous structural solid. (b) Layered structural solid [31].

SOLID185 considers the generalized stress components in a solid body shown in Figure 1.3 and considers 9 independent elasticity constants (orthotropic materials) which establish the proportionality between stress and strains (Eqs. (1.2)) [31]. SOLID185 is represented in global coordinates in Figure 1.12a by eight nodes and with isoparametric natural coordinates (s, t, g) in Figure 1.12b. The element faces are defined by $s, t, g = \pm 1$ and the functions used to describe the element geometry for x, y, z in terms of generalized degrees of freedom a_i 's are:

$$x = a_1 + a_2s + a_3t + a_4g + a_5st + a_6tg + a_7gs + a_8stg \quad (1.27a)$$

$$y = a_9 + a_{10}s + a_{11}t + a_{12}g + a_{13}st + a_{14}tg + a_{15}gs + a_{16}stg \quad (1.27b)$$

$$z = a_{17} + a_{18}s + a_{19}t + a_{20}g + a_{21}st + a_{22}tg + a_{23}gs + a_{24}stg \quad (1.27c)$$

After a large algebraic manipulation, it is possible express the element geometry in terms of the shape function

$$\begin{Bmatrix} x \\ y \\ z \end{Bmatrix} = \sum_{i=1}^8 \left(\begin{bmatrix} N_i & 0 & 0 \\ 0 & N_i & 0 \\ 0 & 0 & N_i \end{bmatrix} \begin{Bmatrix} x_i \\ y_i \\ z_i \end{Bmatrix} \right) \quad (1.28a)$$

where N_i is the shape function defined at i -th node. Such function is given by,

$$N_i = \frac{(1 + ss_i)(1 + tt_i)(1 + gg_i)}{8} \quad i = 1, \dots, 8 \quad (1.28b)$$

where s_i, t_i, g_i are the coordinates of the i -th node.

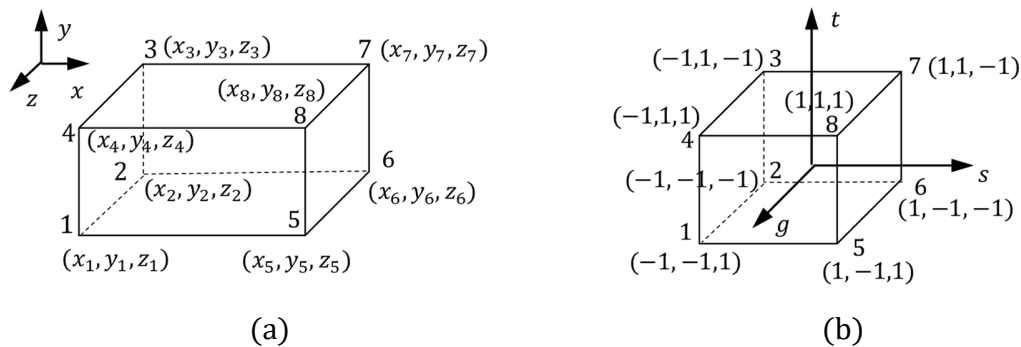


Figure 1.12. Coordinate systems of the SOLID185 element. (a) Global. (b) Natural or intrinsic coordinates s, t and g [30].

If the shape functions are evaluated in a specify node, the function corresponding of this node is 1 and the others are null [30]. Now, evaluating the Eq. (1.28a) in a specific node, it is observed that any point in the natural-coordinates system is mapped to one in the global-coordinate system. The displacement functions of the element SOLID185 is a 3×24 matrix given by,

$$\begin{Bmatrix} u \\ v \\ w \end{Bmatrix} = \sum_{i=1}^8 \left(\begin{bmatrix} N_i & 0 & 0 \\ 0 & N_i & 0 \\ 0 & 0 & N_i \end{bmatrix} \begin{Bmatrix} u_i \\ v_i \\ w_i \end{Bmatrix} \right) \quad (1.29)$$

The linear strain field given by Eq. (1.1) can be expressed in terms of nodal displacement (Eq. 1.26) as

$$\{\varepsilon\} = [B]\{d\} \quad (1.30a)$$

where $[B]$ is a function of s and t coordinates and is called strain-displacement matrix.

$$[B] = [B_1 \quad \dots \quad B_8] \quad (1.30b)$$

being

$$B_i = \begin{bmatrix} \partial N_i / \partial x & 0 & 0 \\ 0 & \partial N_i / \partial y & 0 \\ 0 & 0 & \partial N_i / \partial z \\ \partial N_i / \partial y & \partial N_i / \partial x & 0 \\ 0 & \partial N_i / \partial z & \partial N_i / \partial y \\ \partial N_i / \partial z & 0 & \partial N_i / \partial x \end{bmatrix}; \quad i = 1, \dots, 8 \quad (1.30c)$$

Now, it is possible to determine the stresses applying the Hooke's Law, Eqs. (1.2). The element stiffness matrix to each element is given by,

$$[k] = \int_{-1}^1 \int_{-1}^1 \int_{-1}^1 [B]^T [D] [B] |J| ds dt dg \quad (1.31a)$$

where the Jacobian $|J|$ is given by

$$|J| = \begin{vmatrix} \frac{\partial x}{\partial s} & \frac{\partial y}{\partial s} & \frac{\partial z}{\partial s} \\ \frac{\partial x}{\partial t} & \frac{\partial y}{\partial t} & \frac{\partial z}{\partial t} \\ \frac{\partial x}{\partial g} & \frac{\partial y}{\partial g} & \frac{\partial z}{\partial g} \end{vmatrix} \quad (1.31b)$$

SOLID185 element prevents the shear locking using the enhanced strain formulation method. This is applicable in bending-dominated problems where the shear strain could be considerable. The shear locking is a lock that could happen in FEM when transverse strain is considered within the finite element used. The trend to reach the shear locking increase when the ratio between length/thickness is very high [51] due to the stiffness matrix could become singular. For example, in a beam case, the global stiffness matrix results from the sum of the bending and shear stiffness matrices; when the shear stiffness matrix increases greatly with respect to the other, the lock could happen simulating a null deflection on the beam. Cook [51] points out that to overcome the shear locking the enhanced strain formulation method introduces automatically certain number of internal (and inaccessible) degrees of freedom into the element level and condensed out during the solution phase of the analysis. For example, three shape functions could be considered in SOLID185 to prevent the shear locking (this implies nine new degree of freedom), given a displacement function in u as follow,

$$u = \frac{1}{8}(u_5(1-t)(1-g)(1-s) + u_6(1+t)(1-g)(1-s) + u_2(1+t)(1+g)(1-s) + u_1(1-t)(1+g)(1-s) + u_8(1-t)(1-g)(1-s) + u_7(1+t)(1-g)(1+s) + u_3(1+t)(1+g)(1+s) + u_4(1-t)(1+g)(1+s)) + u_9(1-t^2) + u_{10}(1-g^2) + u_{11}(1-s^2) \quad (1.32)$$

u_9 , u_{10} , and u_{11} represent the tree new degree of freedom associated with the u displacement. The other two displacement functions v and w can be expressed analogously [30, 31, 51]. The displacement function in matrix form considering the enhance strain formulation method to overcome the shear locking is:

$$\begin{Bmatrix} u \\ v \\ w \end{Bmatrix} = \sum_{i=1}^8 \left(\begin{bmatrix} N_i & 0 & 0 \\ 0 & N_i & 0 \\ 0 & 0 & N_i \end{bmatrix} \begin{Bmatrix} u_i \\ v_i \\ w_i \end{Bmatrix} \right) + \sum_{i=9}^{11} \left(\begin{bmatrix} N_i & 0 & 0 \\ 0 & N_i & 0 \\ 0 & 0 & N_i \end{bmatrix} \begin{Bmatrix} u_i \\ v_i \\ w_i \end{Bmatrix} \right) \quad (1.33a)$$

with

$$N_9 = (1-t^2), N_{10} = (1-g^2), N_{11} = (1-s^2) \quad (1.33b)$$



Chapter II. Examination of the plate twist specimen for thick specially orthotropic laminated composites and sandwich plates by using first-order shear deformation theory

2.1 Introduction

The two-point plate twist specimen (PTS) consists of a rectangular plate loaded by two-point forces of magnitude $P/2$ (where P is the total applied force) over two small diagonally opposite areas near the corners and pin supported in the other two [17, 45] (see Figure 2.1). As Timoshenko and Woinowsky-Krieger [12] pointed out, this specimen has been used to verify the bending theory of thin plates [19] since it is a recognized case of anticlastic bending [2, 5, 12, 52], i.e. the deformed shape is a surface with curvatures of opposite sign. Hearmon and Adams [11] employed the PTS to measure the in-plane shear moduli of metals and plywoods by measuring the maximum deflection along diagonals of the panel. Similarly, Tsai [44] used this specimen with three pin supports and one loading pin at the corners to measure the bending and twisting stiffnesses of unidirectional glass fiber/epoxy composites. Both Hearmon and Adams [11] and Tsai [44] employed a solution developed by Thielemann [43] (and also reported by Lekhnitskii [28]) for thin anisotropic plates under uniformly distributed bending and twisting moments. Due to all these developments, simplicity and accuracy, the PTS has become the recommended *ASTM D3044 – 95* standard test method to measure the in-plane shear modulus of thin wood-based structural panels [9]. Mure extended the use of the PTS to determine the twisting stiffness D_{66} of corrugated core cardboard panels [24, 53]. Later, Vinson [6] applied energy principles to this specimen to determine the in-plane shear strength of face sheets, core and adhesive material in sandwich panels. Avilés et al. [17] developed an algebraic expression using classical laminated plate theory (CLPT) to determine D_{66} and analyzed its suitability in compliance calculations for sandwich panels. From their analysis, they concluded that such CLPT expression underestimates the deflections with respect to those computed by the finite element method (FEM) and experiments. In order to consider the effect of transverse shear strains in the deflections of thick PTSs, a semi-empirical shear-corrected expression was proposed by Avilés et al. [42]. However, such formulation required an unknown constant to be calibrated by FEM or experimental data. In a sequel paper, Avilés et al. [16] measured successfully the in-plane shear modulus of glass-vinylester and glass-vinylester/plywood laminated composites, twist stiffness and transverse shear modulus of the core in glass-vinylester/Polyvinyl chloride (PVC) foam sandwich composites by using their shear-corrected formulation. In order to obtain an analytical solution for thick PTSs, Hernández-Pérez et al. [45] developed a Fourier series solution by applying first-order shear deformation theory (FSDT). Such a solution, however, it is only suitable for compliant-cored sandwich materials where the transverse shear strains dominates the elastic response, is mathematically complex and does not provide an easy to implement closed-form solution. Elmalich and Rabinovitch [46] recently analyzed the twist behavior of compliant-cored sandwich panels by developing expressions based on geometrically nonlinear extended high-order plate theory, which considers all stiffness components of the core. They concluded that the in-plane normal and in-plane shear stiffnesses of the core do not contribute significantly to the twist rigidity and that the main contribution comes from the in-plane shear stiffness of the face sheets and transverse shear stiffness of the core; they also pointed out that the actual

stress state is considerably different to the one given by the constant twisting moment stated by CLPT. Beyond its use for shear characterization of laminated composites and sandwich structures, the PTS can assist in understanding complex in-plane shear and tearing fracture mechanisms of composite materials. By including an edge crack along the mid-plane of the PTS, Lee [18] developed the edge crack torsion (ECT) specimen in order to measure the mode III fracture toughness of composite laminates using CLPT. The ECT specimen is still under research for potential standardization of fracture mode III in composite laminates, since FEM analysis has shown important mode II loading contributions along the edges of this specimen [54, 55]. As noticed from this literature background, several authors have rightfully addressed the solution to the deflections of thick composite plates and sandwich panels in the PTS configuration by using different approaches, but to date, an analytical closed-form solution which is free from calibration parameters, independent of FEM and easy to implement is inexistent. Thus, in this work an analytical closed-form expression for the compliance and rotations of thick specially orthotropic PTSs is developed by using FSDT. This solution is compared to experiments, FEM simulations and a previous CLPT solution, conducting an extensive parametric analysis of dimensions and elastic properties. It is expected that this novel and versatile solution contribute to the design of sandwich panels and composite laminates loaded in torsion, the determination of elastic shear properties by using the PTS experimentally, guide to further developments of anticlastic bending problems using shear deformation theories and potentially assist in the compliance solution of cracked composite specimens loaded in torsion.

2.2 Analytical solution using first-order shear deformation theory

2.2.1 The plate twist specimen

The PTS considered here consists in a rectangular panel with side-lengths L'_x and L'_y and thickness h , as depicted in Figure 2.1 for composite laminates (Figure 2.1a) and sandwich plates (Figure 2.1b). For the case of composite laminates, h_i represents the thickness of the i -th ply, Figure 2.1a. For sandwich panels, h_f and h_c denote the face sheet and core thickness, respectively, Figure 2.1b. In the PTS, the vertical forces and pin supports are placed inside the panel in order to avoid sliding of these loads at corners. The distances between the pin supports (span length) along the x and y directions are denoted as L_x and L_y , respectively. In the FSDT solution developed herein, no overhang is considered, i.e., only the in-plane area inside the vertical forces is considered ($L_x \times L_y$ area), i.e., for analytical solutions L_x and L_y dimensions will be used instead of L'_x and L'_y . The free body diagram of the PTS is shown in Figure 2.2a, where the pin supported conditions were replaced by upward transverse force reactions of magnitude $P/2$. According to plate theory, these four transverse forces at the corners can be represented by four transverse loads per unit length (Q_x and Q_y) and four twisting moments per unit length (M_{xy}) applied at the edges, Figure 2.2b. In this figure, Q_x

and Q_y are the through-thickness forces per unit length, tangential to the yz and xz planes, respectively, which are defined as [47],

$$Q_x = \int_{-\frac{h}{2}}^{\frac{h}{2}} \tau_{xz} dz; \quad Q_y = \int_{-\frac{h}{2}}^{\frac{h}{2}} \tau_{yz} dz; \quad M_{xy} = \int_{-\frac{h}{2}}^{\frac{h}{2}} \tau_{xy} z dz \quad (2.1a-c)$$

where τ_{xz} , τ_{yz} and τ_{xy} are the shear stresses acting on the xz , yz and xy planes. Because of the PTS symmetry, only one quarter plate can be analyzed as is shown in Figure 2.2c. According to this figure, equilibrium of forces along the z direction and equilibrium of moments around x and y axes require that

$$M_{xy}(x, y) = \frac{P}{4}; \quad Q_x\left(\frac{L_x}{2}, -\frac{L_y}{2}\right) = -\frac{P}{2L_y}; \quad Q_y\left(-\frac{L_x}{2}, \frac{L_y}{2}\right) = -\frac{P}{2L_x} \quad (2.2a-c)$$

Equations (2.2a – c) point out that inside the PTS exist transverse uniformly distributed loads Q_x and Q_y with constant magnitudes $-P/(2L_y)$ and $-P/(2L_x)$, respectively (negative signs indicate downward direction), which both equilibrate $P/2$ at $(L_x/2, -L_y/2)$. Moreover, there is a uniformly distributed twisting moment per unit of length of constant magnitude $P/4$ on the entire plate, as Timoshenko and Woinowsky-Krieger [12] have pointed out. It should be noted that Q_x and Q_y from Eqs. (2.2b) and (2.2c) are not considered in the CLPT solutions (which consider only $M_{xy} = P/4$ [2, 5, 9, 11, 12, 17, 19, 28, 43, 44, 52]), but they are considered in the FSDT solution.

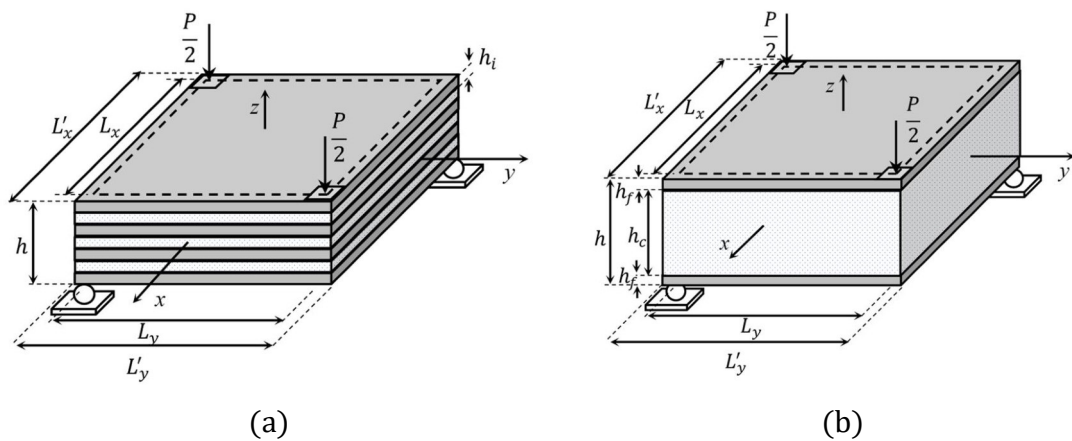


Figure 2. 1. The PTS. (a) Composite laminate. (b) Sandwich panel.

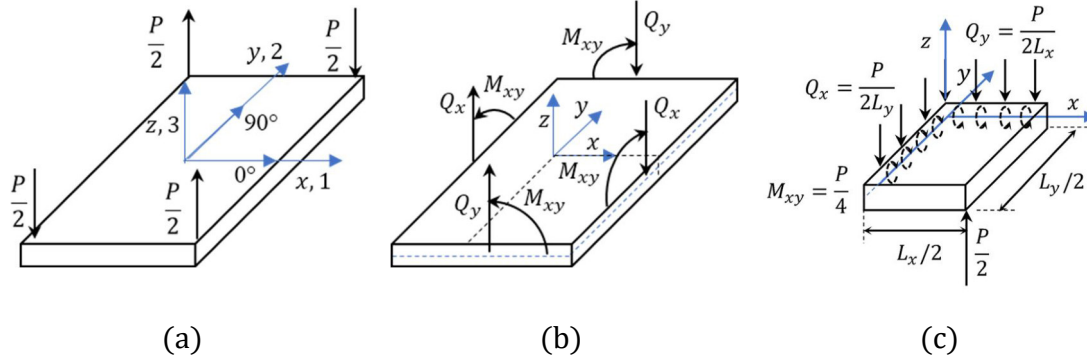


Figure 2.2. Equivalent force and moment diagrams for the PTS. (a) Original free body diagram. (b) Equivalent free body diagram with force and moment resultants. (c) Resultant transverse shear loads and twist moments in one quarter plate.

The boundary conditions of the PTS can be determined from Figure 2.1. According to this figure, at the pin support positions $(-L_x/2, L_y/2)$ and $(L_x/2, -L_y/2)$, the transverse deflection w must vanish, i.e.,

$$w\left(-\frac{L_x}{2}, \frac{L_y}{2}\right) = w\left(\frac{L_x}{2}, -\frac{L_y}{2}\right) = 0 \quad (2.3)$$

In order to employ the FSDT, two rotation functions ϕ_x and ϕ_y are needed to represent the rotation of the plate cross-section with respect to the mid-plane ($z = 0$) along x and y directions. These rotations additionally denote the difference between transverse shear strains and slopes of the deformed mid-plane surface. Because of the symmetry of the PTS and its anticlastic deformed shape, it is expected that at the plate center $(0,0)$, the slope of the deformed mid-plane surface becomes zero. This geometric condition leads to consider that both slopes ($\partial w/\partial x$ and $\partial w/\partial y$) and rotating functions (ϕ_x and ϕ_y) must vanish at the center of the plate, i.e.,

$$\frac{\partial w}{\partial x}(0,0) = 0; \quad \frac{\partial w}{\partial y}(0,0) = 0 \quad (2.4a-b)$$

$$\phi_x(0,0) = 0; \quad \phi_y(0,0) = 0 \quad (2.4c-d)$$

In this work, two specially orthotropic material systems are employed as baseline for the parametric analysis. The first one is a cross-ply composite laminate formed by 24 plies with

a $[(90/0)_6]_s$ stacking sequence, which represents a “stiff” material. Figure 2.1a. 90 and 0 denote the angular orientation of the fibers of each ply according to the x - y - z global coordinate system, with 0 coinciding with the x direction. This cross-ply laminate is a square plate with side-lengths $L'_x = L'_y = 78$ mm and ply thickness $h_i = 0.1875$ mm ($h = 4.5$ mm). Each ply of the $[(90/0)_6]_s$ laminate is made of a unidirectional glass/epoxy prepreg, whose specially orthotropic elastic properties are listed in Table 2.1. The second baseline material is a sandwich plate with aluminum face sheets and a PVC foam core, both considered isotropic, Figure 2.1b; this material system is labeled as “AL/H45” and represent a compliant sandwich material. AL/H45 consists of a square panel with side lengths $L'_x = L'_y = 305$ mm, face sheet thickness $h_f = 2.51$ mm and core thickness $h_c = 13$ mm. The elastic properties of the aluminum and PVC foam are listed in Table 2.1. PVC foam cores may be slightly orthotropic but for simplicity in the parametric analysis they are considered isotropic, without significant changes in the outcomes of this elastic analysis [16]. Both baseline material systems were chosen because they are typically employed in engineering applications where light weight is priority [8, 56, 57].

Table 2.1. Elastic properties of baseline panels.

Unidirectional glass/epoxy prepreg			Stiffness	
$[(0/90)_6]_s$	$E_1 = 47.7$ GPa	$\nu_{13} = 0.278$	$G_{13} = 4.83$ GPa	$D_{66} = 36.9$ Nm
	$E_2 = 12.3$ GPa	$\nu_{12} = 0.278$	$G_{12} = 4.83$ GPa	$A_{44} = 20.9$ MN/m
	$E_3 = 12.3$ GPa	$\nu_{23} = 0.403$	$G_{23} = 4.48$ GPa	$A_{55} = 20.9$ MN/m
Aluminum			H45	Stiffness
AL/H45	$E = 70$ GPa		$E_1 = 39.6$ MPa	$D_{66} = 8.20$ N m
	$\nu = 0.3$		$\nu_{12} = 0.32$	$A_{44} = 195$ kN/m
				$A_{55} = 195$ kN/m

2.2.2 First-order shear deformation solution

FSDT was employed to provide accurate predictions of transverse deflections and strains in thick laminated composites and sandwich panels. The displacement fields in FSDT are given by [3],

$$u(x, y) = u_o(x, y) + z\phi_x(x, y) \quad (2.5a)$$

$$v(x, y) = v_o(x, y) + z\phi_y(x, y) \quad (2.5b)$$

$$w(x, y) = w_o(x, y) \quad (2.5c)$$

where u_o , v_o and w_o denote the mid-plane displacements of an (x, y) point along the x , y and z axes, respectively. Considering that displacements are much smaller than the thickness of the plate ($u, v, w \ll h$) and that strains are much lower than unity (infinitesimal strains, $\epsilon, \gamma \ll 1$), the strain fields in FSDT are customarily defined by [3, 47],

$$\varepsilon_{xx} = \frac{\partial u_o}{\partial x} + z \frac{\partial \phi_x}{\partial x}; \quad \varepsilon_{yy} = \frac{\partial v_o}{\partial y} + z \frac{\partial \phi_y}{\partial y}; \quad \varepsilon_{zz} = 0 \quad (2.6a-c)$$

$$\gamma_{xy} = \left(\frac{\partial u_o}{\partial y} + \frac{\partial v_o}{\partial x} \right) + z \left(\frac{\partial \phi_x}{\partial y} + \frac{\partial \phi_y}{\partial x} \right); \quad \gamma_{xz} = \frac{\partial w_o}{\partial x} + \phi_x; \quad \gamma_{yz} = \frac{\partial w_o}{\partial y} + \phi_y \quad (2.6d-f)$$

According to FSDT, the contribution of both γ_{xz} and γ_{yz} to the deflections are considered by the rotations ϕ_x and ϕ_y as described by Eqs. (2.6e) and (2.6f). An alternative representation of ϕ_x and ϕ_y is obtained by rewriting Eqs. (2.6e) and (2.6f) as,

$$\phi_x = \gamma_{xz} - \frac{\partial w_o}{\partial x}; \quad \phi_y = \gamma_{yz} - \frac{\partial w_o}{\partial y} \quad (2.7a-b)$$

It should be noticed from Eqs. (2.7a, b) that when $\gamma_{xz} = \gamma_{yz} = 0$, the rotation functions become $\phi_x = -\partial w_o / \partial x$ and $\phi_y = -\partial w_o / \partial y$, which returns to the CLPT assumption. According to FSDT, the bending curvatures along the x and y axes (κ_x and κ_y , respectively) and twisting curvature κ_{xy} are defined as [3],

$$\kappa_x = \frac{\partial \phi_x}{\partial x}; \quad \kappa_y = \frac{\partial \phi_y}{\partial y}; \quad \kappa_{xy} = \frac{\partial \phi_x}{\partial y} + \frac{\partial \phi_y}{\partial x} \quad (2.8a-c)$$

Since there are not in-plane forces acting in the PTS (Figure 2.2c) and considering specially orthotropic materials, their constitutive equations are given by [3, 47],

$$\begin{Bmatrix} M_x \\ M_y \\ M_{xy} \end{Bmatrix} = \begin{bmatrix} D_{11} & D_{12} & 0 \\ D_{12} & D_{22} & 0 \\ 0 & 0 & D_{66} \end{bmatrix} \begin{Bmatrix} \kappa_x \\ \kappa_y \\ \kappa_{xy} \end{Bmatrix} \quad (2.9a)$$

$$\begin{Bmatrix} Q_y \\ Q_x \end{Bmatrix} = \begin{bmatrix} K_{11}A_{44} & 0 \\ 0 & K_{22}A_{55} \end{bmatrix} \begin{Bmatrix} \gamma_{yz} \\ \gamma_{xz} \end{Bmatrix} \quad (2.9b)$$

where M_x and M_y are the bending moment resultants along the x and y axes. K_{11} and K_{22} are the shear correction factors employed in FSDT for the yz and xz planes, which correct the discrepancy between the actual transverse shear force distribution through the specimen thickness (parabolic or higher order) and that computed by FSDT (uniform) [24, 47]. A_{44} and A_{55} are the transverse shear stiffness corresponding to the yz and xz planes. These and the other extensional A_{ij} and bending stiffnesses D_{ij} are defined as [3],

$$A_{ij} = \sum_{n=1}^N (\bar{Q}_{ij})_n (z_{n+1} - z_n) \quad (2.9c)$$

$$D_{ij} = \frac{1}{3} \sum_{n=1}^N (\bar{Q}_{ij})_n (z_{n+1}^3 - z_n^3); \quad (i, j = 1, 2, \dots, 6) \quad (2.9d)$$

where $(\bar{Q}_{ij})_n$ is the transformed reduced stiffness of the n th ply ($n = 1, 2, \dots, N$), z_n is the transverse coordinate of the n th ply, and N is the total number of layers ($N = 24$ for the cross-ply laminate and $N = 3$ for the sandwich panel). From Figure 2.2b and 2.2c, it is observed that in the PTS only Q_x , Q_y and M_{xy} are present. Thus, bending moment resultants are zero, i.e., $M_x = M_y = 0$. Including this condition into Eqs. (2.9a) and (2.9b) yields

$$M_x = D_{11}\kappa_x + D_{12}\kappa_y = 0; \quad M_y = D_{12}\kappa_x + D_{22}\kappa_y = 0 \quad (2.10a-b)$$

$$M_{xy} = D_{66}\kappa_{xy} \quad (2.10c)$$

$$Q_y = K_{11}A_{44}\gamma_{yz}; \quad Q_x = K_{22}A_{55}\gamma_{xz} \quad (2.10d-e)$$

Since bending stiffnesses D_{11} , D_{12} , and D_{66} are not negligible, the bending curvatures must vanish according to Eqs. (2.10a) and (2.10b), i.e., κ_x and $\kappa_y = 0$. Therefore, from Eqs. (2.10) is deduced that

$$\kappa_x = \frac{\partial \phi_x}{\partial x} = 0; \quad \kappa_y = \frac{\partial \phi_y}{\partial y} = 0 \quad (2.11a-b)$$

$$M_{xy} = D_{66} \left(\frac{\partial \phi_x}{\partial y} + \frac{\partial \phi_y}{\partial x} \right) \quad (2.11c)$$

$$Q_y = K_{11}A_{44} \left(\frac{\partial w_o}{\partial y} + \phi_y \right); \quad Q_x = K_{22}A_{55} \left(\frac{\partial w_o}{\partial x} + \phi_x \right) \quad (2.11d-e)$$

In order to represent the deformed shape of the PTS and fulfill the equilibrium equations given by Eqs. (2.2) and boundary conditions given by Eqs. (2.3) and (2.4), the following algebraic polynomials are proposed,

$$w(x, y) = C_0 + C_1\phi_x + C_2\phi_y + C_3\phi_x\phi_y \quad (2.12a)$$

$$\phi_x(x, y) = C_4 + C_5x + C_6y \quad (2.12b)$$

$$\phi_y(x, y) = C_7 + C_8x + C_9y \quad (2.12c)$$

where C_i ($i = 0, 1, \dots, 9$) are unknown constants to be determined. Introducing Eqs. (2.12) into (2.4) and (2.11) yields,

$$C_1 = C_2 = C_4 = C_5 = C_7 = C_9 = 0 \quad (2.13a)$$

Substituting Eqs. (2.12b) and (2.12c) into (2.12a) and using the Eq. (2.3) yields,

$$C_o = C_3 C_6 C_8 \frac{L_x L_y}{4} \quad (2.13b)$$

The constants C_0, C_3, C_6, C_8 are determined in two steps. The first step consists in substituting Eqs. (2.12b) and (2.12c) into (2.8c), and then into Eq. (2.10c), and finally equating to Eq. (2.2a). In the second step Eqs. (2.12b) and (2.12c) are substituted into Eqs. (2.6e) and (2.6f), and then into Eqs. (2.9b), (2.2b) and (2.2c), yielding,

$$C_0 = \frac{L_x L_y P}{8} \left(\frac{1}{4D_{66}} + \frac{1}{L_x^2 K_{11} A_{44}} + \frac{1}{L_y^2 K_{22} A_{55}} \right) \quad (2.13c)$$

$$C_6 = \frac{P}{2} \left(\frac{1}{4D_{66}} + \frac{1}{L_x^2 K_{11} A_{44}} - \frac{1}{L_y^2 K_{22} A_{55}} \right) \quad (2.13d)$$

$$C_8 = \frac{P}{2} \left(\frac{1}{4D_{66}} - \frac{1}{L_x^2 K_{11} A_{44}} + \frac{1}{L_y^2 K_{22} A_{55}} \right) \quad (2.13e)$$

Finally, substituting the constants C_0, C_3, C_6, C_8 into Eq. (2.12), the proposed closed-form solution becomes

$$w(x, y) = -\frac{P}{2} \left(\frac{1}{4D_{66}} + \frac{1}{L_x^2 K_{11} A_{44}} + \frac{1}{L_y^2 K_{22} A_{55}} \right) \left(\frac{L_x L_y}{4} + xy \right) \quad (2.14a)$$

$$\phi_y(x) = \frac{P}{2} \left(\frac{1}{4D_{66}} + \frac{1}{L_x^2 K_{11} A_{44}} - \frac{1}{L_y^2 K_{22} A_{55}} \right) x \quad (2.14b)$$

$$\phi_x(y) = \frac{P}{2} \left(\frac{1}{4D_{66}} + \frac{1}{L_x^2 K_{11} A_{44}} - \frac{1}{L_y^2 K_{22} A_{55}} \right) y \quad (2.14c)$$

Eqs. (2.14a – c) represent the FSDT solution developed herein for the PTS. The maximum deflection (w_{max}) takes place at both loaded corners $(L_x/2, L_y/2)$ and $(-L_x/2, -L_y/2)$ and is given by

$$w_{max} = -\frac{P}{4} \left(\frac{L_x L_y}{4D_{66}} + \frac{L_y}{L_x K_{11} A_{44}} + \frac{L_x}{L_y K_{22} A_{55}} \right) \quad (2.15a)$$

The compliance C is defined as the ratio between the maximum deflection and the total applied force, i.e., $C = w_{max}/P$ [24]. Thus, according to Eq. (2.15a) the compliance predicted by FSDT is,

$$C_{FSDT} = \frac{1}{4} \left(\frac{L_x L_y}{4D_{66}} + \frac{L_x}{L_y K_{11} A_{44}} + \frac{L_y}{L_x K_{22} A_{55}} \right) \quad (2.15b)$$

The selection of the shear correction factors (K_{11} and K_{22}) is yet a matter of controversy because they depend on Poisson's ratio, specimen aspect ratio, method of evaluation and type of problem [33, 35, 36]. The most typically accepted ones are $K_{11} = K_{22} = 1, 5/6, 2/3$ and $\pi^2/12$. However, specific shear correction factors for torsion problems have been scarcely discussed in the literature [33, 36, 58]. Therefore, after a dedicated analysis shown in section 2.4.4, $K_{11} = K_{22} = 2/3$ were selected, which matches the suggestions by Whitney [35], Uflyand [59] and Timoshenko [60]. Furthermore, in order to employ Eq. (2.15b) for sandwich composite materials, Zenkert [8] and Avilés et al. [42] have pointed out that transverse shear stiffnesses of a sandwich plate with an isotropic compliant core ($E_c \ll E_f$) and thin face sheets ($h_f \ll h_c$) are reduced to $A_{44} = A_{55} = G_c h_c$. This agrees with sandwich theory [23], which assumes that the transverse shear contribution from thin and stiff face sheets is negligible and the core carries almost all shear forces (Q_x and Q_y). Thus, considering $A_{44} = A_{55} = G_c h_c$ and $K_{11} = K_{22} = 2/3$ for sandwich materials [8, 35, 59], Eq. (2.15b) becomes

$$C_{FSDT} = \frac{L_x L_y}{16D_{66}} + \frac{3}{8G_c h_c} \left(\frac{L_x}{L_y} + \frac{L_y}{L_x} \right) \quad (2.15c)$$

Eqs. (2.15b) and (2.15c) are employed for the parametric analysis of composite laminates and sandwich materials herein, respectively. It should be noticed that when the material studied is stiff or thin, i.e. low ratio of in-plane elastic moduli to interlaminar shear moduli (E_1/G_{23}) and width-to-thickness ratios higher than 10 [47], Eq. (2.15b) is reduced to the solution based on CLPT developed by Avilés et al. [17], which is given by,

$$C_{CLPT} = \frac{L_x L_y}{16D_{66}} \quad (2.16)$$

It should be noticed that Eq. (2.16) does not consider the stiffnesses A_{44} and A_{55} which are important for shear deformable plates. In addition, if a monolithic isotropic stiff material is analyzed, both Eqs. (2.15b) and (2.16) are reduced to the equation developed in the ASTM standard D3044-94 [9] and discussed in Nádai [19], Jones [2], Hearmon and Adams [11], and Tsai [44]. By differentiating Eq. (2.14a) with respect to x and y the slopes of the deformed mid-plane along the x and y axes are obtained

$$\left(\frac{\partial w}{\partial x} \right)_{FSDT} = -\frac{P}{2} \left(\frac{1}{4D_{66}} + \frac{1}{L_x^2 K_{11} A_{44}} + \frac{1}{L_y^2 K_{22} A_{55}} \right) y \quad (2.17a)$$

$$\left(\frac{\partial w}{\partial y} \right)_{FSDT} = -\frac{P}{2} \left(\frac{1}{4D_{66}} + \frac{1}{L_x^2 K_{11} A_{44}} + \frac{1}{L_y^2 K_{22} A_{55}} \right) x \quad (2.17b)$$

γ_{xz} and γ_{yz} are computed by substituting Eqs. (2.17) and (2.14) into Eqs. (2.6e) and (2.6f), which yields

$$\gamma_{xz} = -\frac{P}{L_x^2 K_{11} A_{55}} y; \quad \gamma_{yz} = -\frac{P}{L_y^2 K_{22} A_{55}} x \quad (2.18a-b)$$

For comparison, the displacement field $w(x, y)$, slopes $\partial w/\partial x$ and $\partial w/\partial y$ obtained by Avilés et al. [17] using CLPT are employed in this work, i.e.

$$w(x, y) = -\frac{P}{8D_{66}} \left(\frac{L_x L_y}{4} + xy \right) \quad (2.19a)$$

$$\left(\frac{\partial w}{\partial x} \right)_{CLPT} = -\frac{P}{8D_{66}} y; \quad \left(\frac{\partial w}{\partial y} \right)_{CLPT} = -\frac{P}{8D_{66}} x \quad (2.19b-c)$$

2.3 Finite element analysis

Finite element modeling was conducted in order to analyze and compare the deflections, compliances and transverse shear strains of the investigated panels with those predicted by FSDT. Three-dimensional finite element models were carried out in ANSYS11.0 [31] for 78 mm long square composite laminates and 305 mm long square sandwich panels, both modeled as linear elastic materials, see Figure 2.3 and Table 2.1. The total thickness (h) of both baseline materials was variable due to the parametric analysis conducted. All models employed the SOLID185 element in order to be able to capture the transverse shear deformation. SOLID185 is a brick element defined by eight corner nodes with linear displacement interpolation between nodes. Each node has three translations along x, y and z orthogonal directions, i.e. 24 degrees of freedom. To model $[(0/90)_n]_s$ composite laminates, the layered option of the SOLID185 element was used whereas the AL/H45 specimen employed the homogeneous option. In order to assign the orientation, elastic properties and thicknesses for each ply of the $[(0/90)_n]_s$ laminate, the SOLID185 layered element was used. The enhanced strain formulation method to prevent shear locking during twisting [31]. The elastic properties of both baseline models are listed in Table 2.1. In order to produce twisting in the $[(0/90)_6]_s$ model, two point loads of 500 N ($P = 1$ kN) were applied at two diagonally opposite nodes on the top surface at $(-L_x/2, +L_y/2, +h/2)$ and $(+L_x/2, -L_y/2, +h/2)$ considering a small (1 mm) overhang in each plate side accord to Browning et al. [61], which recommend to use small overhangs to reduce their influence in the compliance of the plate, i.e., $L'_x = L'_y = 78$ mm and $L_x = L_y = 76$ mm, according to figures 2.1a and 2.3a. These loaded nodes were coupled in the z transverse direction in order to obtain symmetric anticlastic bending of the plate, i.e., that both diagonally opposite corners experience the same deflection. The pin supports were modeled by prescribing zero transverse displacements ($w = 0$) in two nodes diagonally opposite at the bottom surface located at $(+L_x/2, +L_y/2, -h/2)$ and $(-L_x/2, -L_y/2, -h/2)$. Additionally, the nodes at the center of the plate (0,0) and corner $(L_x/2, L_y/2)$ were fixed in the x and y directions (i.e., $u = v = 0$ at (0,0) and $(L_x/2, L_y/2)$). The AL/H45 model used the same forces and boundary conditions than the cross-ply laminate; however, since its

size is much larger, the AL/H45 panel employed 5 mm overhang with point forces applied to central areas of $10 \times 10 \text{ mm}^2$ (0.22 % of the panel area) instead of single nodes, see Figure 2.3b. Considering that between plies there is a perfect union without sliding between them, a static analysis was performed in ANSYS employing a single load step, solving static equilibrium matrices by using the sparse direct solver (a Gaussian elimination approach). The compliance was computed as the nodal z displacement of the loaded node located at $(-L_x/2, L_y/2, h/2)$ divided by the value of the total applied force ($P = 1 \text{ kN}$). In order to subtract indentation effects to the compliance, C was calculated by subtracting the deflection of the mid-plane node at $(L_x/2, L_y/2, 0)$ to that located at $(-L_x/2, L_y/2, 0)$ and dividing such difference by the magnitude of applied force. The element size and total numbers of nodes were chosen after obtaining convergence on the values of compliance in models with different mesh sizes. The aspect ratio of the finite elements for sandwich panels varied from 0.5 to 4, whereas for composite laminates varied from 4.16 to 21.3. Such refinements increased the computational time exponentially with no significant change in the compliance (only 0.13 % after 119,072 and 6,084 elements for sandwich panels and composite laminates, respectively). Thus, after the convergence analysis, the models for AL/H45 and $[(0/90)_n]_s$ panels employed 119,072 and 6,084 elements, respectively.

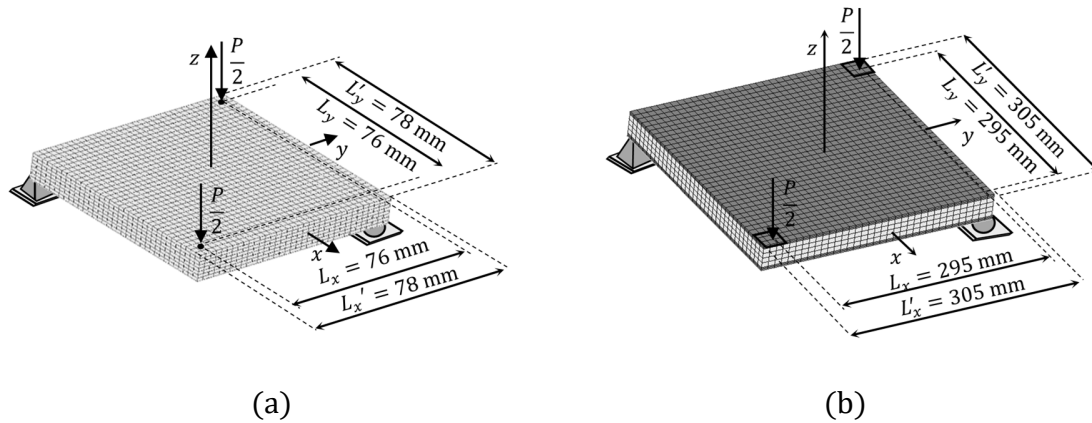


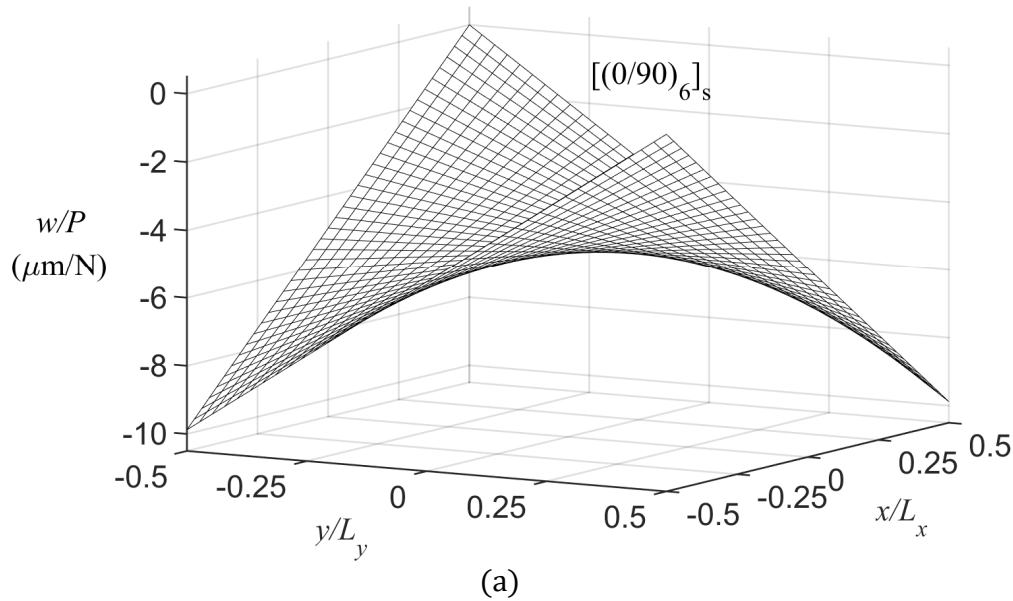
Figure 2.3. Finite element models of the baseline materials. (a) Laminated composite. (b) Sandwich panel.

2.4 Results and discussion

2.4.1 Displacement, rotations, and strain fields

Figure 2.4 illustrates the deformed mid-plane surface ($z = 0$) of the $[(0/90)_n]_s$ composite laminate calculated by FSDT (Figure 2.4a) and FEM (Figure 2.4b). A comparison of normalized mid-plane deflections (w/P) between FSDT (Eq. (2.14a)), FEM and CLPT (Eq. (2.19a)) is conducted in Figure 2.4c. It is observed in Figure 2.4a that the FSDT solution truly represents an anticlastic bending surface; its curvature along the pin supports ($L_x/2, L_y/2$) and $(-L_x/2, -L_y/2)$ is concave (downwards) and its curvature along loading

points is convex. As expected, zero and maximum normalized deflections ($-9.88 \mu\text{m}/\text{N}$) are obtained at pin supports and loading points, respectively. At the plate center $(0,0)$, where both curvatures coincide, a local minimum value of $4.94 \mu\text{m}/\text{N}$ is attained. Similarly, the FEM in Figure 2.4b agrees with the antilastic deformed surface predicted by FSDT with maximum normalized deflections of $-10.33 \mu\text{m}/\text{N}$ at loading points and a minimum local value of $5.07 \mu\text{m}/\text{N}$ at the plate center. It was observed (not shown) that the CLPT solution developed by Avilés et al. [17] (Eq. 2.19a) adequately represents the antilastic deformed shape of the $[(0/90)_6]_s$ baseline laminate, in agreement with FSDT and FEM. Figure 2.4c shows that all approaches predict a linear deflection per unit force along $y = L_y/2$, increasing from 0 at pin support ($x/L_x = +0.5$) to $\sim -9.9 \mu\text{m}/\text{N}$ at loading point ($x/L_x = -0.5$). The agreement between plate theories and FEM points out that CLPT and FSDT can be employed to predict the twist behavior of rigid and thin cross-ply laminates.



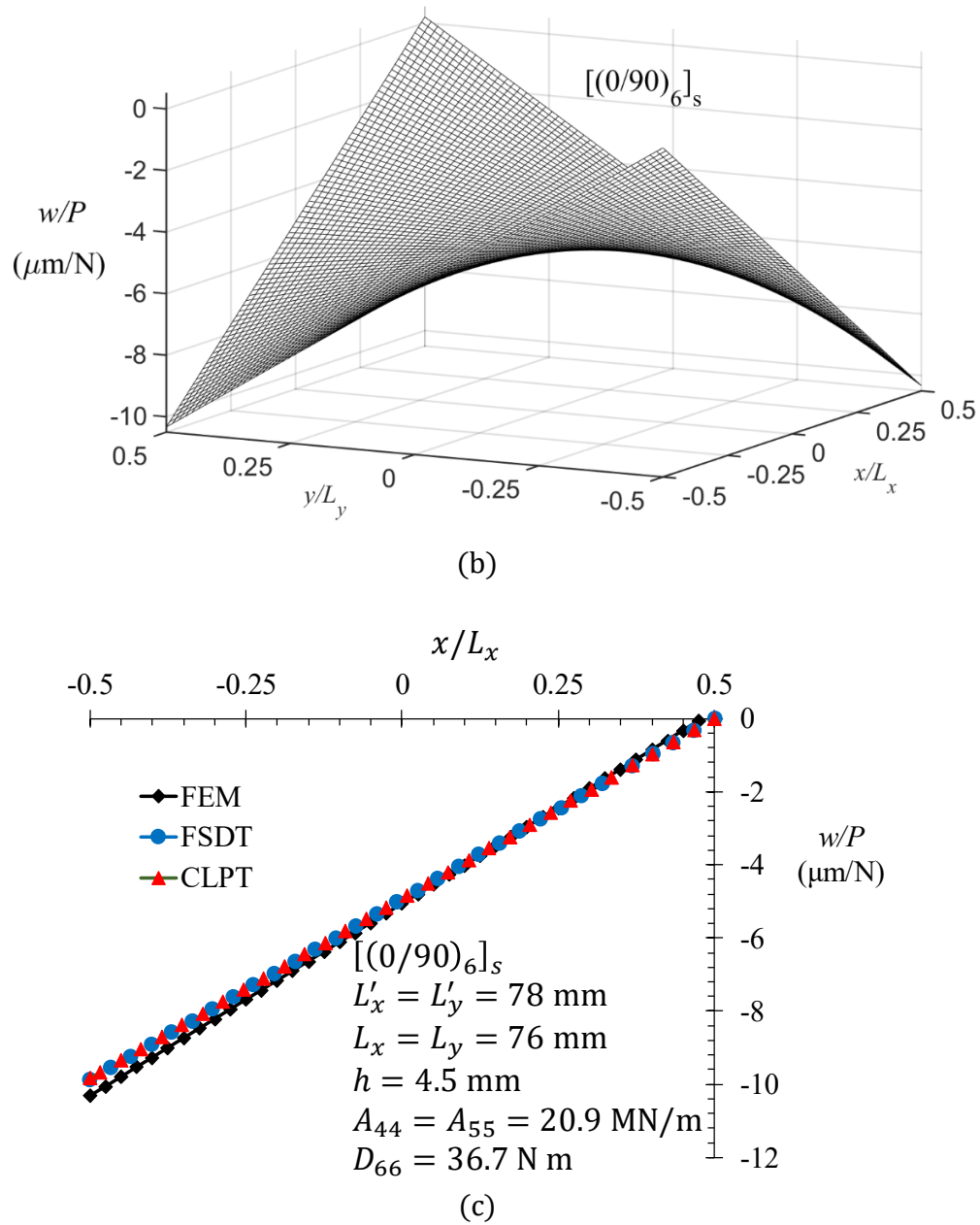
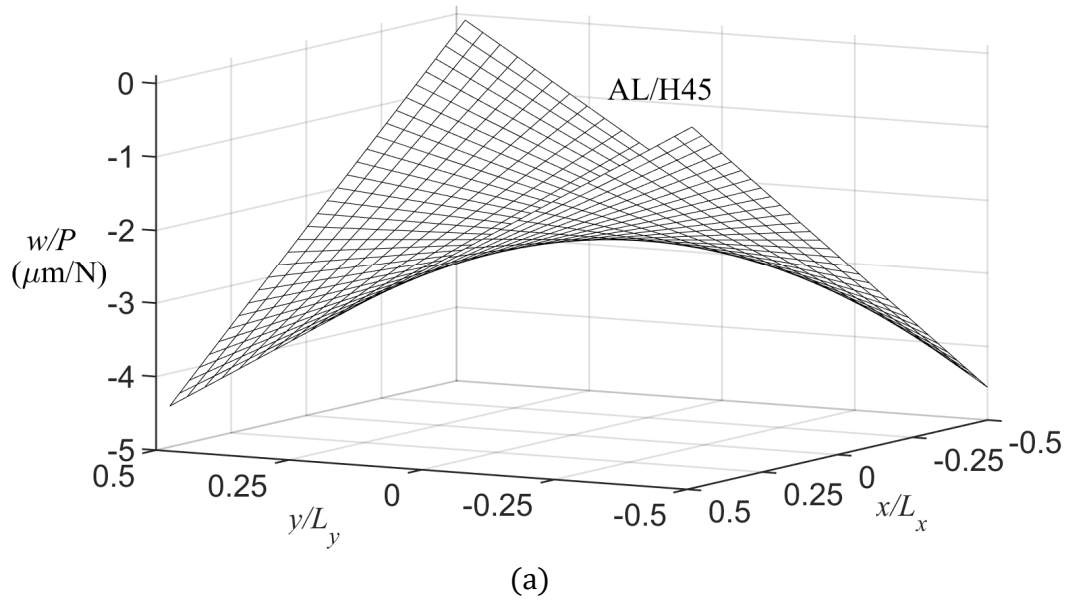


Figure 2.4. Normalized mid-plane deflection (w/P) for the square $[(0/90)_6]_s$ composite laminate. (a) FSDT. (b) FEM. (c) Along $y = L_y/2$.

The transverse displacement field (at the mid-plane) of the AL/H45 panel is also plotted by using FSDT (Figure 2.5a) and FEM (Figure 2.5b). Similar to Figure 2.5a, the FSDT solution adequately represents the anticlastic bending surface of the PTS, reaching a maximum value

of $-4.55 \mu\text{m}/\text{N}$ at $(+L_x/2, -L_y/2)$ and $(-L_x/2, +L_y/2)$ and with a local minimum value of $-2.28 \mu\text{m}/\text{N}$ at the panel center. FEM (Figure 2.5b) also predicts an anticlastic deformed shape with similar deflections to those calculated by FSDT. The normalized deflection (w/P) is also plotted along $y = L_y/2$ of the AL/H45 panel (Figure 2.5c). In this figure, FSDT predicts a linear w/P response, increasing from 0 at $x/L_x = 0.5$ to $-4.55 \mu\text{m}/\text{N}$ at $x/L_x = -0.5$. The deflections computed by FEM coincide with those calculated by FSDT along $y = L_y/2$. However, two small undulations are noticed for FEM, which may be due to influence of the γ_{xz} distribution in the deflection, which is caused by the applied point forces, as will be discussed later. On the other hand, the CLPT approach also presents a linear w/P behavior with a maximum of $-0.71 \mu\text{m}/\text{N}$ at $x/L_x = -0.5$, i.e., much lower deflections than FSDT and FEM. This is because the CLPT formulation does not consider the contribution of γ_{xz} and γ_{yz} to the deflection of the AL/H45 sandwich, whose core is compliant and prone to bend and shear.



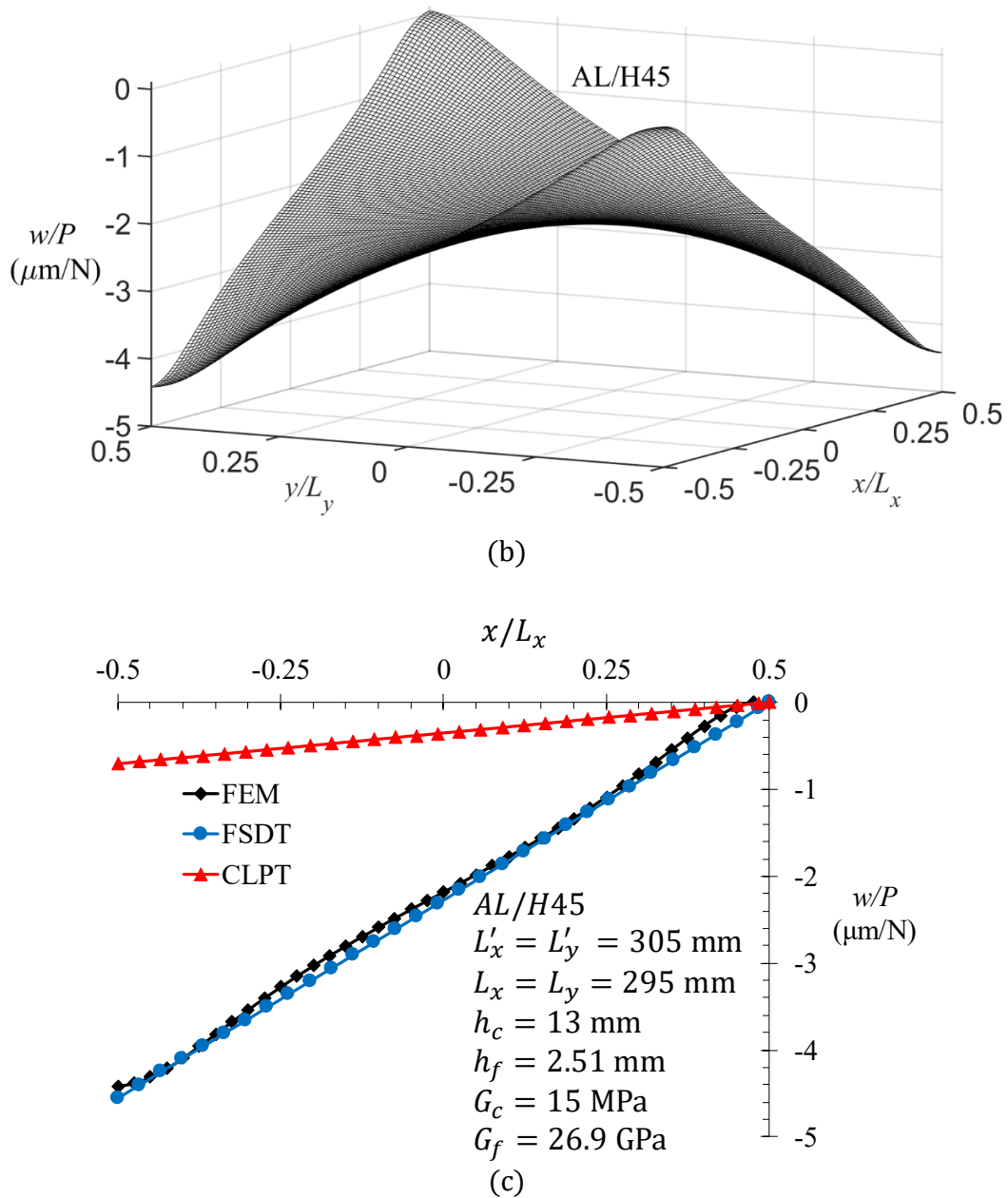
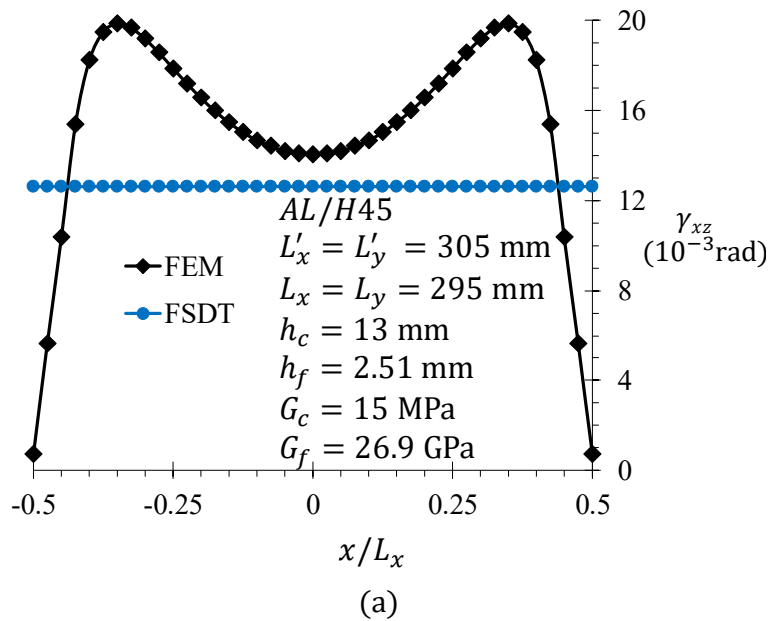


Figure 2. 5. Normalized mid-plane deflection (w/P) of the square AL/H45 sandwich panel. (a) FSDT. (b) FEM. (c) Along $y = L_y/2$.

Transverse shear strain γ_{xz} is plotted along $y = L_y/2$ (Figure 2.6a) and along the $x = 0$ centerline (Figure 2.6b) for AL/H45. Here γ_{xz} is plotted only for AL/H45 since it was observed (not shown) that contribution of γ_{xz} to the maximum deflection of the stiff $[(0/90)_6]_s$ laminate was only 3.37 % (with respect to FEM), which is considered negligible.

This shear contribution was calculated as $1 - w_{CLPT}/w_{FEA}$, and in this case $w_{CLPT} \approx w_{FEA}$ according to Figure 2.6c. In Figure 2.6a, it is observed that γ_{xz} predicted by FEM has a symmetric M-shaped behavior, raising from 0.75×10^{-3} rad at $x/L_x = 0.5$ to a maximum of 19.9×10^{-3} rad at $x/L_x = 0.35$, and then decreasing parabolically until a valley of 14.1×10^{-3} rad is reached at $x = 0$. This predicted shape is due to the two transverse point forces which locally disrupt the constant γ_{xz} distribution along the edge. On the other hand, the FSDT solution predicts a constant $\gamma_{xz} = 12.6 \times 10^{-3}$ rad along the entire edge ($-0.5 \leq x/L_x \leq 0.5$). At $x = 0$ (away from the applied forces), reasonable agreement between the γ_{xz} values predicted by FEM and FSDT is obtained. This points out that the FSDT solution predicts similar γ_{xz} than those by FEM in positions sufficiently far from the zone of applied forces, when compliant or/and shear deformable materials are used as cores. Figure 2.6b shows that FEM predicts a linear γ_{xz} behavior with negative slope along the $x = 0$ centerline with maximum and minimum values of $\gamma_{xz} = \pm 14.1 \times 10^{-3}$ rad at panel ends. Good agreement is noticed between the γ_{xz} distribution computed by FEM and FSDT along the $x = 0$ centerline, which confirms that the proposed functions ϕ_x and ϕ_y are suitable to describe the γ_{xz} and γ_{yz} strain fields of the PTS.



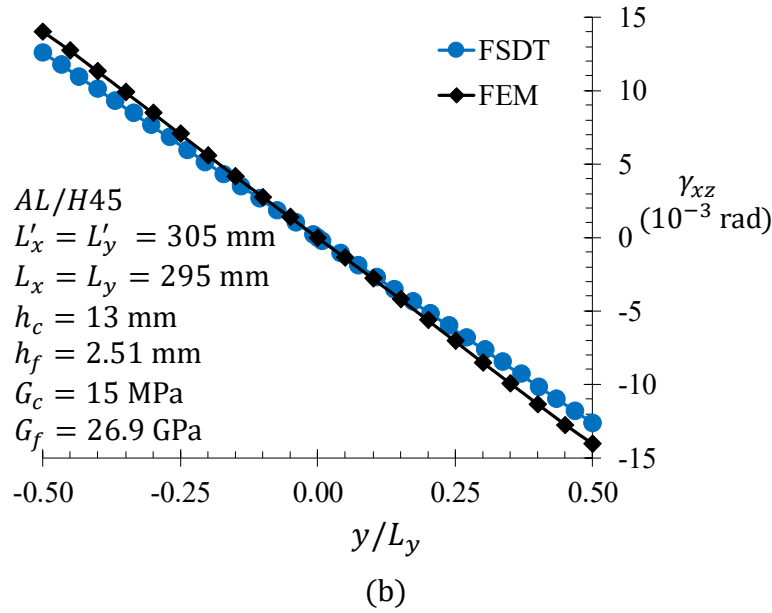


Figure 2.6. Mid-plane transverse shear strain γ_{xz} distribution along the AL/H45 sandwich panel. (a) $y = L_y/2$. (b) $x = 0$ centerline.

Further investigation of the transverse shear strain components from FSDT was conducted for the baseline plates. Figure 2.7 displays ϕ_x (Eq. (2.14c)), γ_{xz} (Eq. (2.18a)), slopes $(\partial w/\partial x)_{FSDT}$ (Eq. (2.17a)) and $(\partial w/\partial x)_{CLPT}$ (Eq. (2.19b)) at the xz plane of the cross-ply laminate (Figure 2.7a) and sandwich panel (Figure 2.7b). For the cross-ply laminate, $(\partial w/\partial x)_{CLPT}$ and $(\partial w/\partial x)_{FSDT}$ have identical linear behaviors with negative slopes, attaining maximum and minimum values of $\pm 130 \times 10^{-3}$ rad at panel ends. This agreement points out that the contribution of A_{44} and A_{55} to the rotations of stiff PTS composites is negligible, which is therefore dominated by D_{66} . It is also noticed that γ_{xz} vanishes. On the other hand, the rotation ϕ_x presents a linear behavior with equal magnitude but opposite signs to those obtained for $(\partial w/\partial x)_{CLPT}$ and $(\partial w/\partial x)_{FSDT}$, i.e., $\phi_x = -\partial w/\partial x$. This confirms that the current FSDT solution converges to CLPT when stiff materials are employed. Moreover, ϕ_x and $\partial w/\partial x$ fulfill the condition of symmetry of being zero at the center of the plate (Eqs. (2.4a) and (2.4c)).

Figure 2.7b shows that all transverse shear strain components keep linear trends along the normalized y/L_y axis, but with different values than those shown in Figure 2.7a. For this compliant-cored sandwich, $(\partial w/\partial x)_{FSDT}$ predicts values 5.43 times higher than $(\partial w/\partial x)_{CLPT}$, which indicates that the cross-section rotation in compliant PTS is mainly due to A_{44} and A_{55} . It is noticed that γ_{xz} can be estimated as the difference between $(\partial w/\partial x)_{FSDT}$ and $(\partial w/\partial x)_{CLPT}$. In other words, the shear contribution to the rotation is approximately $\gamma_{xz} \approx (\partial w/\partial x)_{FSDT} - (\partial w/\partial x)_{CLPT}$. Furthermore, γ_{xz} is 4.43 times larger than $(\partial w/\partial x)_{CLPT}$.

$\partial x)_{CLPT}$, which again points out its importance for compliant materials. As expected, ϕ_x results from the difference between γ_{xz} and $(\partial w/\partial x)_{FSDT}$.

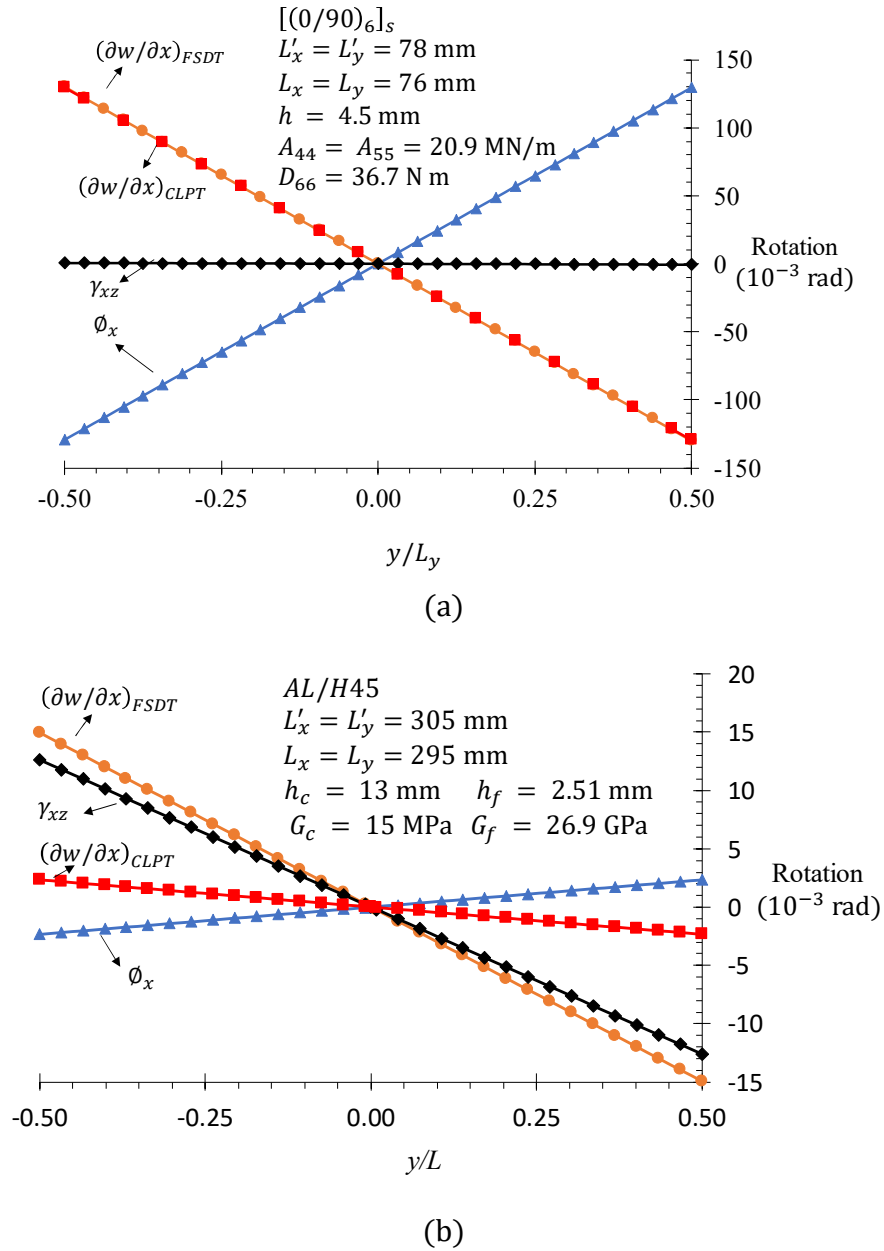
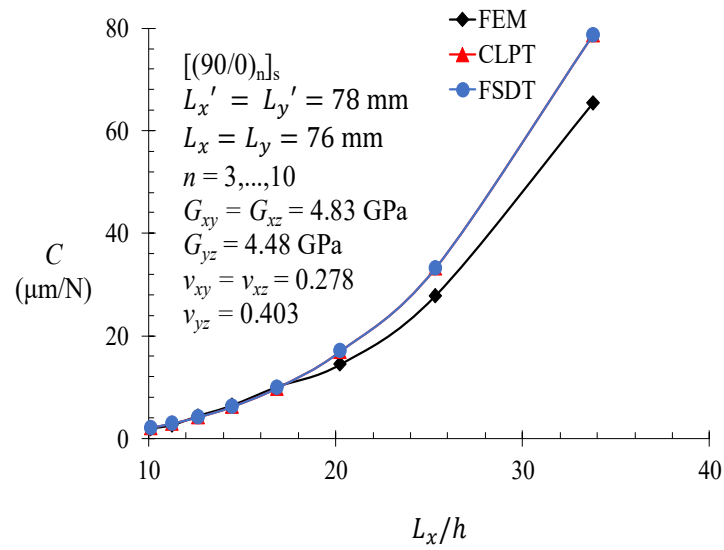


Figure 2.7. Rotation function ϕ_x , slope $(\partial w/\partial x)_{FSDT}$, slope $(\partial w/\partial x)_{CLPT}$ and transverse shear strain γ_{xz} at the xz plane for the (a) [(0/90)₆]_s laminate. (b) AL/H45 sandwich panel.

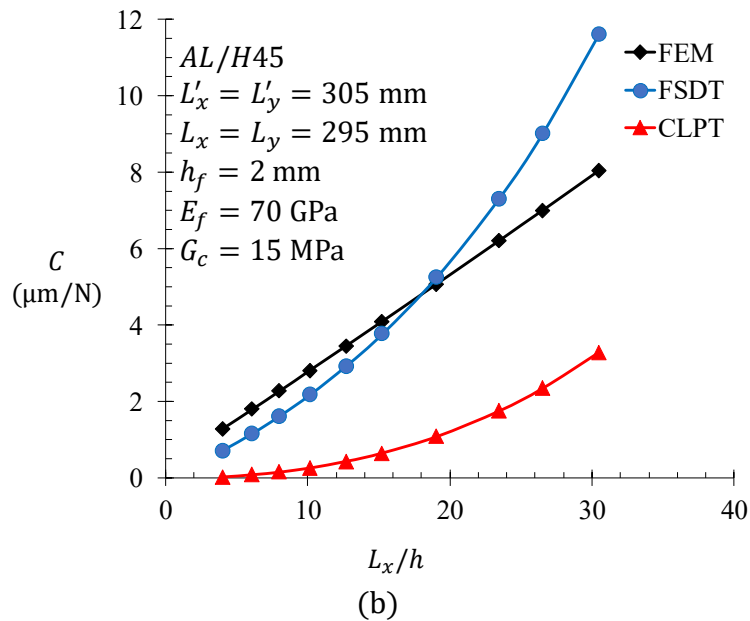
2.4.2 Parametric investigation

Since panel dimensions, orthotropy and stiffness strongly affect the deflections of the PTS, they are investigated here by using the FSDT solution. Figure 2.8 displays the compliance of square $[(0/90)_n]_s$ cross-ply composite laminates (Figure 2.8a) and AL/H45 sandwich panel (Figure 2.8b) with different length-to-thickness ratios (L_x/h). For cross-ply laminates, the total thickness h was increased by adding more (0/90) layers (with $h_i = 0.1875$ mm ply) to its stacking sequence, i.e., the subscript n varies from 3 to 10. Figure 2.8a shows that compliance predicted by FEM increases monotonically from $1.87 \mu\text{m/N}$ at $L_x/h = 10.1$ (thick plates) to $65.4 \mu\text{m/N}$ at $L_x/h = 33.8$ (thin plates). This is because A_{44} (and A_{55}) vary linearly with h , while D_{66} does it cubically. This means that for thick specimens, extensional stiffnesses A_{ij} dominate their bending response whereas for thin specimens, stiffnesses D_{ij} does, which is typically observed in the synclastic bending of thick beams [24, 47]. FSDT also predicts a monotonically rise in compliance from 2.15 to $78.8 \mu\text{m/N}$ in the $10.1 \leq L_x/h \leq 33.8$ range. For the majority of the L_x/h interval, good agreement is observed between C predicted by FEM and FSDT, although an exception is found at $L_x/h = 33.8$, where a difference of 20.5 % is attained. The CLPT solution predicts practically the same compliance values than FSDT for thick and thin plates. Consequently, both CLPT and FSDT approaches can be employed to predict deflections of stiff composite laminates in a wide range of L_x/h slender ratios.

For AL/H45 sandwich plates, Figure 2.8b, the compliance computed by FEM increases linearly from $1.30 \mu\text{m/N}$ for $L_x/h = 4.0$ to $8.05 \mu\text{m/N}$ for plates with $L_x/h = 30.5$. Likewise, the FSDT solution predicts a monotonically increasing behavior of compliance with respect to the L_x/h ratio. C increases from $0.73 \mu\text{m/N}$ at $L_x/h = 4.0$ to $11.6 \mu\text{m/N}$ when $L_x/h = 30.5$. For the $4.0 \leq L_x/h \leq 19.1$ range, FEM and FSDT predict similar C ; however, for extremely thin plates with compliant cores ($L_x/h = 30.5$), the FSDT approach overpredicts C , possibly because the transverse shear contribution dominates the deflection response in the FSDT formulation and/or the in-plane twist stiffness (D_{66}) plays h a minor role in this extreme case. Regardless of the aspect ratios of the compliant-cored sandwich plates shown in Figure 2.8b, CLPT largely underpredicts the compliance with respect to FEM and FSDT, since γ_{xz} is not considered in the CLPT formulation (see, Eq. (2.16)).



(a)



(b)

Figure 2.8. Effect of normalized side-length L_x/h on the compliance of square composites. (a) Cross-ply $[(0/90)_n]_s$ laminate. (b) AL/H45 sandwich panel.

Since FSDT and CLPT solutions strongly depend on G_{12} (due to D_{66}), an analysis of the in-plane shear modulus ratio between the face sheet and core (G_{12f}/G_{12c}) was conducted, keeping $G_{12f} = 29.6 \text{ MPa}$ fixed. Figure 2.9 illustrates the effect of G_{12f}/G_{12c} ratio on the

compliance of square sandwich panels with isotropic cores and face sheets. A close-up of C for $1 \leq G_{12f}/G_{12c} \leq 50$ is included in such a figure. The compliance predicted by FEM increases in a power law fashion from 0.075 to 0.184 $\mu\text{m}/\text{N}$ in the $1 \leq G_{12f}/G_{12c} \leq 10$ range. For G_{12f}/G_{12c} ratios higher than 10, a linear behavior with a positive slope is observed. This linear trend starts from 0.184 $\mu\text{m}/\text{N}$ at $G_{12f}/G_{12c} = 10$ to until 1.44 $\mu\text{m}/\text{N}$ at $G_{12f}/G_{12c} = 1000$. These two different compliance behaviors seem to indicate that D_{66} is the dominant stiffness for $G_{12f}/G_{12c} < 10$, whereas A_{44} and A_{55} control the plate deflection for $G_{12f}/G_{12c} > 10$. Similarly, the FSDT approach predicts a compliance that rises from 0.048 to 0.141 $\mu\text{m}/\text{N}$ in a power law form between $1 \leq G_{12f}/G_{12c} \leq 10$. Larger ratios of G_{12f}/G_{12c} yield a linear growth in compliance, increasing from 0.141 to 0.985 $\mu\text{m}/\text{N}$ for $10 \leq G_{12f}/G_{12c} \leq 1000$. However, these FSDT predictions of C are slightly lower than those by FEM, possibly due to the shear corrected factor employed, which may not be constant in this case due to the high G_{12f}/G_{12c} mismatch between plies. This agrees with the examples of Birman and Bert [39], who pointed out that K approaches to zero as the G_f/G_c ratio increases, which would increase C . Also, the distributions of Q_x and Q_y (Eqs. (2.2b) and (2.2c)) assumed uniform may not be adequate and high order shear deformation theory may be needed for such extremely flexible sandwich cores. On the other hand, CLPT highly underestimates C for the $10 \leq G_{12f}/G_{12c} \leq 1000$ range. This confirms that for the $1 \leq G_{12f}/G_{12c} \leq 10$ range, the D_{66} stiffness dominates the elastic response of the PTS and for the $10 \leq G_{12f}/G_{12c} \leq 1000$ interval the $A_{44}(= A_{55})$ stiffness dominates.

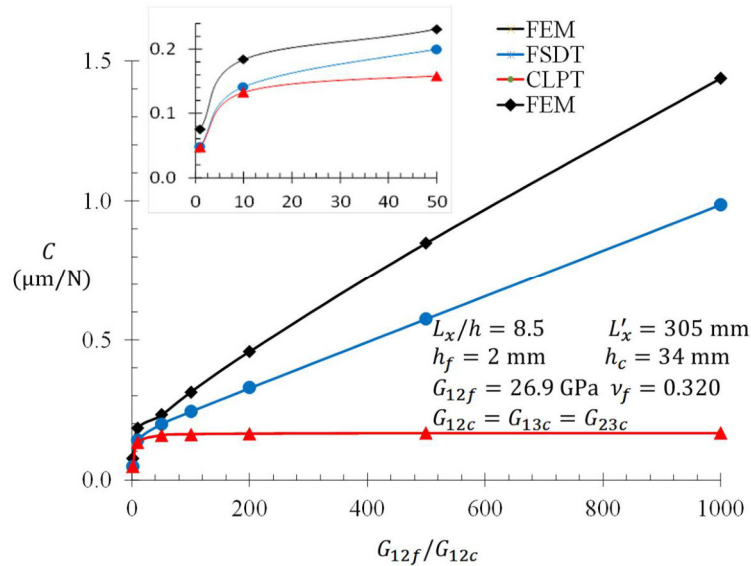


Figure 2.9. Effect of the ratio between in-plane shear stiffness of the face sheet and core (G_{12f}/G_{12c}) on the compliance of square sandwich twist panels.

The effect of variations in the anisotropy of cross-ply laminates is analyzed in Figure 2.10 by plotting their G_{23}/G_{12} shear stiffness ratio against the plate compliance. It is observed that all approaches predict practically constant values of their corresponding compliances for the $1 \leq G_{23}/G_{12} \leq 5$ interval. This points out that for stiff cross-ply laminates, slight differences between G_{12} and G_{23} do not affect significantly the deflections of the PTS. FEM predicts compliance values from 1.10 to 1.04 $\mu\text{m}/\text{N}$, whereas FSDT and CLPT predict C values between 1.25 and 1.23 $\mu\text{m}/\text{N}$, i.e., a 13 % difference between plate theories and FEM predictions. This indicates that FSDT and CLPT solutions are suitable to estimate the compliance of cross-ply laminates with moderated G_{23}/G_{12} ratios.

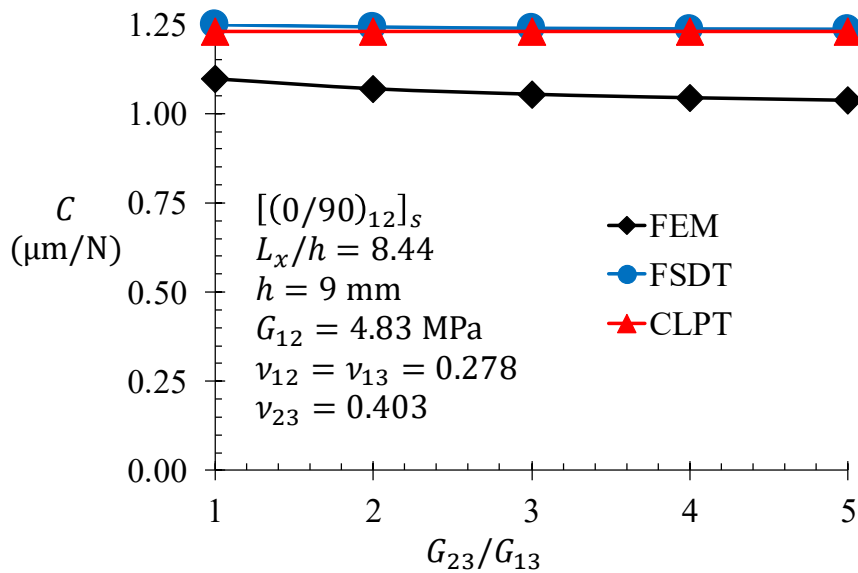


Figure 2.10. Effect of G_{23}/G_{12} shear stiffness ratio on the compliance of cross-ply laminates.

The compliance of $[(0/90)_{12}]_s$ laminates is plotted versus their width/length ratio (L_x/L_y) in Figure 2.11. FEM predicts a 1.16 $\mu\text{m}/\text{N}$ compliance for square specimens ($L_x/L_y = 1$), and as the L_x/L_y ratio enhances, C diminishes monotonically to $\sim 0.24 \mu\text{m}/\text{N}$ for $L_x/L_y = 10$ (slender rectangular specimens). This is due to the second moment of inertia of the plate cross-sections, which is high for large L_x/L_y ratios and low for small L_x/L_y ratios. The FSDT is in very good agreement with FEM for all ratios, while the CLPT diverges for $L_x/L_y > 4$.

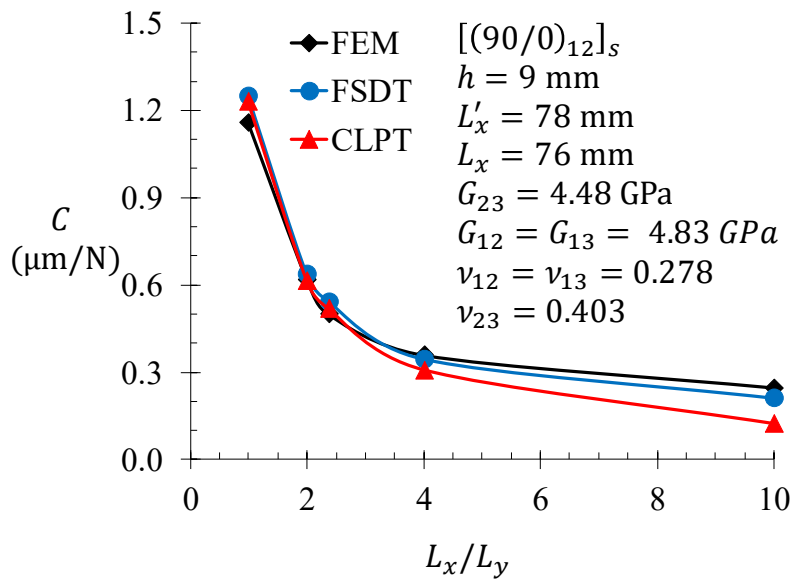


Figure 2.11. Effect of in-plane aspect ratio L_x/L_y in the compliance of $[(0/90)_{12}]_s$ laminates.

2.4.3 Comparison with experiments

Table 2.2 lists the compliance of several monolithic and composite plates measured and predicted by previous works using FEM and CLPT and those predicted by the FSDT solution, Eq. (2.15b). For almost all 14 panels analyzed, good agreement is observed between the compliance measured and that predicted by FSDT. This agreement covers a wide range of materials, from very stiff materials like metals and Maple plywoods [11], moderate stiff sandwich panels like “H200/Thick” [17] to moderate compliant sandwich plates like “AL/H100” [42]. In general, the compliance computed by FEM also agrees well with that measured. Consistently, the CLPT approach underestimates the compliance for moderate and very compliant materials, while it predicts it well for stiff materials.

Table 2.2. Compliance, measured and predicted by other authors and by the current FSDT solution [16, 17, 42] in ($\mu\text{m}/\text{N}$) and [11] in (10^{-4} in/Lb).

Reference	Panel	Previously reported			Eq. (2.15b)	Difference (%)
		EXP	CLPT	FEM	FSDT	$\left(1 - \frac{\text{FSDT}}{\text{EXP}}\right) 100$
Avilés et al. [17]	H80/Thin	4.26	1.42	3.56	3.44	19.2
	H100/Thick1	2.85	0.85	2.23	2.31	18.9
	H200/Thin	2.51	1.42	2.16	2.15	14.3
	H200/Thick	1.82	0.85	1.56	1.59	12.6
Avilés et al. [42]	Al/H45	4.45	0.71	----	4.56	-2.47
	Al/H100	2.85	0.84	----	2.51	11.9
	Al/H200	1.82	0.89	----	1.6	12.1
Avilés et al. [16]	G-VE/PW	1.43	1.55	----	1.66	-16.1
	G-VE/H45	2.82	0.27	----	2.11	25.2
Hearmon and Adams [11]	Maple Plywood (1)	30.7-36.5	----	----	31.8*	5.36
	Maple Plywood (2)	31.0-31.5	----	----	32.7*	-4.64
	Aluminum	5.8-6.0	----	----	6.03*	-2.2
	Brass	4.4-4.6	----	----	4.55*	-1.11
	Mild steel	8.6-9.4	----	----	8.96*	0.44

* FSDT equation is divided by 2 here because the maximum deflection measured in [11] is taken from the plate center to one loading point, i.e., half the displacement between pin support and loading point. "EXP" stands for experiment.

2.5 Conclusions

A closed-form solution based on FSDT has been developed for the PTS. As a reference, the PTS was also analyzed by the FEM and a previously reported solution based on CLPT. A parametric analysis was conducted by employing two baseline materials, viz. a $[(0/90)_6]_s$ cross-ply laminate made of a unidirectional glass/epoxy prepreg and a sandwich panel with aluminum face sheets and PVC foam core. The results indicate that FSDT solution is suitable to predict the transverse deflections of thick specially orthotropic PTS sandwich and laminated composite materials. Analysis of the transverse shear distributions showed that the FSDT approach predicts similar mid-plane transverse shear strains of sandwich panels with compliant cores, with respect to FEM. The analysis of plate size revealed that the FSDT approach properly predicts the compliance of square and rectangular plates ($1 \leq \text{width/length} \leq 10$), thick ($4.0 \leq \text{length/thickness} \leq 8.5$) and thin plates ($8.5 \leq \text{length/thickness} \leq 19.1$). It was also noticed that moderate changes in the transverse shear to in-plane shear moduli ratio (G_{23}/G_{12}) do not significantly affect the accuracy of the FSDT compliance for $1 \leq G_{23}/G_{12} \leq 5$. On the other hand, for sandwich panels with large differences between in-plane shear modulus of the face sheet and core ($G_{12f}/G_{12c} \geq 200$), FSDT underpredicts the compliance ($\sim 40\%$ for $G_{12f}/G_{12c} = 200$) with respect to FEM. Comparison between the FSDT predicted compliance and that previously measured in previous works yielded good agreement for specially orthotropic sandwich panels and Maple plywoods. The proposed FSDT closed-form solution is adequate for stiff and compliant specially orthotropic sandwich and laminated composite materials of moderate compliance with dimensions $1 \leq \text{width/length} \leq 10$ and $4 \leq \text{length/thickness} \leq 19$. Moreover, it is simple and rather accurate, and contributes to the existent knowledge of the PTS. Thus, this solution can be widely applied in the analysis and design of shear deformable specially orthotropic laminates and sandwich panels loaded in torsion, to predict in-plane and transverse shear moduli of face sheets and cores. The proposed solution may also assist in future developments of shear stress analysis of plates with mid-plane cracks under twisting loads.

Chapter III. A closed-form solution for anticlastic bending of laminated composite plates

3.1 Introduction

Laminated composites plates and sandwich panels are widely employed in structural applications where a high stiffness/weight ratio is need. These structures may experience torsion and/or bending during their life-time, as part of wind turbine blades, helicopter rotors, composite shafts, airplanes, and naval structures, among others [7, 24, 40]. Torsion and/or bending loads may lead to a deformed anticlastic surface, which is characterized by having two curvatures with opposite sign at a given point, curved convexly along the longitudinal plane and concavely along the perpendicular section [62]. Investigation about anticlastic bending is important because is a fundamental case of pure bending mentioned in elementary theory of plates [12, 63], being the other fundamental case synclastic bending. Both represent extreme cases, which other general bending loading may be theoretically decomposed in. Pure anticlastic bending is produced if solely twisting moments are uniformly distributed (constants) along the edges of a plate [12]. To achieve this strict condition on thin isotropic plates, Lord Kelvin and Tait in 1883 [64] proposed an statically equivalent replacement of twisting couples at the edges of the plate by two downward concentrated forces at diagonally opposite corners and two upward concentrated forces at the remaining corners. Nowadays, a plate under this antisymmetric loading is named the plate twist specimen (PTS) [9, 10]. In the PTS, each concentrated force bears half of the applied force ($P/2$) yielding a constant $P/4$ twisting moment per unit length (M_{xy}) along the edges of the thin plate [12, 64], i.e. $M_{xy} = P/4$. However, the limits of applicability of this condition on compliant materials and/or thick laminated and sandwich plates have not yet been studied. In 1925, Nádai conducted experiments using the PTS, verifying the elementary solution of anticlastic bending for thin homogeneous plates [19]. Because of the simplicity and accuracy of the PTS, it has been standardized to measure the in-plane shear modulus of plywood panels and unidirectional fiber-reinforced plastic composites [9, 10]. The use of the PTS has also been extended to measure diverse elastic properties and strengths of orthotropic laminated composites. Vinson [6] determined the in-plane shear strength of the face sheets of an aluminum/PVC foam core sandwich panel. To achieve that, Vinson [6] developed a solution for the deflection based on the Ritz method. Tsai [44] used the original PTS configuration to measure the bending and twisting compliances ($S_{66}, S_{11}, S_{12}, S_{22}$) of unidirectional glass epoxy composites; a similar work was developed by Hearmon and Adams [11, 43] to measure the compliances of aluminum, brass, mild steels and plywood plates obtaining good correlation between the measurements and predicted values of bending and twisting stiffnesses in metals and plywoods. Avilés et al. [17] used the Classical Laminated Plate Theory (CLPT) to determine the twisting stiffness (D_{66}) of thin sandwich panels, concluding that such a theory is no appropriate to determine D_{66} . Later, Avilés et al. [42] developed a semi-empirical shear correct formulation for the PTS applied to sandwich panels in order to measure the out-of-plane shear modulus (G_{23}) of the core [16]. Most solutions of the PTS have been developed under the assumptions of CLPT, and only a few works have analytically predicted the elastic response of compliant and/or thick plates under anticlastic bending using higher order theories than CLPT [45, 46, 65]. Hernández-Pérez et al. [45] proposed a solution

for thick PTS using First-Order Shear Deformation Theory (FSDT) and Fourier series. This last solution considered the shear effects and is applicable to compliant-core sandwich materials where the shear contribution is important, but in practice, it may not be easy to implement as a standard reduction model due to the absence of a closed-form. Elmalich and Rabinovitch [46] derived a geometrically nonlinear extended high-order sandwich theory to study the twist behavior of soft-core sandwich plates considering all stiffness components of the core, its Poisson's effect and the direct contribution of the in-plane shear stresses in the core to the twist rigidity. Their theory was implemented in FEM concluding that the in-plane normal and in-plane shear stiffnesses of the core do not have an important contribution to the twist rigidity. More recently, a FSDT solution of the PTS was presented in [65], considering shear effects and obtaining closed-form solutions for rotations and deflection of thick specially orthotropic plates. This solution, however, considers a constant shear correction factor $K = 2/3$ and twisting moment $M_{xy} = P/4$, which brings some limitations in its application range, resulting convenient only to sandwich plates with ratios of $G_{12f}/G_{12c} < 100$ and to cross-ply laminates with moderate G_{23}/G_{12} ratios, less than 5. Although M_{xy} has been recognized as the main driving-load to yield anticlastic bending [12, 64], there is no assessment of the uniformity of the $M_{xy} = P/4$ condition for compliant materials and/or thick plates. In addition, scarce studies and closed-form solutions (only one) have been developed on such specimen despite the importance of the anticlastic bending as a fundamental case of pure bending [65]. Thus, this work examines the M_{xy} distributions of the PTS by FEM and develops an approximate closed-form solution based on FSDT and the Ritz method for the deflection and rotations of anticlastic bending of laminated composite plates, considering both M_{xy} and the shear correction factors as functions of the material system. This solution is expected to assist on the determination of elastic (transverse shear) properties of laminated composites by PTS, and it could probably serve as a stepping stone for fracture mechanics solutions of mode III loading [18].

3.2 First-order shear deformation theory

3.2.1 Kinematics

FSDT extends the kinematics of CLPT by considering the effect of transverse shear deformation on the plate deflections [3], which becomes important for thick plates and compliant materials [4]. As other plate theories, FSDT assumes perfect bonding between the constituent materials, continuous and linear elastic materials, no extension along the thickness, small displacements, small rotations and deformations [3]. To determine the strain field by FSDT, three displacement (u , v and w) and two rotation functions (ϕ_x and ϕ_y) need to be specified [3]. Here u , v and w represent displacements along the x , y and z directions, respectively, i.e.,

$$u = u_0(x, y) + z \phi_x(x, y) \quad (3.1a)$$

$$v = v_0(x, y) + z \phi_y(x, y) \quad (3.1b)$$

$$w = w_0(x, y) \quad (3.1c)$$

where subscript 0 is referred to the mid-plane (at $z = 0$) of the plate, see Figure 1a. The functions ϕ_x and ϕ_y denote mid-plane rotations along the x and y axes, representing the difference between transverse shear strains and slopes of the deflection w along such axes [3, 4], and are of major relevance in this model,

$$\phi_x = \gamma_{xz} - \frac{\partial w}{\partial x}; \quad \phi_y = \gamma_{yz} - \frac{\partial w}{\partial y} \quad (3.2a-b)$$

where γ_{xz} and γ_{yz} are the transverse shear strains at planes xz and yz . Accordingly, the curvatures are defined in FSDT as,

$$\kappa_x = \frac{\partial \phi_x}{\partial x}; \quad \kappa_y = \frac{\partial \phi_y}{\partial y}; \quad \kappa_{xy} = \frac{\partial \phi_x}{\partial y} + \frac{\partial \phi_y}{\partial x} \quad (3.3a-c)$$

being κ_x and κ_y the bending curvatures along x and y axes, whereas κ_{xy} is the twisting curvature.

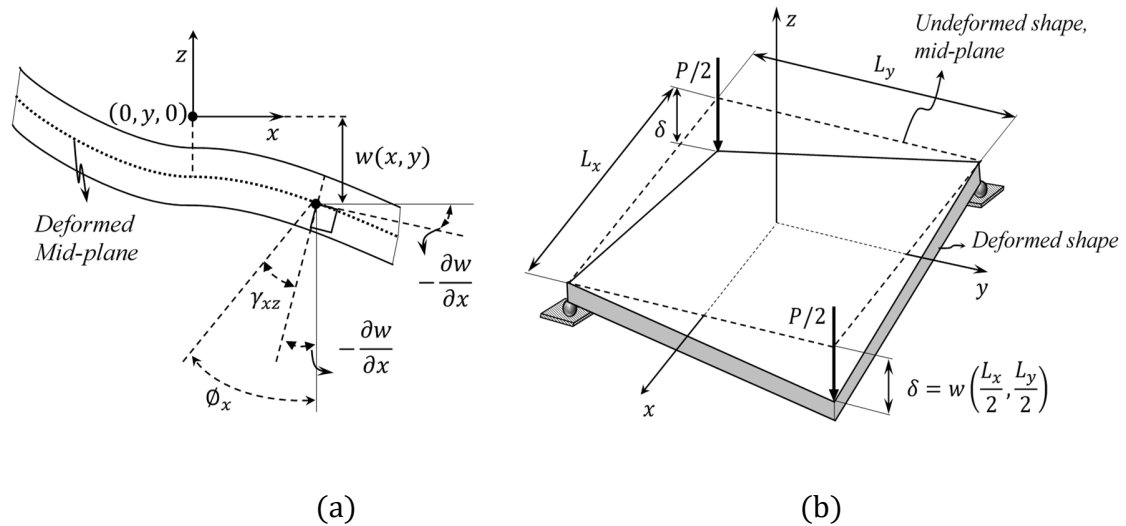


Figure 3.1. Schematic of the PTS. (a) Representation of rotations ϕ_x , slopes $\partial w/\partial x$ and transverse shear strains γ_{xz} . (b) Isometric view.

3.2.2 Governing differential equations

By neglecting all in-plane forces in FSDT (i.e. considering only moment resultants and transverse forces along z axis), the equilibrium equations of a specially orthotropic plate are given by [3, 5, 40, 47],

$$D_{11} \frac{\partial^2 \phi_x}{\partial x^2} + D_{12} \frac{\partial^2 \phi_y}{\partial y \partial x} + D_{66} \left(\frac{\partial^2 \phi_x}{\partial y^2} + \frac{\partial^2 \phi_y}{\partial x \partial y} \right) - K_{22} A_{55} \left(\frac{\partial w}{\partial x} + \phi_x \right) = 0 \quad (3.4a)$$

$$D_{22} \frac{\partial^2 \phi_y}{\partial y^2} + D_{12} \frac{\partial^2 \phi_x}{\partial x \partial y} + D_{66} \left(\frac{\partial^2 \phi_y}{\partial x^2} + \frac{\partial^2 \phi_x}{\partial y \partial x} \right) - K_{11} A_{44} \left(\frac{\partial w}{\partial y} + \phi_y \right) = 0 \quad (3.4b)$$

$$\left(\frac{\partial^2 w}{\partial x^2} + \frac{\partial \phi_x}{\partial x} \right) K_{22} A_{55} + \left(\frac{\partial^2 w}{\partial y^2} + \frac{\partial \phi_y}{\partial y} \right) K_{11} A_{44} + q = 0 \quad (3.4c)$$

Here q represents the load per unit of area (pressure) acting along z direction over the plate. D_{ij} ($i, j = 1, 2, 6$) are the bending stiffnesses and A_{ij} ($i, j = 4, 5$) are the transverse shear stiffnesses of the plate [40]. K_{11} and K_{22} denote the shear correction factors for the planes yz and xz (respectively), which compensate the difference between the real γ_{yz} and γ_{xz} distributions and the constant distributions assumed by FSDT. Herein, K_{11} and K_{22} are calculated for each material system according to the methodology developed by Chow [34], which is summarized in Appendix B. This means that conventional constant values such as $1, 5/6, 2/3$ and $\pi^2/12$ are not assumed upfront for K_{11} and K_{22} [47]. In theory of plates, the pressure q is expressed in terms of moment resultants as [3, 63],

$$q = - \left(\frac{\partial^2 M_x}{\partial x^2} + 2 \frac{\partial^2 M_{xy}}{\partial x \partial y} + \frac{\partial^2 M_y}{\partial y^2} \right) \quad (3.5)$$

where M_x and M_y correspond to the bending moments per unit length along x and y axes. According to FSDT, the moment resultants for a specially orthotropic plate are given by [3],

$$M_x = D_{11} \left(\frac{\partial \phi_x}{\partial x} \right) + D_{12} \left(\frac{\partial \phi_y}{\partial y} \right); \quad M_y = D_{12} \left(\frac{\partial \phi_x}{\partial x} \right) + D_{22} \left(\frac{\partial \phi_y}{\partial y} \right) \quad (3.6a-b)$$

$$M_{xy} = D_{66} \left(\frac{\partial \phi_x}{\partial y} + \frac{\partial \phi_y}{\partial x} \right) \quad (3.6c)$$

By substituting Eq. (3.6) into (3.5) and then Eq. (3.5) into (3.4c), the equilibrium Eq. (3.4c) becomes,

$$\begin{aligned} & \left(\frac{\partial^2 w}{\partial x^2} + \frac{\partial \phi_x}{\partial x} \right) K_{22} A_{55} + \left(\frac{\partial^2 w}{\partial y^2} + \frac{\partial \phi_y}{\partial y} \right) K_{11} A_{44} \\ & = D_{11} \frac{\partial^3 \phi_x}{\partial x^3} + D_{12} \frac{\partial^3 \phi_y}{\partial y^3} + (D_{12} + 2D_{66}) \left(\frac{\partial^3 \phi_x}{\partial y^2 \partial x} + \frac{\partial^3 \phi_y}{\partial x^2 \partial y} \right) \end{aligned} \quad (3.7)$$

Equations (3.4a – b) and (3.7) are the governing differential equations of the anticlastic bending problem, which are third-order partial differential equations on the variables ϕ_x and ϕ_y and second-order on w .

3.3 Plate twist solution

3.3.1 Boundary conditions

Anticlastic bending of a rectangular plate is induced here by using the PTS, see Figure 1b. The rectangular plate has side-lengths L_x and L_y , and thickness h . To obtain a solution for the PTS the boundary conditions discussed in this section are enforced. According to Figure 1b, w is zero at the pin supports, i.e.,

$$w \left(\pm \frac{L_x}{2}, \mp \frac{L_y}{2} \right) = 0 \quad (3.8)$$

Since the anticlastic deformed shape is symmetric with respect to the x and y axes, it is expected that the slopes $\partial w / \partial x$, $\partial w / \partial y$ and rotations ϕ_x and ϕ_y vanish at the center of the plate,

$$\frac{\partial w}{\partial x}(0,0) = 0; \quad \frac{\partial w}{\partial y}(0,0) = 0 \quad (3.9a-b)$$

$$\phi_x(0,0) = 0; \quad \phi_y(0,0) = 0 \quad (3.10a-b)$$

Timoshenko and Woinowsky-Krieger [12] point out that w vanishes along the center lines of a four-point loaded thin PTS. Since this work addresses a PTS with two pin supports and two concentrated forces (Figure 1b), it is then assumed that w remains constant along the axes of symmetry of the anticlastic shape, i.e.,

$$w(x, 0) = w(0, y) = C_0 \quad (3.11a)$$

This is a condition of symmetry that will be evaluated and validated with FEM for flexible and stiff plates, and will be further discussed in the results section. Given this condition, the rate of change of Eq. (3.11a) is zero along the x and y directions, i.e.,

$$\frac{\partial w}{\partial x}(x, 0) = 0; \quad \frac{\partial w}{\partial y}(0, y) = 0 \quad (3.11b)$$

Equations (3.8)-(3.11) constitute the essential boundary conditions of the PTS.

3.3.2 Closed-form polynomial solution

In order to satisfy the FSDT governing equations, Eqs. (3.4a – b) and (3.7), and fulfill the essential boundary conditions of the anticlastic bending problem, Eqs. (3.8)-(3.11), algebraic polynomials for the deflection w , and rotations ϕ_x and ϕ_y are proposed. Using algebraic polynomials keeps the mathematical problem analytically tractable and consequently the solution has a closed-form, which greatly facilitates its implementation by other authors. Differentiating Eq. (3.2a) with respect to x and Eq. (3.2b) with respect to y , the transverse shear strains become,

$$\frac{\partial \gamma_{xz}}{\partial y} = \frac{\partial^2 w}{\partial y \partial x} + \frac{\partial \phi_x}{\partial y}; \quad \frac{\partial \gamma_{yz}}{\partial x} = \frac{\partial^2 w}{\partial x \partial y} + \frac{\partial \phi_y}{\partial x} \quad (3.12a-b)$$

Since w is assumed to be a continuous and well-behaved function, the sequence of its second derivative does not matter ($\partial^2 w / \partial x \partial y = \partial^2 w / \partial y \partial x$) which yields,

$$\frac{\partial^2 w}{\partial x \partial y} = \frac{\partial}{\partial y}(\gamma_{xz} - \phi_x) = \frac{\partial}{\partial x}(\gamma_{yz} - \phi_y) \quad (3.13)$$

Mathematically, the above equation implies three possible cases, but only one is physically plausible. The first case is the trivial one,

$$\gamma_{xz} = \phi_x \quad ; \quad \gamma_{yz} = \phi_y \quad (3.14a-b)$$

Eqs. (3.14a – b) are discarded because they mean that w is constant along whole mid-plane ($\partial w / \partial x = \partial w / \partial y = 0$, see Eq. (3.2)), which would not yield the anticlastic shape. The second case is,

$$\frac{\partial \gamma_{xz}}{\partial y} = -\frac{\partial \phi_y}{\partial x} \quad ; \quad \frac{\partial \gamma_{yz}}{\partial x} = -\frac{\partial \phi_x}{\partial y} \quad (3.14c-d)$$

Substituting Eqs. (3.14c – d) into (3.12a) or (3.12b) yields $-\partial w^2 / \partial x \partial y = \partial \phi_x / \partial y + \partial \phi_y / \partial x$, which according to Eq. (3.3c) is the definition of κ_{xy} by FSDT. Therefore, Eqs. (3.14c – d) imply that $\kappa_{xy} = -\partial w^2 / \partial x \partial y$, which is half of the twisting curvature defined by CLPT [40]. This would mean that transverse shear strains yield exactly half of the

anticlastic curvature all the time, which is numerically impossible in actual tests. Hence, this second condition is also discarded. The third case is,

$$\frac{\partial \gamma_{xz}}{\partial y} = \frac{\partial \gamma_{yz}}{\partial x} \quad ; \quad \frac{\partial \phi_x}{\partial y} = \frac{\partial \phi_y}{\partial x} \quad (3.14e-f)$$

which represents a general valid case where shear strains and rotations are continuous and vary along the x and y axes. Integrating Eq. (3.14f) with respect to x and solving for ϕ_y

$$\phi_y = \int \frac{\partial \phi_x}{\partial y} dx \quad (3.15a)$$

Integrating Eq. (3.14e) with respect to x and solving for γ_{yz}

$$\gamma_{yz} = \int \frac{\partial \gamma_{xz}}{\partial y} dx \quad (3.15b)$$

According to Eqs. (3.15), only polynomials for ϕ_x and γ_{xz} need to be specified. In order to produce a closed-form solution, fifth- and third-order algebraic polynomials are proposed herein for ϕ_x and γ_{xz} , viz.,

$$\phi_x = B_1y + B_2xy + B_3y^2 + B_4x^2y + B_5xy^2 + B_6y^3 + B_7x^3y + B_8x^2y^2 + B_9xy^3 + B_{10}y^4 + B_{11}x^4y + B_{12}x^3y^2 + B_{13}x^2y^3 + B_{14}xy^4 + B_{15}y^5 \quad (3.16a)$$

$$\gamma_{xz} = C_1y + C_2xy + C_3y^2 + C_4x^2y + C_5xy^2 + C_6y^3 \quad (3.16b)$$

The deflection w can be determined by integrating the slope $\partial w / \partial x$ of Eq. (3.2a) with respect to x , i.e.,

$$w = \int \gamma_{xz} dx - \int \phi_x dx = B_1yx + \frac{B_2x^2y}{2} + B_3y^2x + \frac{B_4x^3y}{3} + \frac{B_5x^2y^2}{2} + B_6y^3x + \frac{B_7x^4y}{4} + \frac{B_8x^3y^2}{3} + \frac{B_9x^2y^3}{2} + B_{10}y^4x + \frac{B_{11}x^5y}{5} + \frac{B_{12}x^4y^2}{4} + \frac{B_{13}x^3y^3}{3} + \frac{B_{14}x^2y^4}{2} + B_{15}y^5x - C_1yx - \frac{C_2x^2y}{2} - C_3y^2x - \frac{C_4x^3y}{3} - \frac{C_5x^2y^2}{2} - C_6y^3x + C_o \quad (3.16c)$$

Substituting Eq. (3.16a) into (3.15a) yields,

$$\phi_y = B_1x + \frac{1}{2}B_2x^2 + 2B_3yx + \frac{1}{3}B_4x^3 + B_5x^2y + 3B_6y^2x + \frac{1}{4}B_7x^4 + \frac{2}{3}B_8x^3y + \frac{3}{2}B_9x^2y^2 + 4B_{10}y^3x + \frac{1}{5}B_{11}x^5 + \frac{1}{2}B_{12}x^4y + B_{13}x^3y^2 + 2B_{14}x^2y^3 + 5B_{15}y^4x \quad (3.17a)$$

Substituting Eq. (3.16b) into (3.15b) yields,

$$\gamma_{yz} = C_1x + \frac{1}{2}C_2x^2 + 2C_3yx + \frac{1}{3}C_4x^3 + C_5x^2y + 3C_6y^2x \quad (3.17b)$$

Substituting Eqs. (3.16b), (3.16a) and (3.17a) into (3.4a) yields,

$$\begin{aligned} &K_{22}A_{55}(C_6y^3 + C_4x^2y + C_5xy^2 + C_2xy + C_3y^2 + C_1y) = \\ &D_{11}(12B_{11}x^2y + 6B_{12}xy^2 + 2B_{13}y^3 + 6B_7xy + 2B_8y^2 + 2B_4y) \\ &+ D_{12}(2B_{12}x^3 + 6B_{13}x^2y + 12B_{14}xy^2 + 20B_{15}y^3 + 2B_8x^2 + 6B_9xy \\ &+ 12B_{10}y^2 + 6B_6y + 2B_5x + 2B_3) \\ &+ D_{66}(4B_{12}x^3 + 12B_{13}x^2y + 24B_{14}xy^2 + 40B_{15}y^3 + 4B_8x^2 + 12B_9xy \\ &+ 24B_{10}y^2 + 12B_6y + 4B_5x + 4B_3) \end{aligned} \quad (3.18a)$$

Substituting Eqs. (3.17b), (3.16a) and (3.17a) into (3.4b) yields,

$$\begin{aligned} &K_{11}A_{44} \left(3C_6y^2x + \frac{1}{3}C_4x^3 + C_5x^2y + \frac{1}{2}C_2x^2 + 2C_3yx + C_1x \right) = \\ &D_{22}(2B_{13}x^3 + 12B_{14}x^2y + 60B_{15}xy^2 + 3B_9x^2 + 24B_{10}xy + 6B_6x) \\ &+ D_{12}(4B_{11}x^3 + 6B_{12}x^2y + 6B_{13}xy^2 + 4B_{14}y^3 + 3B_7x^2 + 4B_8xy + 3B_9y^2 \\ &+ 2B_4x + 2B_5y + B_2) \\ &+ D_{66}(8B_{11}x^3 + 12B_{12}x^2y + 12B_{13}xy^2 + 8B_{14}y^3 + 6B_7x^2 + 8B_8xy \\ &+ 6B_9y^2 + 4B_4x + 4B_5y + 2B_3) \end{aligned} \quad (3.18b)$$

From Eqs. (3.18), the following system of equations are formed,

$$C_2 = C_3 = C_5 = B_2 = B_3 = B_5 = B_7 = B_8 = B_9 = B_{10} = B_{12} = B_{14} = 0 \quad (3.19a)$$

$$3A_{44}K_{11}C_6 + A_{55}K_{22}C_4 - 12D_{11}B_{11} - 12(D_{12} + 2D_{66})B_{13} - 60D_{22}B_{15} = 0 \quad (3.19b)$$

$$K_{22}A_{55}C_4 = 12D_{11}B_{11} + 6(D_{12} + 2D_{66})B_{13} \quad (3.19c)$$

$$K_{22}A_{55}C_6 = 2D_{11}B_{13} + 20(D_{12} + 2D_{66})B_{15} \quad (3.19d)$$

$$K_{22}A_{55}C_1 = 2D_{11}B_4 + 6(D_{12} + 2D_{66})B_6 \quad (3.19e)$$

$$K_{11}A_{44}C_4 = 6D_{22}B_{13} + 12(D_{12} + 2D_{66})B_{11} \quad (3.19f)$$

$$K_{11}A_{44}C_6 = 20D_{22}B_{15} + 2(D_{12} + 2D_{66})B_{13} \quad (3.19g)$$

$$K_{11}A_{44}C_1 = 6D_{22}B_6 + 2(D_{12} + 2D_{66})B_4 \quad (3.19h)$$

Equations (3.19b) – (3.19h) represent a system of 7 equations with 8 unknown constants ($B_4, B_6, B_{11}, B_{13}, B_{15}, C_1, C_4, C_6$). Moreover, the constant B_1 does not appear in Eqs. (3.19), since it vanishes when conducting the derivatives of \emptyset_x and \emptyset_y in the right-hand side of Eqs. (3.4a) and (3.4b). To solve this problem, the Ritz method [35, 40] (theorem of minimum potential energy) is employed to create two additional equations to determine C_1 (arbitrarily chosen) and B_1 . According to FSDT, the potential energy (V) of the plate is given by [3, 40],

$$\begin{aligned}
V = \int_{-L_x/2}^{L_x/2} \int_{-L_y/2}^{L_y/2} & \left[\frac{D_{11}}{2} \left(\frac{\partial \phi_x}{\partial x} \right)^2 + D_{12} \frac{\partial \phi_y}{\partial y} \frac{\partial \phi_x}{\partial x} + \frac{D_{22}}{2} \left(\frac{\partial \phi_y}{\partial y} \right)^2 + K_{22} A_{55} \left(\frac{\phi_x^2}{2} + \phi_x \frac{\partial w}{\partial x} + \right. \right. \\
& \left. \left. \frac{1}{2} \left(\frac{\partial w}{\partial x} \right)^2 \right) + K_{11} A_{44} \left(\frac{\phi_y^2}{2} + \phi_y \frac{\partial w}{\partial y} + \frac{1}{2} \left(\frac{\partial w}{\partial y} \right)^2 \right) + D_{66} \left(\frac{1}{2} \left(\frac{\partial \phi_x}{\partial y} \right)^2 + \frac{\partial \phi_x}{\partial y} \frac{\partial \phi_y}{\partial x} + \frac{1}{2} \left(\frac{\partial \phi_y}{\partial x} \right)^2 \right) \right] + \\
& \frac{P}{2} w \left(\frac{L_x}{2}, \frac{L_y}{2} \right) + \frac{P}{2} w \left(-\frac{L_x}{2}, -\frac{L_y}{2} \right) - \frac{P}{2} w \left(\frac{L_x}{2}, -\frac{L_y}{2} \right) - \frac{P}{2} w \left(-\frac{L_x}{2}, \frac{L_y}{2} \right)
\end{aligned} \tag{3.20}$$

To determine the constants C_1 and B_1 , V is minimized separately with respect to those unknowns,

$$\frac{\partial V}{\partial C_1} = 0 \tag{3.21a}$$

$$\frac{\partial V}{\partial B_1} = 0 \tag{3.21b}$$

After performing Eqs. (3.21), Eqs. (3.19b)-(3.19h) and (3.21) are solved altogether to determine the unknowns constants, yielding

$$B_{11} = B_{13} = B_{15} = C_4 = C_6 = 0 \tag{3.22a}$$

$$C_1 = -\frac{6P}{L_x^2 K_{11} A_{44} + L_y^2 K_{22} A_{55}} \tag{3.22b}$$

$$B_1 = \left(\frac{1}{8D_{66}} + \frac{L_y^2 S_2 - L_x^2 S_1}{4S} \right) P \tag{3.22c}$$

$$B_4 = \frac{3S_1 P}{S} \tag{3.22d}$$

$$B_6 = -\frac{S_2 P}{S} \tag{3.22f}$$

where,

$$S_1 = K_{11} A_{44} (D_{12} + 2D_{66}) - K_{22} A_{55} D_{22}; \tag{3.23a}$$

$$S_2 = K_{11} A_{44} D_{11} - K_{22} A_{55} (D_{12} + 2D_{66}) \tag{3.23b}$$

$$S = (D_{11} D_{22} - D_{12}^2 - 4D_{12} D_{66} - 4D_{66}^2) (L_x^2 K_{11} A_{44} + L_y^2 K_{22} A_{55}) \tag{3.23c}$$

Finally, a closed-form solution for the anticlastic bending of plates is obtained by substituting Eqs. (3.22) and (3.23) into Eqs. (3.16), and (3.17), yielding,

$$w = (C_1 - B_1)xy - \frac{1}{3}B_4x^3y - B_6y^3x + w_0 \quad (3.24a)$$

$$\phi_x = B_1y + B_4x^2y + B_6y^3 \quad (3.24b)$$

$$\phi_y = B_1x + \frac{1}{3}B_4x^3 + 3B_6y^2x \quad (3.24c)$$

$$\gamma_{xz} = C_1y \quad (3.24d)$$

$$M_{xy} = 2D_{66}(B_1 + B_4x^2 + 3B_6y^2) \quad (3.24e)$$

the constant w_0 is determined by using the symmetry condition given by Eq. (3.11a), yielding,

$$C_0 = \left(\frac{L_y L_x}{4}\right) \left(C_1 - B_1 - \frac{1}{12}B_4L_x^2 - \frac{1}{4}B_6L_y^2\right) \quad (3.25)$$

It should be noticed that the solution given by Eqs. (3.24) fulfills the boundary conditions given by Eqs. (3.8)-(3.11) and the equilibrium equations given by Eqs. (3.4a – b) and (3.7). The proposed solution, Eqs. (3.24) is general since it considers the influence of bending curvatures κ_x and κ_y and transverse shear forces Q_x and Q_y . This allows to take into account the effect of D_{11} , D_{12} , D_{22} , A_{44} and A_{55} stiffnesses in the anticlastic deflection. For the case of composite plates with isotropic layers ($K_{11} = K_{22}$, $A_{44} = A_{55}$ and $D_{11} = D_{22}$), algebraic manipulations of Eqs. (3.22) leads to simplification of B_1 , B_4 , B_6 and C_1 as,

$$B_1 = \frac{P}{8} \left(\frac{1}{D_{66}} + \frac{1}{D_{22}} \right) \quad (3.26a)$$

$$B_4 = -\frac{3P}{2(L_x^2 + L_y^2)D_{22}} \quad (3.26b)$$

$$B_6 = -\frac{P}{2(L_x^2 + L_y^2)D_{22}} \quad (3.26c)$$

$$C_1 = -\frac{6P}{(L_x^2 + L_y^2)K_{22}A_{55}} \quad (3.26d)$$

Notice also that if the transverse shear forces and bending moments are not considered (i.e. $C_1 = B_4 = B_6 = 0$), the present solution for w is reduced to the solution obtained by Allen [23], Jones [2], the ASTM standard D3044 – 95, Tsai [44], Gay et al. [66], Hearmon and Adams [11], Avilés et al. [17] and Lekhnitskii [28], using CLPT. The compliance (C) is introduced here to compare with previous results by several authors. C is defined as the maximum deflection δ ($w(\pm L_x/2, \pm L_y/2)$) divided by the total applied load P [24], i.e.,

$$C = \frac{\delta}{P} \quad (3.27)$$

3.4 Finite element analysis

For a basis of comparison against the FSDT model, FEM is conducted herein using the commercial software ANSYS11 [31]. To be able to capture the transverse shear strains and compute accurate twisting moments, brick element (SOLID185) with linear interpolation are employed in the FEM. This element is defined by eight corner nodes having three degrees of freedom at each node (translations along the x , y and z axes). In order to analyze the anticlastic bending of plates, two (baseline) specially orthotropic plates with different stiffnesses are employed herein. The first panel is referred to as “LM” (for laminate composite) which represents a stiff laminate composite with $[(0/90)_6]_s$ lamination and properties of an unidirectional glass/epoxy prepreg, typically employed to build structures like shafts, car bumpers, rockets, among others [8, 57]. The second panel is named “SW” and corresponds to a sandwich panel with stiff face sheets and a compliant core, typically used in aircrafts, wind turbines, buildings (as wall and roof panels) and ships (decks and hulls) [8, 57]. SW represents a sandwich panel with aluminum face sheets and PVC foam core which is usually identified as AL/H45. LM and SW are selected because they represent a stiff and a moderately flexible plate, respectively. LM aims to represent a flexural rigid thin plate which carries loads by internal bending and twisting moments, having negligible mid-plane deformations and membrane forces. SW aims to represent a moderately flexible plate which carries external loads by the combined action of internal moments and transverse shear forces. Table 3.1 lists the size and elastic properties of the baseline plates used in main analyses. For the parametric analysis, the thickness h varied from 4 to 100 mm in order to obtain different aspect ratios. Figure 3.2 shows a schematic of the FEM and the boundary conditions used, where the origin of the coordinate system is placed at the center of the plate. In order to avoid excessive deflections at corners and discontinuous shear strain distributions along the edges, a small overhang of 5 mm per side was allowed in the FEM. This means that the point forces are applied along a diagonal line with is 7 mm away from the loaded plate corners, see Figure 3.2. Thus, two downward nodal forces of 500 N ($P = 1$ kN) were applied in the z -direction at nodes located at $(\pm L_x/2, \pm L_y/2, h/2)$. The nodes placed at $(\pm L_x/2, \mp L_y/2, -h/2)$ were fixed ($u = v = 0$) whereas nodes at $(L_x/2, -L_y/2, z)$ were constrained along the z -direction ($w = 0$) to simulate pin support conditions. Additionally, nodes at the central surface of the plate $(0,0,z)$ were fixed along x and y axes ($u = v = 0$) to avoid free-body motion. An analysis of convergence was conducted to investigate the effect of meshing size on C . For this purpose, elements of nominal size ranging from $5 \times 5 \times 6.40 \text{ mm}^3$ to $1.25 \times 1.25 \times 0.565 \text{ mm}^3$ were analyzed with a criterion of 0.15 % as maximum variation on C . The results of this stringent convergent analysis yielded typical models consisting of 119,070 elements with nominal element size of $2.5 \times 2.5 \times 1.13 \text{ mm}^3$. M_{xy} is computed by FEM by discretizing its common integral expression in plate theory [40] as,

$$M_{xy} = \frac{1}{2} \sum_{i=1}^n (\tau_{xy}^i - \tau_{xy}^{i-1})(z_i^2 - z_{i-1}^2) \quad (3.28)$$

where i represents the i -th node and n denotes the number of nodes along the model thickness at (x, y) position ($n = 9$ for most FEM models). In order to obtain a representative value of M_{xy} for a specific plate, the average $(M_{xy})_{ave}$ value inside the entire mid-plane is computed as,

$$(M_{xy})_{ave} = \frac{1}{L_x L_y} \int_{-L_x/2}^{L_x/2} \int_{-L_y/2}^{L_y/2} M_{xy} dy dx \quad (3.29)$$

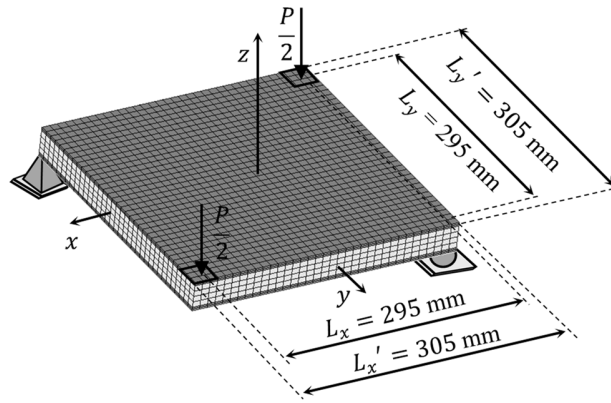


Figure 3. 2. Schematic of the FEM of the PTS.

Table 3.1. Dimensions and properties of the baseline orthotropic panels.

Panel	Stacking sequence	Dimensions (mm)	Elastic properties	Stiffnesses
LM	$[(0/90)_6]_s$	$h = 4.5$ $L_x = L_y = 76$ $L_x' = L_y' = 78$	$E_1 = 47.7$ GPa $E_2 = 12.3$ GPa $E_3 = 12.3$ GPa $G_{12} = 4.83$ GPa $G_{13} = 4.83$ GPa $G_{23} = 4.48$ GPa $\nu_{12} = 0.278$ $\nu_{13} = 0.278$ $\nu_{23} = 0.403$	$A_{44} = A_{55} = 20.9$ MN/m $D_{11} = 249$ N m $D_{22} = 215$ N m $D_{12} = 26.4$ N m $D_{66} = 36.9$ N m
SW	AL/H45	$h_f = 2.51$ $h_c = 13.0$ $L_x = L_y = 295$ $L_x' = L_y' = 305$	$E_f = 70$ GPa $\nu_f = 0.30$ $E_c = 39.6$ MPa $\nu_{12} = 0.32$	$A_{44} = A_{55} = 135$ MN/m $D_{11} = D_{22} = 23.5$ kN m $D_{12} = 7.03$ kN m $D_{66} = 8.20$ kN m

3.5 Results and discussion

In order to first build up the confidence in the FSDT solution and FEM model, both outcomes are first compared against compliance measurements for isotropic, laminated composites and sandwich panels, as listed in Table 3.2. It is observed that FSDT predicts similar compliances than those experiments previously reported (usually less than 10 % difference). Good agreement between FSDT and experiments is observed for isotropic stiff metals, glass-vinylester/PVC foam based sandwich panels and aluminum/PVC foam based sandwich panels. A slight overprediction for C by FSDT is noticed for the Al/H45 ($\sim 32\%$) and G – VE/PW ($\sim 35\%$) panels, which may be due to the high sensitivity of FSDT to the input parameters (accurate elastic properties, dimensions and overhang measurements), the lack of large numbers of test specimens in some cases, and the natural scattering of experimental data, which is around 10 – 20 % for the plate twist test [16, 17, 42]. Particularly, the indentation of soft cores and the assumption that plywoods are isotropic might affect the results for the Al/H45 and G – VE/PW panels, respectively. In order to determine the limits of applicability of the FSDT solution to a particular material system and geometry, an extensive parametric analysis will be conducted in section 5.3. Compliance predictions by FEM also agrees with measurements (less than 10 % of difference) with the exception of the G – VE/PW panel where a 37 % of difference is obtained. The overall good agreement with experiments brings certainty and confidence for the subsequent parametric analysis conducted.

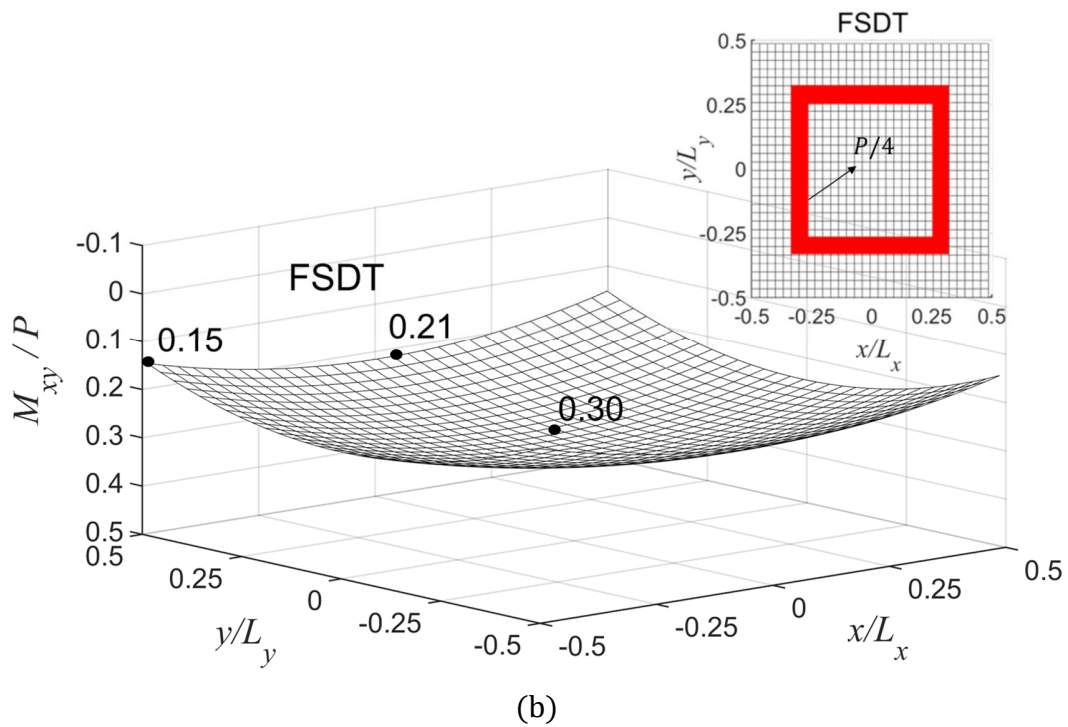
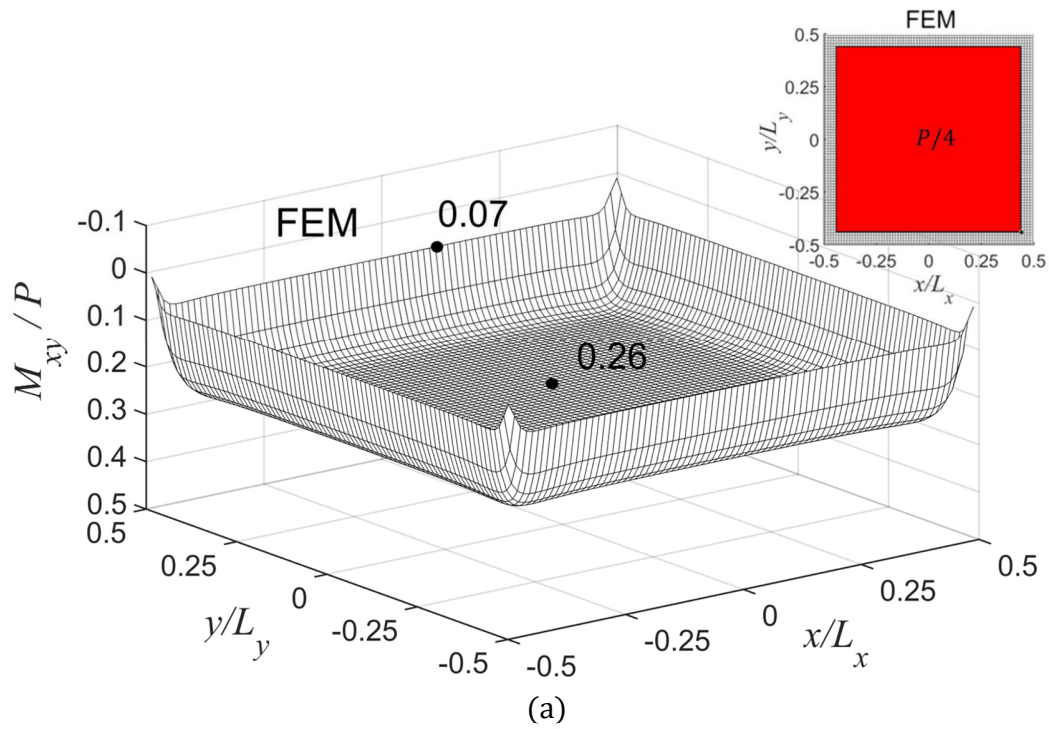
Table 3.2. Comparison between previously reported compliance measurements and predictions by FEM and FSDT of this work.

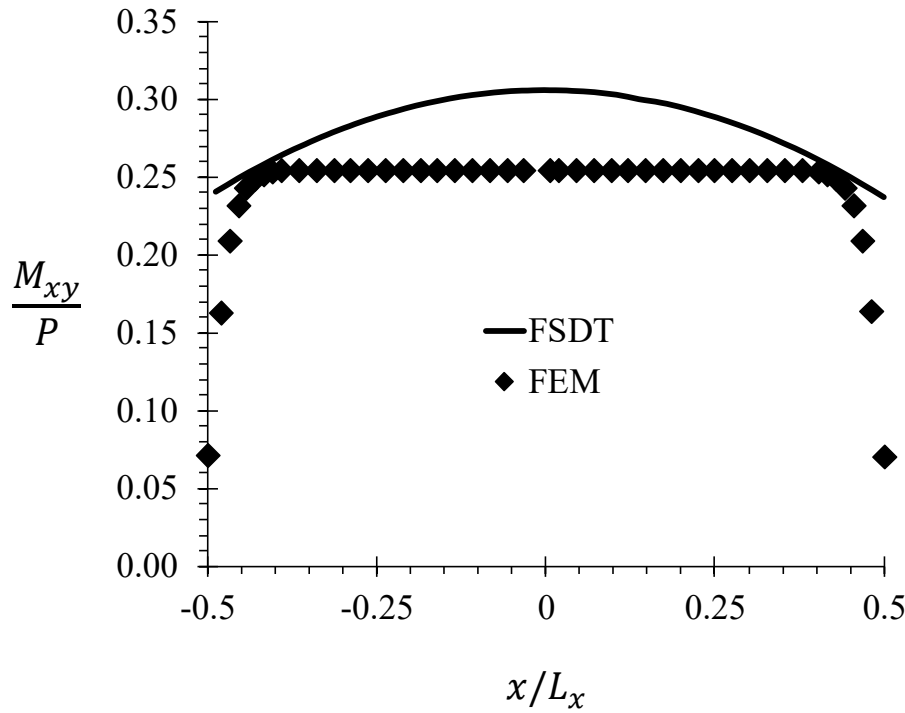
Reference	Panel	C ($\mu\text{m}/\text{N}$)			Ratio (%)	
		EXP	FSDT Eq.(3.27)	FEM	FSDT/EXP	FEM/EXP
[17]	H80/Thin	4.26	4.60	4.26	7.98	0.00
	H100/Thick1	2.85	2.93	2.58	2.81	9.47
	H200/Thin	2.51	2.55	2.59	1.59	3.19
	H200/Thick	1.82	1.87	1.80	2.75	1.10
[42]	Al/H45	4.45	6.02	4.44	35.3	0.22
	Al/H100	2.85	3.22	2.79	13.0	2.11
	Al/H200	1.82	1.90	1.82	4.40	0.00
[16]	G – VE/PW	1.43	1.89	1.96	32.2	37.1
	G – VE/H45	2.82	2.78	2.91	1.42	3.19
[11]*	Aluminum	3.37	3.45	3.38	2.37	0.40
	Brass	2.60	2.60	2.49	0.13	3.98
	Mild Steel	5.11	5.12	4.91	0.14	3.87

*: FEM and FSDT values were converted to $\mu\text{m}/\text{N}$ and divided by 2 here because the compliance reported in [11] was determined with the deflection w from the plate center to one loading point, i.e., half the displacement between pin support and loading point.

3.5.1 Examination of the twisting moment

Standard theory of plates indicates that M_{xy} is the main external loading which yields anticlastic bending [12, 28]. However, the condition $M_{xy}/P = 0.25$ (which theoretically leads to pure twisting [12, 64]) has not been analyzed for compliant and/or thick plates. For this purpose, Figures 3 and 4 displays the normalized twisting moment M_{xy}/P distributions predicted within the mid-plane ($z = 0$) for LM and SW baseline panels (see Table 3.1). At the top-right corner of Figures 3a, 3b, 4a and 4b there is an insert of the top view of the mid-plane, where the region marked in dark red color represents locations where $M_{xy}/P = 0.25$. Figures 3c and 4c makes a direct comparison between M_{xy}/P computations by FEM and FSDT along the $y = 0$ center line. Figure 3.3a (FEM predictions) shows that M_{xy}/P attains values around 0.25 ± 0.01 within the mid-plane with a maximum of 0.26 at the center of the plate; an exception is found at the edges $x = \pm 0.5 L_x$ and $y = \pm 0.5 L_y$ where a 0.07 value is reached. These spurious M_{xy}/P values at the corners are because τ_{xy} is singular at those locations [67-69]. The top-right insert of Figure 3.3a confirms that FEM attains $M_{xy}/P = 0.25$ at most mid-plane. This behavior matches classical theoretical predictions by Lord Kelvin for thin homogeneous plate [64]. In Figure 3.3b it is observed that FSDT predicts a M_{xy}/P symmetric parabolic behavior with respect to the x and y axes, increasing from 0.21 at mid-length of the edges $(0, \pm 0.5 L_y)$ and $(\pm 0.5 L_x, 0)$ up to a maximum of 0.30 at the center of the plate $(0,0)$; the insert of Figure 3.3b shows that FSDT attains $M_{xy}/P = 0.25$ only inside a symmetric rectangular strip zone defined by outer corners $(\pm 0.30, \pm 0.30)$ and inner corners $(\pm 0.20, \pm 0.20)$. Figure 3.3c illustrates the M_{xy}/P parabolic behavior of FSDT and the plateau trend of FEM along $y = 0$ for the LM panel, reaching their corresponding maximum and minimum values at the center and edges of the plate. Despite the M_{xy}/P behavior predicted by FEM and FSDT are not equal, the attained values are similar, specially at the center of the plate where a small difference of 0.04 is found. This indicates that FSDT is able to rightfully capture the essentials of the τ_{xy} stress field yielded by the four $P/2$ vertical forces at corners. The small differences between FEM and FSDT on M_{xy} calculations may be due to their inherent approximated nature, FEM is a numerical approximation and considers an overhang, whereas FSDT does not; furthermore, FEM is sensitive to the loaded areas by the $P/2$ concentrated forces.



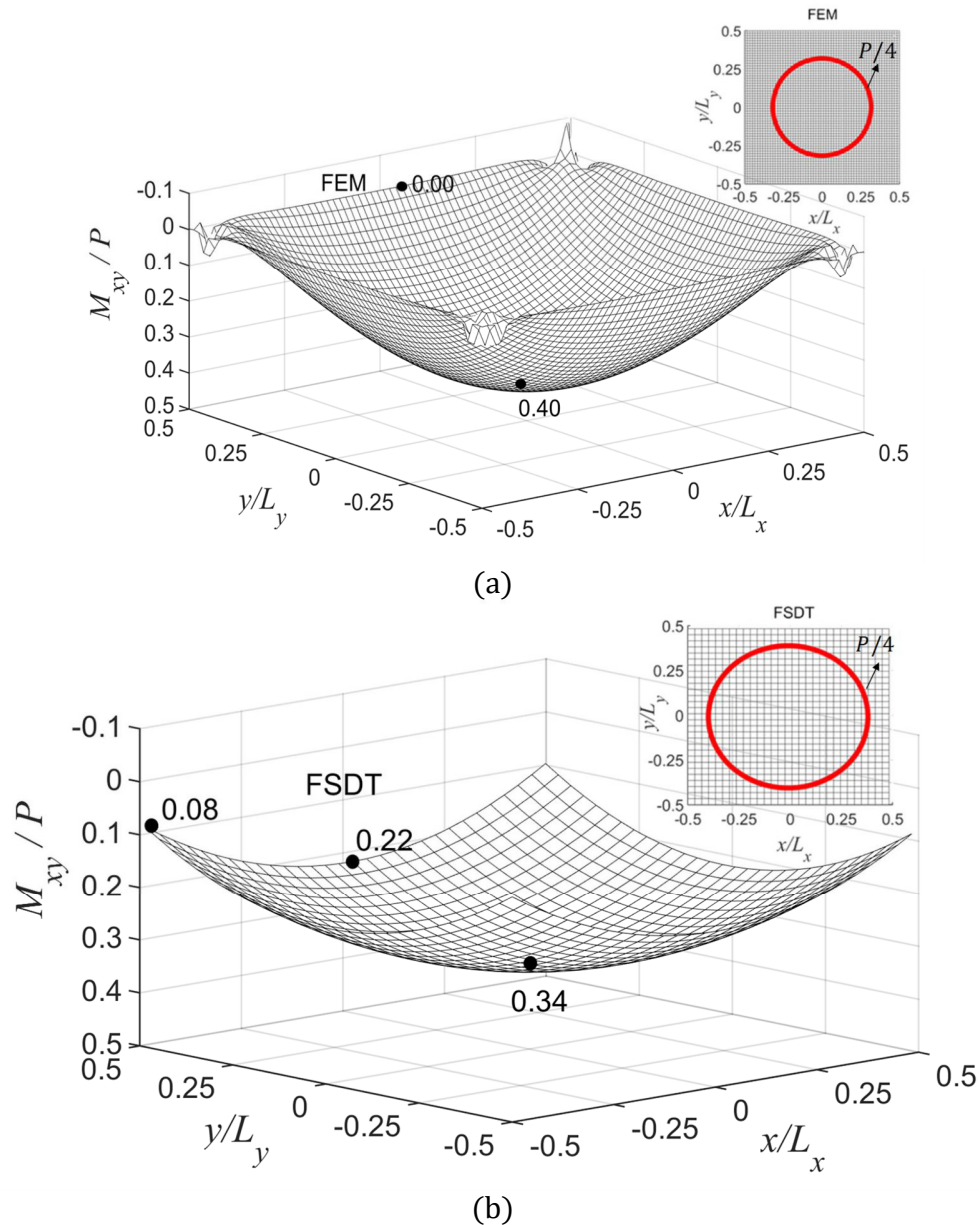


(c)

Figure 3.3. Distribution of normalized twisting moment M_{xy}/P calculated by FSDT and FEM at the mid-plane ($z = 0$) of the LM baseline panel. (a) FEM. (b) FSDT. (c) along the center line $y = 0$.

Figure 3.4a shows that the SW panel (which is more compliant than LM, compare D_{66} in Table 3.1) has a parabolic M_{xy}/P distribution at mid-plane, raising from 0 at the edges until a maximum of 0.40 at the center of the plate (0,0); the dark red zone of the insert of Figure 3.4a shows that FEM reached $M_{xy}/P = 0.25$ only inside a small ring of radius $0.30 \leq \sqrt{(x/L_x)^2 + (y/L_y)^2} \leq 0.34$. By comparing Figures 3a and 4a (FEM), it is observed that not only M_{xy} depends on the material system, but also the shape of its distribution within the mid-plane, i.e., M_{xy} becomes more uniform (flat) as the stiffnesses of the plate increases (see D_{ij} stiffnesses in Table 3.1). This observation suggests that M_{xy} is not fully constant ($P/4$) within whole mid-plane, as assumed by CLPT and previous works [11, 17], specially for compliant plates. Such inhomogeneity on the M_{xy} distribution indicates that a pure twisting state is not fully reached in this specimen, due to the influence of the shear deformation of compliant materials [5, 17, 47]. FSDT also predicts a parabolic distribution of M_{xy}/P (Figure 3.4b), although it attains minimum and maximum values of 0.28 and 0.34 at the corners and center, respectively; from the insert of Figure 3.4b, it is observed that FSDT only attains $M_{xy}/P = 0.25$ inside a small ring region bounded by $0.38 \leq$

$\sqrt{(x/L_x)^2 + (y/L_y)^2} \leq 0.42$. Figure 3.4c shows that the M_{xy} parabolic responses by FEM and FSDT along center line $y = 0$ are slightly dissimilar in shape and minimum values at the edges (0 for FEM and 0.28 for FSDT). However, both approaches have similar peak values at the center of the plate (difference of 0.06) and their average M_{xy}/P are comparable, as will be further discussed in connection to Figure 3.5.



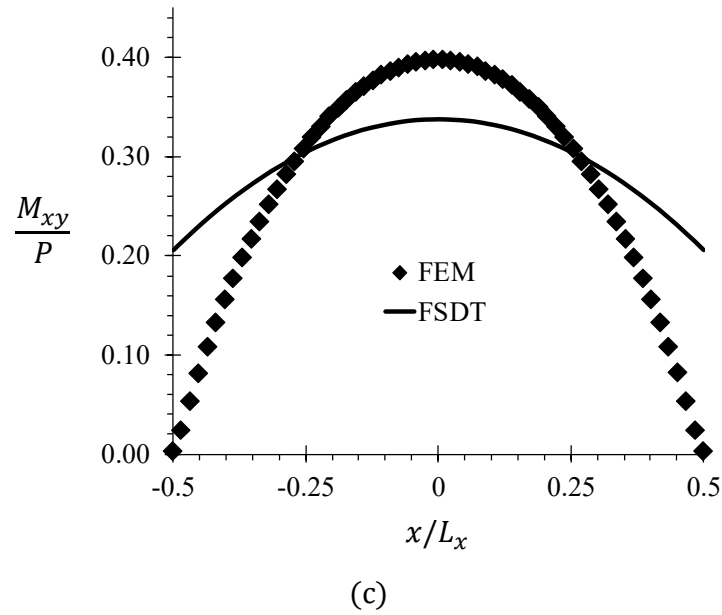
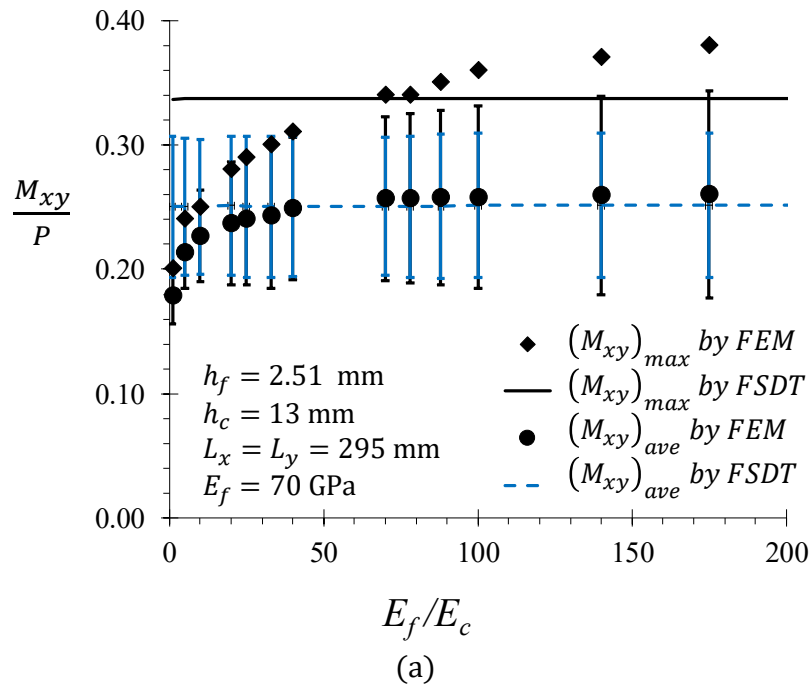


Figure 3.4. Distribution of normalized twisting moment M_{xy}/P calculated by FSDT and FEM at the mid-plane ($z = 0$) of the SW baseline panel. (a) FEM. (b) FSDT. (c) along the center line $y = 0$.

Given the variation and importance of the M_{xy} distribution shown in Figure 3.4 for compliant plates (such as SW), the average ($(M_{xy})_{ave}/P$, see Eq. (3.29)) and maximum ($(M_{xy})_{max}/P$) normalized twisting moment are plotted against different E_c/E_f ratios of sandwich panels (based on SW) in Fig 5. Here $(M_{xy})_{ave}$ with its standard deviation (computed from all M_{xy} values at mid-plane) and $(M_{xy})_{max}$ are parameters which aim to encompass the homogeneity and dispersion of M_{xy} within the same plate, with respect to an ideally constant value. In other words, if M_{xy} would be constant ($P/4$), average and maximum values would be identical and scattering bars would be inexistent. Figure 3.5a is depicted for $1 \leq E_f/E_c \leq 200$ (stiff cores) and Figure 3.5b for $200 < E_f/E_c \leq 1768$ (compliant cores). In these figures it is observed that $(M_{xy})_{ave}/P$ predicted by FEM attains 0.18 ± 0.02 for the isotropic case ($E_c/E_f = 1$) and raises non-linearly until to 0.24 ± 0.05 at $E_c/E_f = 20$; for $E_c/E_f > 20$ $(M_{xy})_{ave}/P$ increases slightly with respect to E_c , keeping mean values around 0.24 and 0.27. Because the $(M_{xy})_{ave}/P$ mean values varied from 0.18 to 0.27, the assumption of $M_{xy} = P/4$ is not fully valid for compliant materials, and is approximated only for $1 \leq E_f/E_c \leq 20$ according to Figures 5a and 5b (using a criterion of 16 % as maximum difference of M_{xy} with respect to $(M_{xy})_{ave}$). On the other hand, the standard deviation of $(M_{xy})_{ave}/P$ by FEM follows a similar trend than its mean values, i.e., for $E_c/E_f = 1$ the standard deviation reached a minimum of ± 0.02 but varies slightly

between ± 0.05 and ± 0.09 for $20 \leq E_f/E_c \leq 1768$. This scatter indicates the large inhomogeneity of the τ_{xy} stress distribution within mid-plane, confirming that M_{xy} is not constant for compliant materials. It is observed that $(M_{xy})_{max}/P$ predicted by FEM follows a similar nonlinear trend than $(M_{xy})_{ave}/P$, although much higher values are obtained (a minimum of 0.20 at $E_c/E_f = 1$ and maximum of 0.42 at $E_c/E_f = 700$). The significant difference between $(M_{xy})_{max}$ and $(M_{xy})_{ave}$ indicates that the highest τ_{xy} obtained at the center of the plate is much higher than the nominal value inside the mid-plane. In Figures 5a and 5b it is observed that $(M_{xy})_{max}$ and $(M_{xy})_{ave}$ calculated by FSDT predicts constant values of 0.34 and 0.25 ± 0.06 , respectively. It is also observed that FSDT and FEM predict the same $(M_{xy})_{ave}$ in a large range of compliant cores ($20 \leq E_f/E_c \leq 1768$) but for $1 \leq E_f/E_c < 20$ the average capture by FSDT differs from FEM between 4 % to 38 %. This difference is due to the parabolic M_{xy} predicted by FSDT, compared to the flat shape predicted by FEM for small ratios of E_f/E_c (see, Figures 3). However, the scattering bars overlap showing that there is no statistical difference. It also shows that for the range in which FSDT and FEM predicts the same $(M_{xy})_{ave}$, the maximum constant value of $M_{xy} = 0.34$ predicted by FSDT at the center of the plate is in good agreement with the FEM predictions at the same location, with maximum differences of 16 %. These observations let to conclude that the M_{xy} expression found using FSDT is a good approximation to predict the M_{xy} behavior in the entire plate for $20 \leq E_f/E_c \leq 1768$.



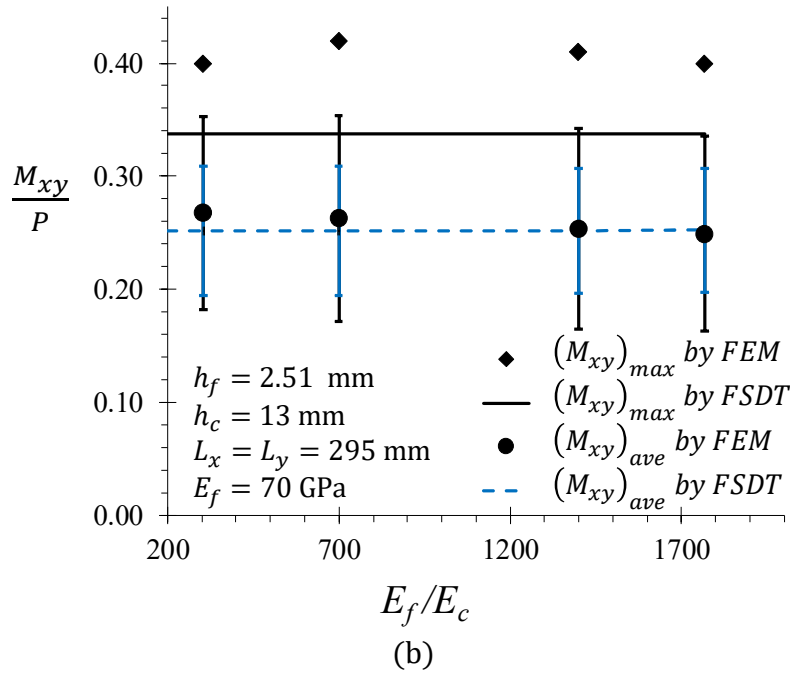
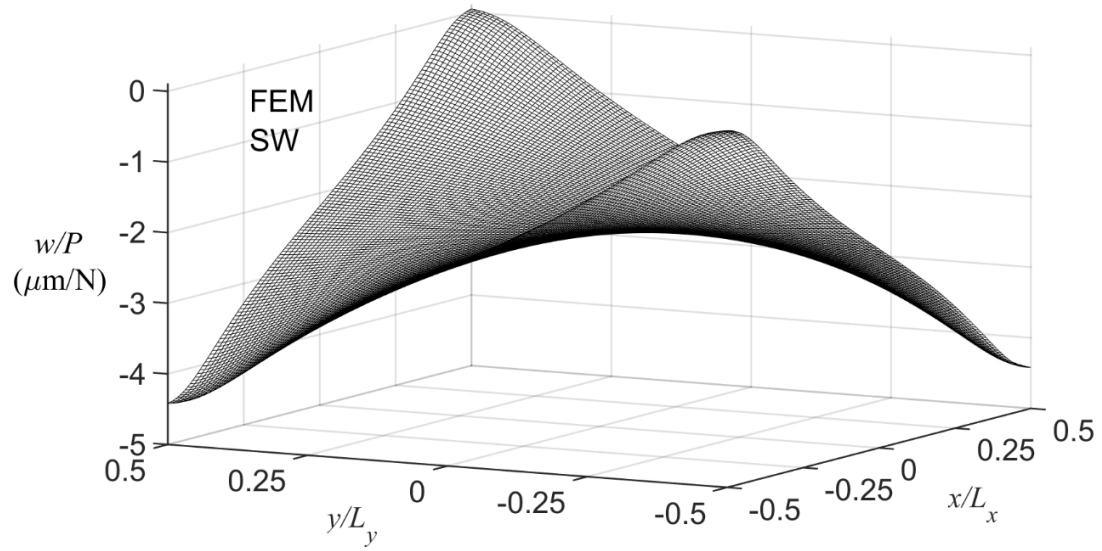


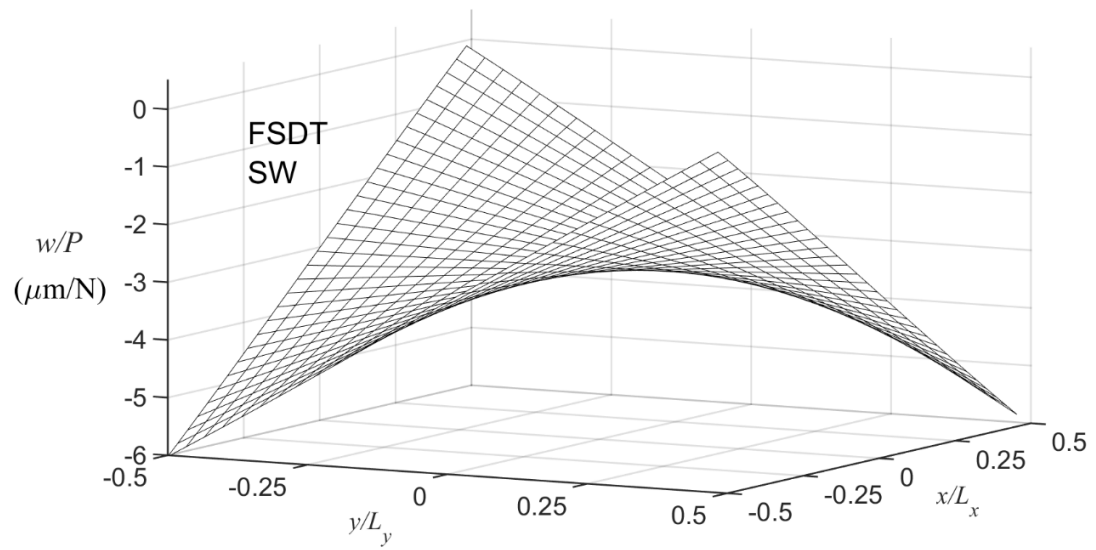
Figure 3.5. Maximum and average M_{xy}/P (Eq. (3.29)) versus E_f/E_c ratios for different sandwich panels using the panel SW as baseline. (a) $1 \leq E_f/E_c \leq 200$. (b) $200 \leq E_f/E_c \leq 1768$.

3.5.2 Prediction of displacements and transverse shear strains

Three-dimensional plots of the normalized transverse deflection field (w/P) at mid-plane ($z = 0$) of the SW baseline panel (Table 3.1) are plotted in Figures 6a (FEM) and 6b (FSDT). A comparison between both approaches for the center line $y = 0$ is shown in Figure 3.6c. Both, Figures 6a and 6b, show that w forms an anticlastic deformed shape, i.e., two parabolic shapes with opposite signs are observed along the perpendicular diagonals of the plate. This anticlastic shape vanishes at the pin support locations ($x/L_x \pm 0.5, y/L_y = \mp 0.5$) and attains a maximum value of $4.5 \mu\text{m}/\text{N}$ (FEM) and $6.0 \mu\text{m}/\text{N}$ (FSDT) at the location of the applied loads ($\pm 0.5, \pm 0.5$). This difference between the maximum deflections predicted by FSDT and FEM are due to high influence of the overhang and point-loaded areas considered only by the FEM model for this sandwich panel with a highly flexible core (better agreement was obtained for stiffer cores, e.g. see Table 3.2). Figure 3.6c shows that the normalized deflection w/P predicted by FEM reached a constant value of $2.2 \mu\text{m}/\text{N}$ along the center line $y = 0$ for SW, which validates the assumption given by Eq. (3.11a) and agrees with the observation by Lord Kelvin and Tait [64] and Timoshenko and Woinowsky-Krieger [12] for the anticlastic bending of thin isotropic plates. As expected, FSDT predicts a constant value w/P along $y = 0$, reaching $3.0 \mu\text{m}/\text{N}$, which approximates to the FEM predictions.



(a)



(b)

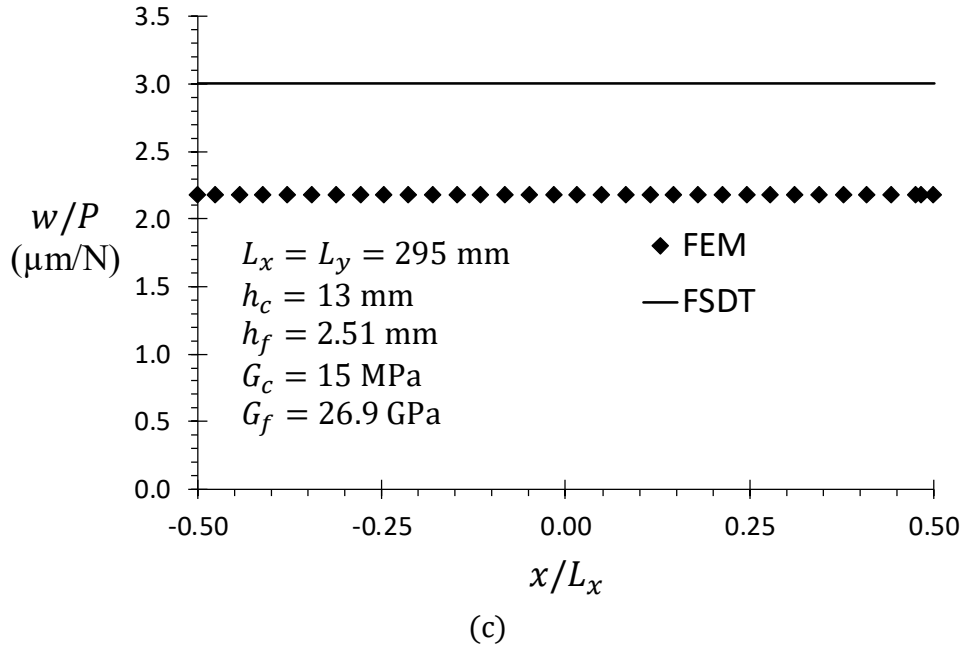
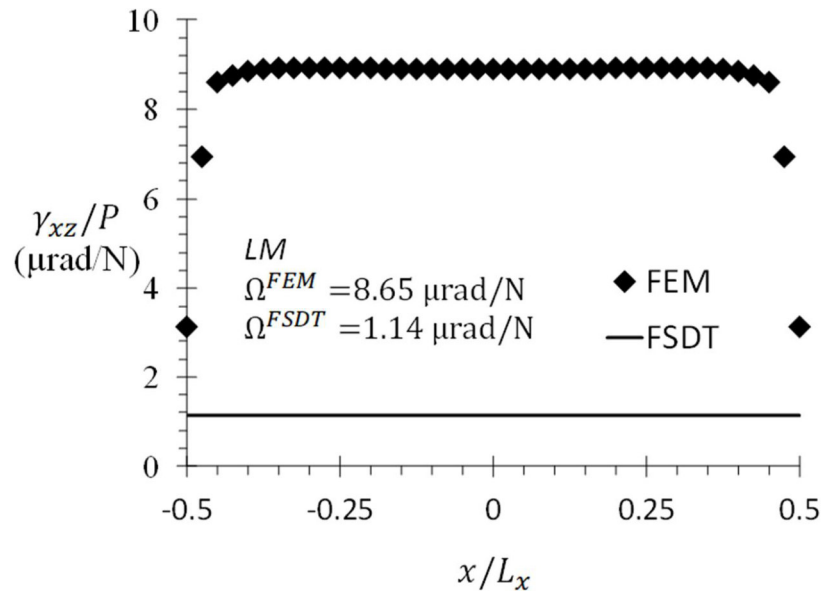


Figure 3.6. Normalized displacement fields $w(x, y)/P$ for the baseline SW at mid-plane ($z = 0$). (a) FEM. (b) FSDT. (c) along center line $y = 0$.

Because transverse shear strains have a great influence on the deflection of compliant and thick plates, Figure 3.7 displays the normalized transverse shear distribution (γ_{xz}/P) along the edge $y = L_y/2$ at the mid-plane for baseline panels LM (Figure 3.7a) and SW (Figure 3.7b) using FEM and FSDT (all γ_{xz} are considered positive). In Figure 3.7a is observed that FEM predicts a practically constant $\gamma_{xz}/P = 8.91 \mu\text{rad}/\text{N}$ behavior along the edge $y = L_y/2$, with exception of zones near the corners $0.45 \leq |x/L_x| \leq 0.5$ where γ_{xz} tends to vanish due to the free-edge border condition [4, 47, 63]. In order to obtain a representative statistically γ_{xz}/P value, the area under the curve γ_{xz}/P vs x/L_x is calculated and represented by the symbol Ω , which indicates the mean γ_{xz}/P value along the x/L_x axis. FEM averaged $\Omega^{FEM} = 8.65 \mu\text{rad}/\text{N}$ which is close to that obtained along the plateau trend. Similarly, FSDT predicts a constant γ_{xz}/P distribution along x/L_x , attaining $\Omega^{FSDT} = 1.14 \mu\text{rad}/\text{N}$. Despite this value is much lower than that obtained by FEM, it is expected that the γ_{xz} contribution to the transverse deflections of stiff laminated composites is negligible, as several authors have demonstrated [17, 45, 47]. This is because the anticlastic bending is dominated by the effect of bending stiffnesses D_{ij} for those stiff plates, instead of transverse shear stiffness A_{44} and A_{55} [17, 65]. Figure 3.7b shows that for the panel SW, according to FEM, γ_{xz}/P raises linearly with a large gradient from $1 \mu\text{rad}/\text{N}$ at the corner $x/L_x = 0.5$ to a peak value of $19.9 \mu\text{rad}/\text{N}$ at $x/L_x = 0.35$. Then γ_{xz}/P decreases parabolically towards

the middle of the edge until a local minimum of $14.1 \mu\text{rad/N}$ at $x/L_x = 0$. It is noted that the shape of the γ_{xz} distribution is symmetric with respect to the vertical axis of Figure 3.7b. On the other hand, FSDT (Eq. (3.16b)) predicts a constant $\gamma_{xz}/P = 17.4 \mu\text{rad/N}$ along the x axis, yielding $\Omega^{FSDT} = 17.4 \mu\text{rad/N}$, which is very similar to that computed by FEM ($15.5 \mu\text{rad/N}$). The fact that FSDT is not exactly representing the detailed nonlinear behavior of γ_{xz} estimated by FEM is due to the chosen algebraic polynomial, $\gamma_{xz} = C_1 y$, see Eq. (3.24d). Herein γ_{xz} is inversely proportional to the sum of products of shear correction factors and transverse shear stiffnesses, which is strongly related to the constitutive equations of transverse shear resultants by FSDT [47]. This fact allows the FSDT solution to nominally capture the through-thickness distributions of τ_{xz} and τ_{yz} in the plate by their shear correction factors. Thus, the FSDT has a similar average γ_{xz} than that predicted by FEM (Ω^{FEM}), which means that the proposed solution is able to represent the distribution of γ_{xz} for sandwich materials with compliant cores in a smeared out manner.



(a)

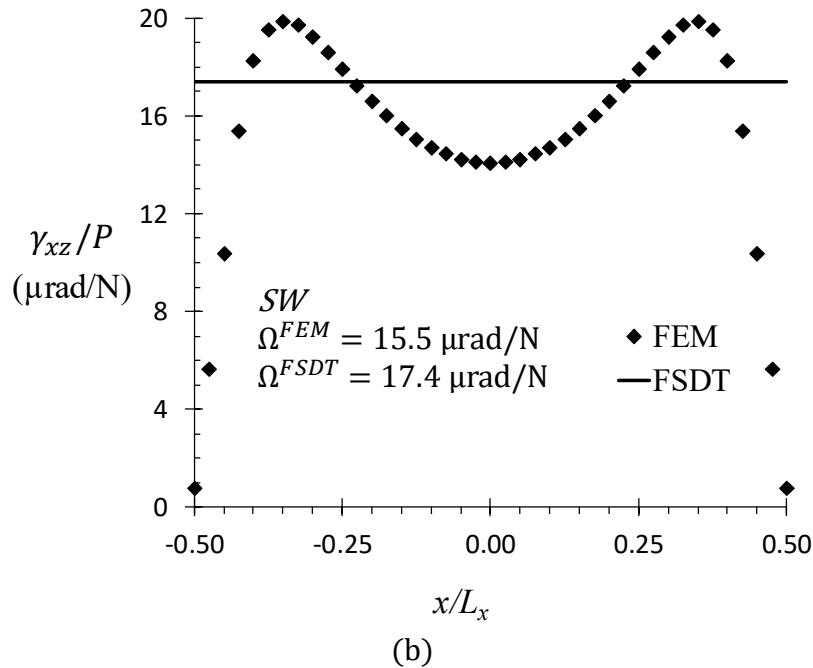


Figure 3.7. Comparison of normalized mid-plane transverse shear strain (γ_{xz}/P) for the baseline panels listed in Table 3.1 at the edge $y = L_y/2$. (a) LM. (b) SW.

3.5.3 Parametric analysis

The effects of the panel slenderness (L_x/h) on the compliance of square orthotropic plates are analyzed in Figures 3.8a and 3.8b, which are based on LM and SW, respectively. In these figures, h was increased keeping the side-lengths constants ($L_x = 76$ mm for LM and $L_x = 295$ mm for SW). In order to increase the thickness of the laminate (Figure 3.8a), the number of plies increased according to $[(0/90)_n]_s$ where $n = 1 \dots 12$ ($n = 1$ implies 4 plies, and $n = 12$ implies 48 plies). This figure illustrates that for a moderately thick panel ($L_x/h = 8.4$) with 48 plies, FEM predicts a compliance of $1.87 \mu\text{m}/\text{N}$, and such compliance raises parabolically as the L_x/h ratio grows, achieving $2035 \mu\text{m}/\text{N}$ for $L_x/h = 101$ (thin plate with 4 plies). FSDT also predicts a parabolic raising of the compliance as the L_x/h ratio grows, obtaining good matching with FEM along the whole range $8.4 \leq L_x/h \leq 101$ (small differences around 5 % of FSDT with respect to FEM were obtained). Figure 3.8b shows that the compliance calculated by FEM increases in a nearly linear fashion with increasing panel aspect ratio L_x/h . It is observed that FSDT slightly overpredicts the compliance with respect to FEM for $4 \leq L_x/h \leq 61$, obtaining a difference of 20 ± 5 % in the range $26.5 \leq L_x/h \leq 61$. These differences are attributed to the consideration of the concentrated forces in a small nodal area in the FEM model. The agreement between both models points out that FSDT captures the nominal transverse shear strains distributions with sufficient accuracy by using specific shear correction factors for each sandwich structure with different slenderness ratio.

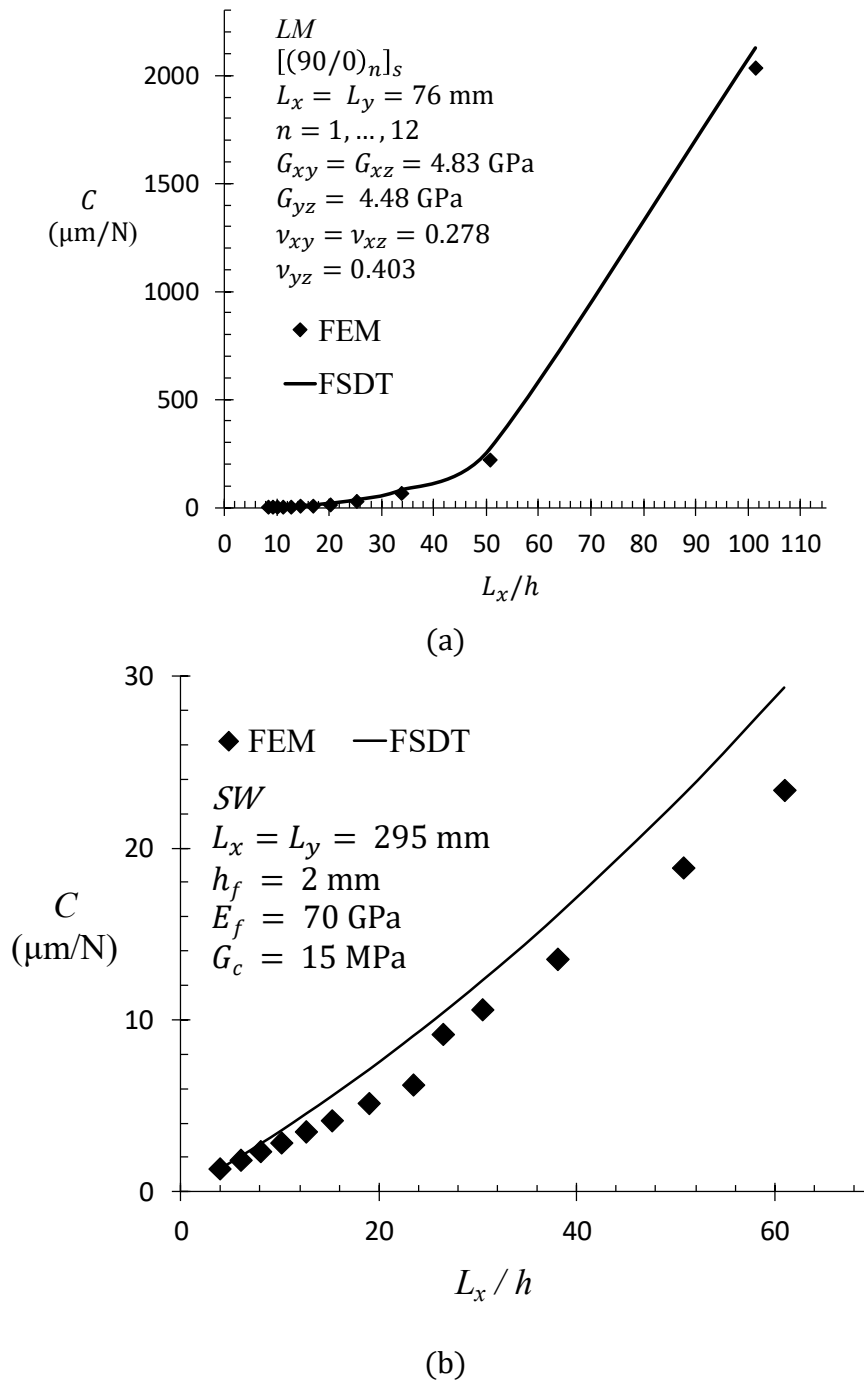


Figure 3.8. Effect of normalized length L_x/h on the compliance of square panels based on baselines plates. (a) LM. (b) SW with $h_f = 2\text{mm}$.

Since the core carries most shear stresses in sandwich structures, the shear moduli ratio between face sheet and core (G_f/G_c) on the compliance of square sandwich panels (based on SW) are plotted in Figure 3.9. It is observed that the compliance predicted by FEM and FSDT increases with respect to the G_f/G_c ratio. As seen from the insert, the compliance attains a power-law behavior for the interval $1 \leq G_f/G_c \leq 50$, which corresponds to stiff panels. However, a linear trend is observed for panels with compliant cores in the range $50 < G_f/G_c \leq 1800$. For $G_f/G_c \leq 1000$ the compliance predicted by both models is similar, reaching a maximum difference of 12 % for $G_f/G_c = 1000$. However, for $G_f/G_c > 1000$, FSDT overpredicts the compliance with respect to FEM with a maximum difference of 21 % for $G_f/G_c = 1800$, which corresponds to the SW panel (a sandwich panel with a very flexible core, $G_c = 15$ MPa). The results of the parametric analysis shown in Figures 3.8 and 3.9 show that the present solution is able to accurately predict (less than 20 % of difference) the anticlastic bending behavior of specially orthotropic plates with different dimensions ($4 \leq L_x/h \leq 61$) and elastic properties ($1 \leq G_f/G_c \leq 1000$).

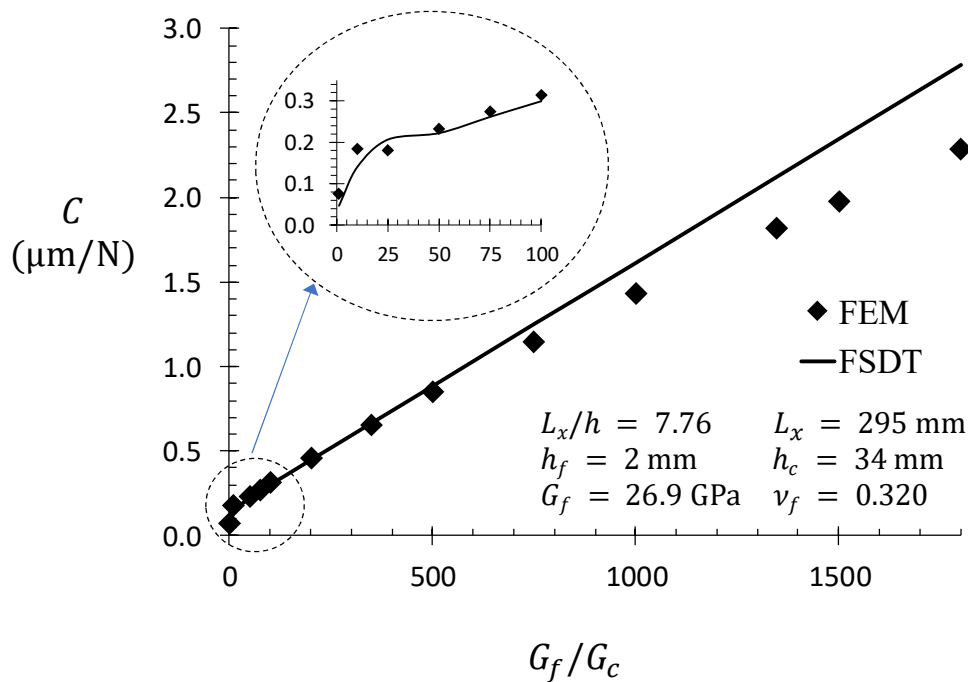


Figure 3.9. Effect of the in-plane shear modulus ratio on the compliance of the square sandwich panels.

3.6 Conclusions

A closed-form solution to the plate twist specimen (PTS, yielding anticlastic bending) of specially orthotropic plates including laminated composites and sandwich structures is developed using first-order shear deformation theory (FSDT) and the theorem of minimum potential energy. The proposed approximate solution for the transverse shear strain and rotations of the cross-section of the plate are fifth- and third-order algebraic polynomials (for γ_{xz} and ϕ_x , respectively) which fulfil the governing equations and essential boundary conditions of the PTS, and their algebraic form greatly facilitates further use of the solution. For comparison, a finite element model (FEM) is performed by using three-dimensional brick elements with linear interpolation. Both FSDT solution and FEM were first validated by comparing against previously reported measurements of compliance (ratio of maximum deflection to applied force P) for a large variety of isotropic and orthotropic plates, finding reasonable agreement. The deflection field showed that the FSDT solution accurately represents the anticlastic deformed shape of orthotropic plates under twisting. Good agreement (less than 20 % of difference) was also observed between compliance predictions by FEM and FSDT when the aspect ratio of square laminated composite plates is varied between $8.4 \leq L_x/h \leq 101$, and sandwich panels with aspect ratio of $4 \leq L_x/h \leq 61$ or shear moduli ratio of $1 \leq G_f/G_c \leq 1000$. One of the most important findings is that the distribution of the twisting moment M_{xy} within the mid-plane is not constant but has a parabolic behavior for sandwich structures with compliant cores, being maximum at the center and zero (minimum) at the edges. This parabolic trend becomes more uniform (flatter) as the stiffness increases, approaching the classical value of $P/4$ for thin and stiff plates. FEM showed that $M_{xy} \approx P/4$ mostly within the mid-plane of unidirectional glass/epoxy $[(0/90)_6]_s$, whereas the average M_{xy} varies from $0.18P$ to $0.27P$ for sandwich panels with face-to-core elastic modulus ratios of $1 \leq E_f/E_c \leq 1768$. This significantly differs from the classical assumption of $M_{xy} = P/4$ considered by CLPT principles for thin homogeneous plates [12, 64]. Good matching on the maximum and average M_{xy} between FEM and FSDT is obtained for a large variety of sandwich structures, indicating that the FSDT solution is able to represent a nominal τ_{xy} stress state on the anticlastic bending of such composite materials. Since the FSDT solution proposed is approximated (two constants are determined by the theorem of minimum potential energy), it predicts a constant distribution of transverse shear strains (γ_{xz} and γ_{yz}) along lines parallel to the y and x axis. Despite of this, the constant γ_{xz} predicted by FSDT agrees reasonably well with the average value predicted by FEM for sandwich panel in the wide range of $350 \leq G_f/G_c \leq 1745$. The solution proposed here can predict the transverse deflection, rotations of the cross-section, twisting moments and averaged transverse shear strains of both stiff thin laminated composites and sandwich structures with compliant cores. Furthermore, from the practical point of view, their algebraic closed-form is easy to implement/code and may be useful to determine shear elastic constants by measuring the compliance from experimental testing (e.g., G_{xy} , G_{xz} and G_{yz} can be measured from D_{66} , A_{44} and A_{55}). Their variable shear correction factors for a specific



material system allows to capture the nominal transverse shear strain field for a large collection of plates with different slenderness ratios and different face-to-core elastic modulus ratios (for sandwich structures).



Universidad
Guanajuato

Conclusions

Orthotropic laminate composites under twisting loads were analyzed theoretically, numerically using the PT test. Two polynomial closed-form solutions are developed to predict the deflection and compliance of rectangular specially orthotropic plates under twisting loads; FEM simulations are performed to analyze rigid composite plates and sandwich panels; and experimental measurements previously reported in the literature were employed to verify the FEM model. The two closed-form solutions show good agreement with FEM and reported results. Analysis of the plate size in the first closed-form solution revealed that the FSDT approach properly predicts the compliance of square and rectangular laminated plates in the following ranges ($1 \leq \text{width/length} \leq 10$), thick ($4.0 \leq \text{length/thickness} \leq 8.5$) and thin plates ($8.5 \leq \text{length/thickness} \leq 19.1$). Moderate changes in the transverse shear to in-plane shear moduli ratio (G_{23}/G_{12}) do not significantly affect the accuracy of the FSDT compliance for $1 \leq G_{23}/G_{12} \leq 5$. On the other hand, for sandwich panels with large differences between in-plane shear modulus of the face sheet and core ($G_{12f}/G_{12c} \geq 200$), FSDT underpredicts the compliance ($\sim 40\%$ for $G_{12f}/G_{12c} = 200$). The first solution is adequate for stiff and compliant specially orthotropic sandwich and laminated composite materials of moderate compliance with dimensions $1 \leq \text{width/length} \leq 10$ and $4 \leq \text{length/thickness} \leq 19$. Analysis of plate size in the second closed-form solution revealed that the distribution of the twisting moment M_{xy} by FEM within mid-plane indicates that M_{xy} has a parabolic behavior for compliant cores although this M_{xy} tends to be constant as the core stiffness enhances, which coincides with Timoshenko's observation that $M_{xy} = P/4$ for thin isotropic plates. The maximum M_{xy} value, $(M_{xy})_{max}$, was obtained at the center of the plate, which increases in a non-linear fashion with respect to E_f/E_c until a peak value, which remains almost constant to larger E_f/E_c ratios. For the variety of orthotropic plates analyzed, $(M_{xy})_{max}$ oscillates between $0.2P$ to $0.5P$. Parametrical analysis reveals that this solution is applicable in the following ranges ($1 \leq \text{length/thickness} \leq 61$) and shear moduli ratio between plies (range $1 \leq G_f/G_c \leq 1000$) to sandwich panels and ($8 \leq L_x/h \leq 100$) to composite laminates. Accord to the comparison between FSDT and CLPT, the transversal shear loads, which are attributed to the shear strains take relevant importance in sandwich panels when the ratio $G_f/G_c > 10$. It is concluded that both solutions predict accurately the deflection and rotations of compliant and stiff specially orthotropic plates loaded under anticlastic bending on the specified ranges. By the other hand, the shear correction factor K_{ij} , which depends of the materials properties, dimensions and ply orientation, must be carefully selected or determined as is indicated in the appendix A and B, respectively, because this strongly affects the shear strains which become too important in plates with moderate or large thickness and

sandwich panels with compliant cores. It is recommended that when the dimensions and properties of the plates are within the application ranges indicated by the parametrical analysis of the first solution, the required calculations, for simplicity, should be done using this solution because the calculation of K_{ij} is avoided, selecting this as a constant ($K_{ij} = 2/3$), otherwise, the second solution must be employed.

Appendix A: Effect of the shear correction factor

Since the shear correction factor K_{ij} has a great influence on FSDT solutions, four values of K_{ij} typically employed in the literature ($K_{11} = K_{22} = 1, 5/6, 2/3$ and $\pi^2/12$) are specifically analyzed in this section. Figure A-1 displays the normalized mid-plane deflection w/P at the edge $y = L_y/2$ of the AL/H45 panel by using FEM, CLPT and FSDT (Eq. (2.15c)) approaches. Although CLPT and FEM trends were already discussed in Figure 2.5c, they are plotted again herein for comparative purposes. It is observed that the shape of the deflection curve predicted by FSDT is independent of the value of K_{ij} employed, but the magnitude of the deflection changes. The panel deflection increases as K_{ij} decreases, with $K_{ij} = 1$ yielding the lowest deflection, and $K_{ij} = 2/3$ yielding the highest deflection. The results with $K_{ij} = 1, 5/6$ and $\pi^2/12$ underestimates w/P with respect to FEM, whereas $K_{ij} = 2/3$ yields the best agreement. This indicates that Timoshenko's beam theory with $K_{ij} = 2/3$ is suitable for bending/torsion problems, since the anticlastic bending of the PTS yields bending along the x and y axes.

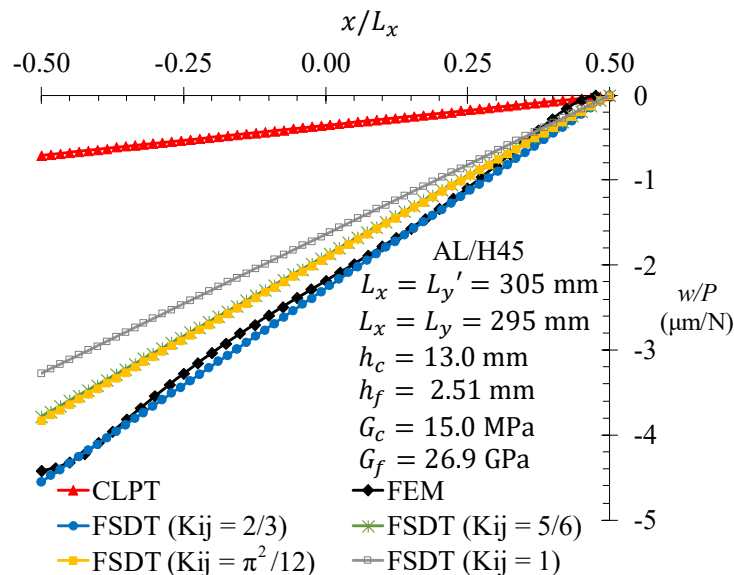


Figure A – 1. Normalized mid-plane deflection (w/P) predicted by FEM, CLPT and FSDT (employing four values of K_{ij}) for the square AL/H45 sandwich panel at the edge $y = L_y/2$.

Appendix B: Calculation of the shear correction factors

The shear correction factors K_{11} and K_{22} (to correct the γ_{yz} and γ_{xz} distributions of FSDT) are determined herein using the methodology suggested by Chow. By conducting one-dimensional bending analyses of laminated plates along x and y directions, Chow found that the through-thickness distributions of τ_{xz} and τ_{yz} may be represented by,

$$\tau_{xz}(z) = \frac{Q_x g_x(z)}{D_{11}} \quad \tau_{yz}(z) = \frac{Q_y g_y(z)}{D_{22}} \quad (\text{B.1a-b})$$

where z is the coordinate along the plate thickness. $g_x(z)$ and $g_y(z)$ are continuous functions given by

$$g_x(z) = -\frac{1}{2} \sum_{k=1}^z \bar{Q}_{11}^{(k)} (z^2 - z_k^2) \quad g_y(z) = -\frac{1}{2} \sum_{k=1}^z \bar{Q}_{22}^{(k)} (z^2 - z_k^2) \quad (\text{B.2a-b})$$

where k is the k -th ply of the laminated composite. $\bar{Q}_{11}^{(k)}$ and $\bar{Q}_{22}^{(k)}$ represent the reduced transformed stiffnesses of the k -th ply along the material 1 (longitudinal) and 2 (transverse) axis, respectively. Analyzing the strain energy with Eq. (B. 1), Chow found that,

$$K_{11} = \frac{(D_{11})^2}{A_{55}H_{11}(z)} \quad K_{22} = \frac{(D_{22})^2}{A_{44}H_{22}(z)} \quad (\text{B.3a-b})$$

where $H_{11}(z)$ and $H_{22}(z)$ are functions through the plate thickness given by,

$$H_{11}(z) = \sum_{k=1}^N \int_{z_k}^{z_{k+1}} \frac{[g_x^2(z)]_k}{G_{13}^{(k)}(z)} dz \quad H_{22}(z) = \sum_{k=1}^N \int_{z_k}^{z_{k+1}} \frac{[g_y^2(z)]_k}{G_{23}^{(k)}(z)} dz \quad (\text{B.4a-b})$$

where $G_{13}^{(k)}(z)$ and $G_{23}^{(k)}(z)$ are the transverse shear modulus at material planes 13 and 23 of the k -th ply, and N is the total amount of plies. It should be noted that $G_{13}^{(k)}(z)$ changes at each ply, i.e., the second ply is rotated 90 degrees respect to the first ply, the third ply is rotated 90 degrees respect to the second ply and so on. As an example, to determine the factor K_{11} for a laminated composite with 3 plies ($k = 3$), the three functions $g_x(z)$ are calculated as,

$$[g_x(z)]_1 = -\frac{1}{2}(\bar{Q}_{11}^1(z^2 - z_1^2)) \quad (\text{B.5a})$$

$$[g_x(z)]_2 = -\frac{1}{2}[\bar{Q}_{11}^1(z_2^2 - z_1^2) + \bar{Q}_{11}^2(z^2 - z_2^2)] \quad (\text{B.5b})$$

$$[g_x(z)]_3 = -\frac{1}{2}[\bar{Q}_{11}^1(z_2^2 - z_1^2) + \bar{Q}_{11}^2(z_3^2 - z_2^2) + \bar{Q}_{11}^3(z^2 - z_3^2)] \quad (\text{B.5c})$$

$H_{11}(z)$ is determined by substituting Eqs. (B.5) into (B.4a), i.e.,

$$H_{11}(z) = \int_{z_1}^{z_2} \frac{[g_x^2(z)]_1}{G_{13}^{(1)}(z)} dz + \int_{z_2}^{z_3} \frac{[g_x^2(z)]_2}{G_{13}^{(2)}(z)} dz + \int_{z_3}^{z_4} \frac{[g_x^2(z)]_3}{G_{13}^{(3)}(z)} dz \quad (\text{B.6})$$

where $G_{13}^{(1)}(z) = G_{13}^{(1)}$; $G_{13}^{(2)}(z) = G_{23}^{(2)}$; and $G_{13}^{(3)}(z) = G_{13}^{(3)}$. Finally, K_{11} is determined by evaluating Eq. (B.6) and such a value is included into Eq. (B.3).



References

- [1] D. F. Adams, L. A. Carlsson, and R. B. Pipes, *Experimental characterization of advanced composite materials*. Boca Raton: CRC Press, 2003.
 - [2] R. M. Jones, *Mechanics of composite materials*, Second ed. Philadelphia: Taylor & Francis, 1999.
 - [3] J. N. Reddy, *Mechanics of laminated composite plates and shells*, Second ed. Boca Raton: CRC Press, 2004.
 - [4] C. M. Wang, J. N. Reddy, and K. H. Lee, *Shear deformable beams and plates*. Eastbourne: Elsevier, 2000.
 - [5] E. Ventsel and K. Theodor, *Thin plates and shells*. New York: Marcel Dekker, 2001.
 - [6] J. R. Vinson, "In-plane shear strength determination of composite materials laminated and sandwich plates," *Appl Mech Rev*, vol. 50, no. 11, 1997.
 - [7] J. R. Vinson, *Plate and panel structures of isotropic, composite and piezoelectric materials, including sandwich construction*. Netherlands: Springer, 2005.
 - [8] D. Zenkert, *An introduction to sandwich construction*. London: EMAS, 1997.
 - [9] ASTM-D3044-95, "Standard test method for shear modulus of wood-based structural panels," ed. West Conshohoken, PA: ASTM, 2000.
 - [10] ISO-15310, "Fibre-reinforced plastic composites-Determination of the in-plane shear modulus by the plate twist method," ed. Geneva: ISO, 1999.
 - [11] R. F. S. Hearmon and E. H. Adams, "The bending and twisting of anisotropic plates," *British Journal of Applied Physics*, vol. 3, pp. 150-156, 1951.
 - [12] S. Timoshenko and S. Woinowsky-Krieger, *Theory of plates and shells*, Second ed. New York: McGraw-Hill, 1959.
 - [13] A. P. Boresi and R. J. Schmidt, *Advanced mechanics of materials*, 6th ed. United States of America: Jhon Willey and Sons, 2003.
 - [14] ASTM-E143-87, "Standar test method for shear modulus at room temperature," ed. Conshohocken: ASTM, 1998.
 - [15] G. D. Sims, W. Nimmo, A. F. Johnson, and D. H. Ferriss, "Analysis of plate-twist test for in-plane shear modulus of composite materials," National Phisycal Laboratory, Teddington. DMM(A)54*, 1994.
 - [16] F. Avilés, F. Couoh-Solis, L. A. Carlsson, A. Hernández-Pérez, and A. May-Pat, "Experimental determination of torsion and shear properties of sandwich panels and laminated composites by the plate twist test," *Composite Structures*, vol. 93, pp. 1923-1928, 2011.
 - [17] F. Avilés, L. A. Carlsson, G. Browning, and K. Millay, "Investigation of the sandwich plate twist test," *Experimental Mechanics*, vol. 49, pp. 813-822, 2009.
 - [18] S. M. Lee, "An edge crack torsion method for mode III delamination fracture testing," *Journal of Composites Technology & Research*, vol. 15, no. 3, pp. 193-201, 1993.
 - [19] A. Náđai, *Die elastischen platten*. Berlin: Springer, 1968.
 - [20] J. Q. Ye, *Laminated composite plates and shells*. London: Springer, 2003.
 - [21] J.-M. Berthelot, *Composite materials* (Mechanical Engineering Series). New York: Springer-Verlag Berlin Heidelberg, 1999.
-

-
- [22] V. Birman and G. A. Kardomateas, "Review of current trends in research and applications of sandwich structures," *Composites Part B*, vol. 142, pp. 221-240, 2018.
- [23] H. G. Allen, *Analysis and design of structural sandwich panels* Oxford: Pergamon, 1969.
- [24] L. A. Carlsson and G. A. Kardomateas, *Structural and failure mechanics of sandwich composites*. New York: Springer, 2011.
- [25] J. M. Davies, *Lightweight sandwich construction*. Oxford: Blackwell Science, 2001.
- [26] A. Hernández-Pérez, R. Hägglund, L. A. Carlsson, and F. Avilés, "Analysis of twist stiffness of single and double-wall corrugated boards," *Composite Structures*, vol. 110, pp. 7-15, 2014.
- [27] J. J. Wijker, *Spacecraft Structures*. Heidelberg: Springer-Verlag Berlin Heidelberg, 2008.
- [28] S. G. Lekhnitskii, *Anisotropic Plates*. New York: Gordon & Breach Science Publishers, 1968.
- [29] S. G. Lekhnitskii, *Theory of elasticity of an anisotropic body*. Moscow: Mir Publishers, 1981.
- [30] D. L. Logan, *A first course in the finite element method*, 4th ed. United States of America: Thomson, 2007.
- [31] ANSYS, "Ansys User's manual: Theory reference," 11.0 ed. Houston: Swanson Analysis System Inc, 2007.
- [32] M. W. Hyer, *Stress analysis of fiber-reinforced composite materials*. Singapore: WCB/McGraw Hill, 1998.
- [33] V. Birman and C. W. Bert, "On the choice of shear correction factor in sandwich structures," *Journal of Sandwich Structures and Materials*, vol. 4, pp. 83-95, 2002.
- [34] T. S. Chow, "On the propagation of flexural waves in an orthotropic laminated plate and its response to an impulsive load," *Journal of Composites Technology & Research*, vol. 5, pp. 306-319, 1971.
- [35] J. M. Whitney and N. J. Pagano, "Shear deformation in heterogeneous anisotropic plates," *Journal of Applied Mechanics*, vol. 37, pp. 1031-1036, 1970.
- [36] T. Kaneko, "On Timoshenko's correction for shear in vibrating beams," *Journal of Physics D: Applied Physics*, vol. 8, pp. 1927-1936, 1975.
- [37] J. M. Whitney, "Shear correction factors for orthotropic laminates under static load," *Journal of Applied Mechanics*, vol. 40, no. 1, pp. 302-304, 1973.
- [38] J. M. Whitney, "The effect of transverse shear deformation on the bending of laminated plates," *Journal of Composite Materials*, vol. 3, pp. 534-547, 1969.
- [39] C. W. Bert, "Simplified analysis of static shear factors for beams of nonhomogeneous cross section," *Journal of Composite Materials*, vol. 7, pp. 525-529, 1973.
- [40] J. R. Vinson and R. L. Sierakowski, *The behavior of structures composed of composite materials*. Dordrecht: Kluwer Academic Publishers, 1987.
- [41] J. G. Sloan, "The behavior of rectangular composite materials plates under lateral and hygrothermal loads," MMAE thesis, Department of mechanical and aerospace engineering, University of Delaware, 1979.
- [42] F. Avilés, L. A. Carlsson, and A. May-Pat, "A shear-corrected formulation for the sandwich twist specimen," *Experimental Mechanics*, vol. 52, pp. 17-23, 2012.
-

-
- [43] W. Thielemann, "Contributions to the problem of buckling of orthotropic plates with special reference to plywood," NACA TM1950, vol. 1263.
- [44] S. W. Tsai, "Experimental determination of the elastic behavior of orthotropic plates," *Journal of Engineering for Industry*, vol. 63, pp. 315-317, 1965.
- [45] A. Hernández-Pérez, F. Avilés, and L. A. Carlsson, "First-order shear deformation analysis of the sandwich plate twist specimen," *J Sandw Struct Mater*, vol. 14, no. 3, pp. 229-245, 2012.
- [46] D. Elmalich and O. Rabinovitch, "Twist in soft-core sandwich plates," *Journal of Sandwich Structures and Materials*, vol. 16, no. 6, pp. 577-613, 2014.
- [47] J. M. Whitney, *Structural analysis of laminated anisotropic plates*. Lancaster: Technomic Publishing Company, 1987.
- [48] H. Hsu, *Applied Fourier Analysis*. San Diego: C.A: Harcourt Brace Jovanovich, 1984.
- [49] S. Moaveni, "Finite element analysis," New Jersey: Prentice Hall, 1999.
- [50] S. S. Rao, *The finite element method in engineering*, 4th ed. Miami: Elsevier Science and Technology Books, 2004.
- [51] R. D. Cook, D. S. Nalkus, and M. E. Plesha, *Concepts and applications of finite element analysis*, 3rd ed. United States of America: John Wiley and Sons, 1989.
- [52] A. C. Ugural, *Stresses in beams, plates, and shells*, Third ed. Boca Raton: CRC Press, 2010.
- [53] M. Mure, "Corrugated board-a new method: anticlastic rigidity [in French]," *Rev ATIP*, vol. 40, pp. 325-330, 1986.
- [54] J. Li, S. M. Lee, E. W. Lee, and T. K. O'Brien, "Evaluation of the edge crack torsion (ECT) test for mode III interlaminar fracture toughness of laminated composites," *Journal of Composite Technology and Research*, vol. 19, no. 3, pp. 174-183, 1997.
- [55] J. G. Ractliffe, "Characterization of the edge crack torsion (ECT) test for mode III fracture toughness measurement of laminated composites," National Aeronautics and Space Administration, Langley-Virginia, 2004.
- [56] M. F. Ashby, *Materials selection in mechanical design*, Second ed. Woburn: Butterworth-Heinemann, 1999.
- [57] M. F. Ashby, A. G. Evans, N. A. Fleck, G. L. J, J. W. Hutchinson, and H. N. G. Wadley, *Metal foams: a design guide*. Woburn: Butterworth-Heinemann, 2000.
- [58] J. Freund and A. Karakoc, "Shear and torsion correction factors of Timoshenko beam model for generic cross section," *Research on Engineering Structures and Materials*, vol. 2, pp. 19-27, 2016.
- [59] Y. Uflyand, "The propagation of the waves in the transverse vibrations of bars and plates [in russian].," *Akad Nauk SSSB, Prikl. MAT. i Mekhanika*, vol. 12, pp. 287-300, 1948.
- [60] S. Timoshenko, *Strength of Materials*. Princeton: D von Nostrand, 1955.
- [61] G. Browning, L. A. Carlsson, and J. Ratcliffe, "Redesign of the ECT Test for mode III delamination testing. Part I: Finite element analysis," *J Compos Mater*, vol. 44, no. 15, pp. 1867-1881, 2010.
- [62] Merriam-Webster. (2019, 29 october). *Definition of anticlastic*. Available: <https://www.merriam-webster.com/dictionary/anticlastic>
-

- [63] J. R. Vinson, *Structural mechanics: The behavior of plates and shells*. New York: John Wiley and Sons, 1974.
- [64] L. L. D. Kelvin and P. Guthrie, *Treatise on natural philosophy*. Cambridge: Cambridge University Press, 1883.
- [65] R. Guillén-Rujano, A. Hernández-Pérez, and F. Avilés, "Examination of the plate twist specimen for thick specially orthotropic laminated composites and sandwich plates by using first-order shear deformation theory," *J Sandw Struct Mater*, vol. 0, pp. 1-27, 2017.
- [66] D. Gay, S. V. Hoa, and S. W. Tsai, *Composite materials*. Boca Raton: CRC Press, 2003.
- [67] C. S. Huang, "Stress singularities at angular corners in first-order shear deformation plate theory," *International Journal of Mechanical Sciences*, vol. 45, pp. 1-20, 2003.
- [68] A. Kotousov, "On stress singularities at angular corners of plates of arbitrary thickness under tension," *International Journal of Fracture*, vol. 132, pp. L29-L36, 2005.
- [69] G. L. Ghiringhelli and G. Sala, "Influence of stacking sequence and interlaminar layer on stress singularities at free edge of composite laminates," *Meccanica*, vol. 25, pp. 32-39, 1990.